STATISTICAL METHODS FOR HIGH-DIMENSIONAL DATA WITH COMPLEX CORRELATION STRUCTURE APPLIED TO THE BRAIN DYNAMIC FUNCTIONAL CONNECTIVITY STUDY

Maria Aleksandra Kudela

Submitted to the faculty of the University Graduate School
in partial fulfillment of the requirements
for the degree
Doctor of Philosophy
in the Department of Biostatistics,
Indiana University

May 2017

Accepted by the Graduate Faculty, Indiana University, in partial fulfillment of the requirements for the degree of Doctor of Philosophy.

Jaroslaw Harezlak, Ph.D., Chair

Mario Dzemidzic, Ph.D.

Doctoral Committee

Constantin Yiannoutsos, Ph.D.

January 6, 2017

Shanshan Li, Ph.D.

Chunyan He, Ph.D.

Dedication

To my loving family

Acknowledgments

I would like to express sincere gratitude to my advisor Prof. Jaroslaw Harezlak for his shared wisdom, encouragement, support, friendship, timely manner revisions, and mentorship. I am very grateful for all provided opportunities to share my research, extend my knowledge, learn from an amazing group of people and grow in this wonderful area of research. I would like to thank the committee members Prof. Constantin Yiannoutsos, Prof. Shanshan Li and Dr. Chunyan He for their inputs, suggestions and constructive criticism.

Especially, I would like to thank Prof. Mario Dzemidzic for his friendship, kindness, shared knowledge, wisdom, guidance, time, Croatian optimism, and an office door that was always open. The list is really, really long. His continuous encouragement and supportive mentorship have always given me the necessary energy to push forward and overcome many challenges. I deeply appreciate his tremendous support and contributions to my research, without which this work would have been impossible.

I would also like to thank Prof. Xiaochun Li for her help, support and advice during my time at Indiana University, Prof. Martin Lindquist for his support, contributions, comments and valuable input, and my collaborators from the Neuroscience field Prof. David Kareken, Prof. Brandon Oberlin and Prof. Joaquin Goñi for their thorough feedbacks, shared knowledge about brain imaging concepts, contributions and support, openness to discuss new ideas and learning new statistical methods.

I would like to give my special thanks to the Chair of Biostatistics Department Dr. Barry Katz, all faculty and staff members at Biostatistics department for creating a friendly and interdisciplinary research environment.

Finally, I would like to thank my family and friends for their unconditional love and support. I really appreciate that you are always there for me.

Maria Aleksandra Kudela

STATISTICAL METHODS FOR HIGH-DIMENSIONAL DATA WITH COMPLEX CORRELATION STRUCTURE APPLIED TO THE BRAIN DYNAMIC FUNCTIONAL CONNECTIVITY STUDY

A popular non-invasive brain activity measurement method is based on the functional magnetic resonance imaging (fMRI). Such data are frequently used to study functional connectivity (FC) defined as statistical association among two or more anatomically distinct fMRI signals (Friston, 1994). FC has emerged in recent years as a valuable tool for providing a deeper understanding of neurodegenerative diseases and neuropsychiatric disorders, such as Alzheimer's disease and autism. Information about complex association structure in high-dimensional fMRI data is often discarded by a calculating an average across complex spatiotemporal processes without providing an uncertainty measure around it.

First, we propose a non-parametric approach to estimate the uncertainty of dynamic FC (dFC) estimates. Our method is based on three components: an extension of a bootstrapping method for multivariate time series, recently introduced by Jentsch and Politis (2015); sliding window correlation estimation; and kernel smoothing.

Second, we propose a two-step approach to analyze and summarize dFC estimates from a task-based fMRI study of social-to-heavy alcohol drinkers during stimulation with flavors. In the first step, we apply our method from the first paper to estimate dFC for each region-subject combination. In the second step, we use semiparametric additive mixed models to account for complex correlation structure and model dFC on a population level following the study's experimental design.

Third, we propose to utilize the estimated dFC to study the system's modularity defined as the mutually exclusive division of brain regions into blocks with intra-connectivity greater than the one obtained by chance. As a result, we obtain brain partition suggesting the existence of common functionally-based brain organization.

The main contribution of our work stems from the combination of the methods from the fields of statistics, machine learning and network theory to provide statistical tools for studying brain connectivity from a holistic, multi-disciplinary perspective.

Jaroslaw Harezlak, Ph.D., Chair

Table of contents

List of tables

List of figures

Chapter 1

Introduction

The human brain is one of the most complex biological systems. It consists of approximately 100 billion neurons and 100 trillion of synapses which work together in the temporal and topological domain (Fornito et al. (2016)). Malfunctions of this complicated system manifest as neurodegenerative diseases, neuropsychiatric and substance abuse disorders, all of which pose major public health concerns. Clinicians and researchers from many fields have been studying these disruptive brain changes. However, the advances in medical imaging provide novel, previously unavailable insights. One of the popular medical imaging techniques to probe brain (dys)function is provided by functional magnetic resonance imaging (fMRI).

fMRI has been extensively used in the past twenty years, spurring a growth of neuroimaging software suites. However, commonly used statistical methods do not account for the rapid technological advancement of neuroimaging field and hence a complex correlation structure in high-dimensional fMRI data. In many modern studies, time-varying measurements have a complex association organization, which can either have the biological source or be induced by the experimental design. Researchers often calculate a one number summary (e.g. average) across these complex spatiotemporal measurements without providing an uncertainty measure, thereby not considering a full information from fMRI data.

In this dissertation, we extended traditional statistical approaches to the brain connectivity, known as dynamic functional connectivity (dFC). dFC analysis quantifies the association between two or more time series from anatomically different brain regions (Friston (1994)), and is emerging as an important tool to better understands how the brain works. Recently, the neuroimaging community has realized that assessing FC as a stationary measure across time does not give a full picture of underlying changes in associations occurring in the brain (Chang and Glover (2010); Hutchison et al. (2013)). However, dFC

analysis is challenging due to the complex structure of the fMRI data (high dimensionality and time-dependence). In this dissertation, we addressed a class of problems associated with the standard dFC analysis. The novelty of this work stems from the combination of statistical, machine learning and network theory methodology and its ability to provide statistical implementation of brain connectivity estimation from a holistic, multi-disciplinary perspective. Below, I present a brief summary of my contributions.

In the first part of my dissertation work, I developed an algorithm to quantify uncertainty for a "sliding window" method, which is a commonly used approach assessing dFC between two fMRI time series. The proposed algorithm consists of three components: an extension of a bootstrapping method for multivariate time series, recently introduced by Jentsch et al. (2015); sliding window correlation estimation; and kernel smoothing. We evaluated the empirical performance of this algorithm through an extensive simulation study. To assess the estimation accuracy of the proposed algorithm, we measured the mean square error (MSE) between an estimated dynamically changing correlation and the true value of correlation. We applied the proposed algorithm to the "Multimodal MRI Reproducibility Resource" study (Landman, Huang, Gifford, Vikram, Lim, and et al. (Landman et al.); publicly available data set). As a result, we showed that the estimated dynamic correlation is extremely variable and that providing only point estimates of the correlation is not always representative and can sometimes be misleading. Uncertainty estimation enables us to decrease the chance of making false positive statements about either non-zero association or static behavior of the connectivity. A full description of the methodology and the empirical results can be found in Chapter 3.

In the second part of my dissertation, I examined how the association between two time-varying processes with complex correlation structure changes under different conditions on a population level. This work is applied to a task-based fMRI study of social-to-heavy alcohol

drinkers during stimulation with beer and Gatorade® flavors. We first estimated the time-varying association among 278 functionally defined brain regions (Shen et al. (2013)) at a subject level using the algorithm developed in the first part of my dissertation. As a result, for each subject and scan, we obtained a smooth trajectory and its confidence interval for $38{,}503 (= 278 * 279/2 - 278)$ pairwise time-varying associations. Then these subject-specific estimates were used to model population-averaged dynamically changing association for each stimulus.

To deal with the complex correlation structure of the data and model the time-varying association between each pair of the 278 brain regions on a population level, we used the idea of the penalized splines within the framework of semiparametric additive mixed effects models. This approach allowed us to take into consideration the design of the experiment by accounting for scan effects as well as subject- and task-specific variability. As a result, we combined the information across subjects to obtain a population level estimate of time-varying association and its confidence intervals for each flavor and the difference between flavors.

Next, we proposed steps to summarize the result from 38,503 population level pairwise associations for each flavor and the difference between flavors by calculating the proportion of time points when associations were either significantly positive or negative. Resulting dFC estimates yielded patterns closely resembling the resting state networks. On the regional level, we found that brain regions prominently involved in reward were positively associated during scans with beer flavor stimulation. In addition, we found significant association for right ventral striatum and ventral anterior insula, two brain regions where the main activation-based results were found in previous study (Oberlin et al. (2016)). Most notably, dFC uncovered numerous associations undetected by the traditional static FC analysis.

The proposed approach is applicable not only to the fMRI data but also other types of time series data. A full description of this project can be found in Chapter 3.

In the third part of my dissertation, I examined a different approach to utilize and summarize the results for dFC measures obtained in Chapter 4 by analyzing the system's modularity. This network metric quantifies communities, i.e. mutually exclusive divisions of brain regions with intra-connectivity greater than the one obtained by chance. One of the popular methods to detect such communities is based on the modularity maximization. This method divides a network into non-overlapping communities with densely connected nodes based on maximization of the quality function, Q (Mucha et al. (2010); Newman (2006)), which compares the number of intra-community edges to what one would expect to obtain by chance. Modularity results were summarized on the population and the subject level by calculating network- and region-based entropy (a measure of uncertainty of group assignment) for each flavor. The modularity analysis using dFC of the gustatory task fMRI data yielded three functional modules that were generally comprised of the known resting state networks with major resting state networks contained within each of the derived modules. At the network level, three predominant communities emerged for both flavors involving: 1) visual-subcortical, 2) somatomotor-attentional, and 3) frontoparietal-default mode network regions suggesting the existence of common functionally-based brain organization. On the regional level, we found significant associations for reward-related orbitofrontal and ventrostriatal regions, known to be implicated in the alcohol cue response (Oberlin et al. (2016)). The main advantage of proposed methodology is that it provides a data-driven, flexible approach of assessing associations between brain regions and networks from a distinctly different perspective and discovering relationships that would otherwise remain hidden.

The main contribution of this work is in its unique mixture of methodology from the fields of statistics, machine learning and network theory to provide statistical tools for studying dynamic brain connectivity from a comprehensive, integrative perspective. The methodology proposed here offer a novel analytical framework to uncover numerous associations in task and resting state time series data, undetected by traditional analysis.

Chapter 2

Assessing uncertainty in dynamic functional connectivity

Functional connectivity (FC) – the study of the statistical association between time series from anatomically distinct regions (Friston (1994, 2011)) – has become one of the primary areas of research in the field surrounding resting state functional magnetic resonance imaging (rs-fMRI). Although for many years researchers have implicitly assumed that FC was stationary across time in rs-fMRI, it has recently become increasingly clear that this is not the case and the ability to assess dynamic changes in FC is critical for better understanding of the inner workings of the human brain (Chang and Glover (2010); Hutchison et al. (2013)). Currently, the most common strategy for estimating these dynamic changes is to use the sliding-window technique. However, its greatest shortcoming is the inherent variation present in the estimate, even for null data, which is easily confused with true time-varying changes in connectivity (Lindquist et al. (2014)). This can have serious consequences as even spurious fluctuations caused by noise can easily be confused with an important signal. For these reasons, assessment of uncertainty in the sliding-window correlation estimates is of critical importance. Here we propose a new approach that combines the multivariate linear process bootstrap (MLPB) method and a sliding-window technique to assess the uncertainty in a dynamic FC estimate by providing its confidence bands. Both numerical results and an application to rs-fMRI study are presented, showing the efficacy of the proposed method.

Introduction

Functional connectivity (FC), the study of the statistical association between two or more anatomically distinct time-series (Friston (1994),Friston (2011)), has become one of the primary areas of research in the field surrounding functional magnetic resonance imaging (fMRI). Although researchers implicitly assumed that FC was stationary across time, par-

ticularly in resting-state fMRI (rs-fMRI), it has recently become increasingly clear that the ability to assess dynamic changes in FC is critical for a better understanding of the inner workings of the human brain (Chang and Glover (2010); Hutchison et al. (2013)). The association between changes in connectivity and various diseases has been described in a number of studies (Filippini et al. (2009)), and the hope is that this will provide the beginning of a new and deeper understanding of neurodegenerative diseases and neuropsychiatric disorders, such as Alzheimer's disease (Jones et al. (2012)) or autism (Starck et al. (2013)). The results also support the belief that changes in neural activity patterns associated with dynamically changing FC can provide greater understanding of the fundamental properties of brain networks in both healthy subjects and patients suffering from various mental disorders.

Despite the increased attention, the results of dynamic FC analyses are often difficult to interpret. This is due in part to the inherent low signal-to-noise ratio in the data, physiological artifacts, and variation over time in both the mean and variance of the blood-oxygen-level dependent (BOLD) signal. These issues conspire together to create problems with the interpretation of transient fluctuations in FC (Hutchison et al. (2013)), and it is often difficult to determine whether they are in fact due to neuronal activity or simply a byproduct of random noise (Hindriks et al. (2016); Lindquist et al. (2014)). In addition, a lack of clear analytical strategy and guidelines for proper interpretation of the results further contribute to this ambiguity. As a consequence, significant research and methodological developments are necessary to move the field forward.

A number of approaches have been proposed to assess dynamic FC in resting-state fMRI data, including independent component analysis, time-frequency coherence analysis (Chang and Glover (2010)), time series models (Lindquist et al. (2014)), and change-point detection methods (Cribben et al. (2012, 2013); Xu and Lindquist (2015)). To date, the so-

called sliding-window approach (Allen et al. (2012); Chang and Glover (2010); Handwerker et al. (2012)) has been the most common analysis strategy, and it is the focus of this work. This approach has a number of benefits, including the fact that it is appealingly simple in both application and intuition. However, in spite of these benefits, the approach has several drawbacks. These include the arbitrary choice of window length and the fact that all observations within the window are weighted equally (Lindquist et al. (2014)). However, its greatest shortcoming is possibly the inherent variation present in the estimate, even for null data, which is easily confused with true time-varying changes in connectivity (Hindriks et al. (2016); Lindquist et al. (2014)). This can have serious consequences as even spurious fluctuations caused by noise can easily be confused with important signal.

For these reasons, the ability to assess the level of uncertainty in sliding-window correlation estimates is of critical importance. In particular, the introduction of confidence intervals for the correlation estimates could help identify, and screen for, changes in connectivity that are driven purely by random noise. One possible approach towards obtaining such intervals is to use the bootstrap procedure. Standard bootstrap methods are not readably applicable to time series data due to the dependence structure (Kreiss and Paparoditis (2011)). For this reason, in the past few years, new techniques have been proposed for bootstrapping dependent and stationary time series data (see Kreiss and Paparoditis (2011) for a summary of these methods). To date, this work has primarily focused on estimation of the sample mean and does not consider statistics of order higher than two. To circumvent this problem, Jentsch et al. (2015) introduced the multivariate linear process bootstrap (MLPB) method. They employ a tapered covariance matrix estimator, which gives higher weights to observations in a close proximity and lower weights to observations farther apart. Application of this procedure results in a stable and consistent estimator of the covariance

matrix arising from multivariate time series. These properties of an estimator are critical for accurate estimation of dynamic FC, and standard bootstrap methods do not share them.

In this work, we propose a new non-parametric model-free approach that combines the MLPB and a sliding-window technique in order to assess the uncertainty in dynamic FC estimates by providing confidence bands. Specifically, we divide time series into adjacent blocks. We use data within each block to generate bivariate time series bootstrap samples. We combine generated data from adjacent blocks into time series. Next, we define a moving time window of size w and use data within that window to calculate the correlation coefficient. Subsequently, the window is moved forward step-wise through time, and the procedure is repeated for each shift. As a result, a time-varying measure of correlation between brain regions is obtained as well as dynamically changing confidence bands. Our algorithm, denoted Dynamic Connectivity Bootstrap Confidence Bands (DCBootCB), provides a valid estimate of the confidence band for the sliding-window estimator of the correlation coefficient.

The properties of the proposed estimator are studied in a series of simulation studies. Our simulations provide evidence that the MLPB approach to bootstrapping correlated time series gives valid model-free time-varying connectivity estimates together with their associated confidence bands. In addition, they show that the theoretical properties of the proposed approach are supported by empirical evidence. We conclude by applying the DCBootCB algorithm to resting state fMRI data.

The article is organized as follows: Section 2.2 introduces a statistical framework of our problem; Section 2.3 presents our approach for estimating the time-varying functional connectivity and its confidence bands; Section 2.4 and 2.5 provides the description and the results of the simulation study; Section 2.6 presents an application of our method to rs-fMRI data; and Section 2.7 contains conclusions and a discussion.

Statistical framework

Our work is concerned with the principled estimation of confidence bands for the time-varying functional connectivity between two time series measured at uniformly sampled time points $t = 1, \ldots, T$. Let a two dimensional time series be denoted by $\{\mathbf{y}(t), t = 1, \ldots, T\}$ with $\mathbf{y}(t) = (y_1(t), y_2(t))^\top$, where $\top$ means transpose. Further, assume that:

$$\mathbf{y}(t) = \mu(t) + \varepsilon(t) \tag{2.1}$$

where $\mu(t)$ is the mean of $\mathbf{y}(t)$ conditioned on all observations obtained up to time t, defined by $E(y(t)|y(1), \ldots, y(t-1))$, and $\varepsilon(t)$ is the error term at time t with mean zero and covariance matrix also conditioned on all observations obtained up to time t given by:

$$\Sigma(t) = \begin{pmatrix} \sigma_{11}(t) & \sigma_{12}(t) \\ \\ \sigma_{21}(t) & \sigma_{22}(t) \end{pmatrix}. \tag{2.2}$$

The diagonal terms of the matrix $\Sigma(t)$ are the time-varying variances of the two time series $y_1(t)$, $y_2(t)$. The off-diagonal term is the covariance between the two time series $y_1(t), y_2(t)$. All of these terms are conditioned on all observations obtained till time t . Equivalently, the conditional covariance matrix can be expressed as:

$$\Sigma(t) = D(t)R(t)D(t) = D(t) \begin{pmatrix} 1 & \rho(t) \\ \\ \rho(t) & 1 \end{pmatrix} D(t) \tag{2.3}$$

where the conditional standard deviations of time series are represented in the diagonal matrix $D(t)$; $R(t)$ is the correlation matrix conditioned on all observations obtained till time t, and $\rho(t)$ is the correlation coefficient conditioned on the observations collected up

to time t, which is defined as:

$$\rho(t) = \frac{\sigma_{12}(t)}{\sqrt{\sigma_{11}(t)\sigma_{22}(t)}}. \tag{2.4}$$

The main goal of this paper is to estimate the confidence bands for $\rho(t)$ by applying a modified sliding-window technique. The general idea behind the basic sliding-window technique is based on calculating the correlation coefficient from the data contained within a window of fixed length w. By moving the window, the correlation coefficient can be computed at each time point. This can be expressed as follows:

$$\hat{\rho}(t) = \frac{\sum_{k=t}^{t+w-1}(y_1(k) - \mu_1(k))(y_2(k) - \mu_2(k))}{\sqrt{\sum_{k=t}^{t+w-1}(y_1(k) - \mu_1(k)) \sum_{k=t}^{t+w-1}(y_2(k) - \mu_2(k))}} \tag{2.5}$$

There are a number of potential drawbacks of using the sliding-window approach directly, including its inability to handle sudden changes, the equal weighting of all observations within a window, and the arbitrary selection of window length Lindquist et al. (2014). Due to these shortcomings, it is important to be able to critically evaluate the uncertainty present in the sliding-window estimate. However, the sliding-window technique does not provide valid and straightforward non-parametric estimates for the confidence bands. The most commonly used approach for computing the confidence interval for the correlation estimator is to use a parametric, asymptotic Fisher approximation for the correlation coefficient. However, as we show in this paper, this approach has a number of shortcomings in practice and is not valid for correlated time series.

Estimation of time-varying functional connectivity and its confidence bands

In this section, we introduce the DCBootCB algorithm for estimating the time-varying correlation coefficient and its confidence bands. In order to understand the DCBootCB algorithm, we begin by giving a brief summary of statistical concepts used in our study and the MLPB method proposed by Jentsch and Politis (2015) Jentsch et al. (2015).

We start by providing short overview of a number of statistical concepts. A *confidence interval* at a given confidence level, for example 95%, implies that if the same population is sampled on many occasions and interval estimates are calculated each time, the resulting intervals would include the true population parameter in approximately 95 % of the cases.

The *coverage probability* is used to assess the empirical performance of a method that has been shown to behave well in theory. Specifically, in the simulation studies we estimate it by counting the number of timepoints in which the true parameter value is contained within the confidence interval. For example in the case of a 95% confidence interval, we expect that on average in 95% of the simulations the true parameter will be within the confidence interval limits. In our simulation study, for each time point, we calculate the percentage of times that the confidence interval covers the true parameter. A final estimate of the coverage probability over the whole time domain is calculated by averaging the pointwise coverage probabilities.

Finally, we introduce the terms *non-zero coverage* and *non-static coverage* to indicate the percentage of time when the confidence interval does not contain "zero" and a "constant correlation" value, respectively. Specifically, large non-zero coverage percentage signifies that the dFC is frequently significantly different from zero, whereas large non-static coverage percentage signifies that the dFC is frequently significantly different from the static correlation. The latter indicates that an assumption of static (non-time varying) correlation between two brain regions fails to account for a dynamically changing association between them.

Next we present a short overview of MLPB method. MLPB is a general bootstrap method that gives consistent estimates for statistics of orders two and higher, with both the sample autocovariance and the sample autocorrelation being special cases.

We begin by defining functions used in the MLPB algorithm, including the flat-top kernels and the tapered covariance matrix. The flat-top kernels are the tapered weight functions used in the covariance matrix estimation. They leave the diagonal elements unchanged and progressively decrease the impact on the covariance estimation of observations located farther away from the off-diagonal. McMurry and Politis (2010) McMurry and Politis (2010) defined them formally as follows:

Definition 1. The tapered weight function κ is given by

$$\kappa(x) = \begin{cases} 1 & if\ |x| \leq 1 \\ g(|x|) & if\ 1 < |x| \leq c_\kappa \\ 0 & if\ |x| > c_\kappa \end{cases} \tag{2.6}$$

where $g(\cdot)$ is a function satisfying $|g(x)| < 1$ and c_k a constant satisfying $c_k \geq 1$.

A trapezoid function, which is used in our approach, is an example of a tapered kernel function which meets the requirements of Definition 1. We follow the definition in Jentsch et al. (2015):

$$\kappa(x) = \begin{cases} 1 & if\ |x| \leq 1 \\ 2 - |x| & if\ 1 < |x| \leq 2 \\ 0 & if\ |x| > 2 \end{cases} \tag{2.7}$$

Jentsch and Politis Jentsch et al. (2015) in their approach proposed to use a l-scale version of a flat top kernel, which is defined as $\kappa_l(x) = \kappa(\frac{x}{l})$ for some value of $l > 0$ McMurry and Politis (2010). In our approach, following the example presented in Jentsch and Politis Jentsch et al. (2015) and the author's guidelines on the selection of tuning parameters Jentsch et al. (2015), we set $l = 1$. However, for consistency in notation with the original paper Jentsch et al. (2015) we kept l as an index in the tapered covariance matrix estimator.

We next describe the use of the tapered covariance matrix estimator. Let $\underline{X} = \{X_1, ..., X_{dn}\}^\top$ be a dn-long vectorized version of the $(d \times n)$ data matrix, where n is the number of time points and d the number of time series (brain regions), in our case $d = 2$. Let Γ_{dn} be the covariance matrix of $\underline{X}$, where $\Gamma_{dn}(i,j)$ is the covariance between the i^{th} and j^{th} entry of $\underline{X}$. We estimate Γ_{dn} using the sample autocovariance function $\widehat{C}(h) = \frac{1}{n}\sum_{t=max(1,1-h)}^{min(n,n-h)}(\underline{X}_{t+h} - \overline{X})(\underline{X}_t - \overline{X})^\top$. Following the work of Jentsch et al. (2015) the estimator of Γ_{dn} can then be defined as:

$$\widehat{\Gamma}_{dn} = \Big(\widehat{C}(i-j); i,j = 1,\ldots,n\Big) = \Big(\widehat{\Gamma}_{dn}(i,j); i,j = 1,\ldots,dn\Big).$$

Jentsch and PolitisJentsch et al. (2015) point out that an estimator in this form is not consistent. As a consequence, they proposed to instead use the tapered covariance matrix estimator defined as $\widehat{\Gamma}_{\kappa,l} = \Big(\kappa_l(i-j)\widehat{C}(i-j); i,j = 1,\ldots,n\Big) = \Big(\widehat{\Gamma}_{\kappa,l}(i,j); i,j = 1,\ldots,dn\Big)$, where κ_l was specified in equation 7. To ensure positive definiteness of the obtained estimator of Γ_{dn}, Jentsch and PolitisJentsch et al. (2015) first represented $\widehat{\Gamma}_{\kappa,l}$ as a product of the variance and correlation matrices, and then decomposed the correlation matrix using its spectral factorization. To guarantee positive semidefinitness of $\widehat{\Gamma}_{\kappa,l}$ matrix, they replaced the negative eigenvalues by a small positive constant and showed that the resulting estimate affects the convergence of the estimator only slightly. The procedure can be summarized by the following formula Jentsch et al. (2015): $\widehat{\Gamma}^{\varepsilon}_{\kappa,l} = \widehat{V}^{\frac{1}{2}}\widehat{R}^{\varepsilon}_{\kappa,l}\widehat{V}^{\frac{1}{2}} = \widehat{V}^{\frac{1}{2}}SD^{\varepsilon}S\widehat{V}^{\frac{1}{2}}$, where $\widehat{V}$ is the diagonal matrix of sample variances, $\widehat{R}^{\varepsilon}_{\kappa,l}$ is a correlation matrix with adjusted values, S is a $(dn \times dn)$ orthogonal matrix containing eigenvectors, and $D^{\varepsilon} = diag(r^{\varepsilon}_1, \ldots, r^{\varepsilon}_{dn})$ is a diagonal matrix of eigenvalues of $\widehat{R}^{\varepsilon}_{\kappa,l}$, where negative diagonal entries are adjusted according to the formula $r^{\varepsilon}_i = max(r_i, \varepsilon n^{-\beta})$ with β and ε representing two tuning parameters. McMurry and Politis McMurry and Politis (2010) found in simulation studies that $\beta = 1$ and $\varepsilon = 1$ perform well and affect the MLPB results only slightly. In our work, we made the

same assumptions regarding the values of β and ε. Full description and further details of how to obtain estimator $\widehat{\Gamma}^{\varepsilon}_{\kappa,l}$ of covariance matrix Γ_{dn} can be found in Jentsch et al. (2015).

Up to this point, we have discussed how to obtain a proper estimate of the covariance matrix, which is needed in the MLPB algorithm. Next, the inverse Cholesky decomposition of the estimated covariance matrix is used to decorrelate the constructed vector $\underline{X}$. The decorrelated vector is further centered and standardized. This newly constructed residual vector can be assumed to be independent and identically distributed (*i.i.d.*) with zero mean and unit variance. By randomly selecting these residuals with replacement, bootstrap samples are created. To obtain a bootstrap sample with covariance that is approximately the same as the covariance structure of the original data, the vector of (*i.i.d.*) residuals is multiplied by the Cholesky matrix itself. Formal description of the algorithm, originally presented in Jentsch et al. (2015), is provided below.

MLPB bootstrap algorithm

Step 1. Let $\mathbf{X}$ be the $(d\times n)$ data matrix consisting of $\mathbb{R}^d$-valued time series data $\underline{X}_1,\ldots,\underline{X}_n$ of sample size n. Compute the centered observations $\underline{Y}_t = \underline{X}_t - \overline{\underline{X}}$, where $\overline{\underline{X}} = \frac{1}{n}\sum_{t=1}^{n}\underline{X}_t$, let $\mathbf{Y}$ be the corresponding $(d\times n)$ matrix of centered observations and define $\underline{Y} = vec(\mathbf{Y})$ to be the dn-dimensional vectorized version of $\mathbf{Y}$.

Step 2. Compute $\underline{W} = (\widehat{\Gamma}^{\epsilon}_{\kappa,l})^{-\frac{1}{2}}\underline{Y}$, where $(\widehat{\Gamma}^{\epsilon}_{\kappa,l})^{\frac{1}{2}}$ denotes the lower left triangular matrix $\mathbf{L}$ of the Cholesky decomposition $\widehat{\Gamma}^{\epsilon}_{\kappa,l} = \mathbf{L}\mathbf{L}^{\top}$.

Step 3. Let $\underline{Z}$ be the standardized version of $\underline{W}$, that is, $Z_i = \frac{W_i-\overline{W}}{\widehat{\sigma}_W}$, $i=1,\ldots,dn$ where $\overline{W} = \frac{1}{dn}\sum_{t=1}^{dn}W_t$ and $\widehat{\sigma}^2_W = \frac{1}{dn}\sum_{t=1}^{dn}(W_t-\overline{W})^2$.

Step 4. Generate $\underline{Z}^{\star} = (Z^{\star}_1,\ldots,Z^{\star}_{dn})^{\top}$ by performing i.i.d. resampling from $\{Z_1,\ldots,Z_{dn}\}$.

Step 5. Compute $\underline{Y}^\star = (\widehat{\Gamma}^{\epsilon}_{\kappa,l})^{\frac{1}{2}}\underline{Z}^\star$ and let $\mathbf{Y}^\star$ be the matrix obtained by placing this vector column-wise into a $(d \times n)$ matrix with columns denoted by $\underline{Y}^\star_1, \ldots, \underline{Y}^\star_n$. Define $\mathbf{X}^\star$ to be a $(d \times n)$ matrix consisting of columns $\underline{X}^\star_t = \underline{Y}^\star_t + \overline{\underline{X}}$

Next, we extend this algorithm to estimate the time-varying FC confidence bands. We begin by giving an intuitive description before providing the full DCBootCB algorithm.

In the first step, each time series of length n is divided into k adjacent blocks of length v ($n = kv$). Within each of the k blocks, we generate MLPB bootstrap samples as described above. Subsequently, adjacent blocks of bootstrap samples are combined into a single time series of length n, forming a bootstrap sample of the original time series. In the second step, we apply the sliding-window technique to the obtained bootstrap sample to estimate the dynamically changing correlation. Further, we use a kernel smoothing technique based on a Gaussian kernel to smooth its trajectory. The bootstrapping procedure is repeated B times, producing B estimates of the dynamically changing correlation coefficient trajectory. In the third step, we compute the 95% confidence bands using the empirical quantiles of the entire set of smoothed trajectories. Using the quantiles gives us simultaneous confidence bands, and we do not rely on the selection of constants or pointwise standard error estimation as is commonly done in parametric approaches to confidence band estimation.

The formal steps of the proposed algorithm are presented below. We use the following notation, $\mathbf{X}$ is a $(2 \times n)$ data matrix consisting of vectors $\underline{X}_1, \underline{X}_2$ of size n representing the fMRI time series from two ROIs, and v is an integer-valued block length.

DCBootCB algorithm

Step 1. Partition the matrix $\mathbf{X}$ into $(2 \times k)$ adjacent blocks, where $k = \frac{n}{v}$.

Step 2. Apply MLPB to draw a bootstrap sample within each adjacent block to obtain a single $2 \times v$ bootstrap sample. Combine k adjacent blocks of bootstrap samples into a single $(2 \times n)$ data matrix $\mathbf{X}^{\star}$.

Step 3. Let $\mathbf{X}_{i,v}$ be a $2 \times v$ bootstrap block of v consecutive observations starting at time index i from matrix $\mathbf{X}^{\star}$. For each $\mathbf{X}_{i,v}$ estimate the correlation at time index i.

Step 4. Use a Gaussian kernel smoothing technique to obtain the estimated correlation trajectories.

Step 5. Repeat steps 2 and 3 B times.

Step 6. Calculate the empirical quantiles at each time point to get 95% confidence bands.

We evaluate the properties of the DCBootCB algorithm in a series of simulation studies presented in Section 2.4 and apply it to resting-state fMRI data in Section 2.6.

Simulation study

In the following sections, we present in detail the data generating mechanism used in the simulations and summarize the obtained results.

Data generation

We generated a two-dimensional time series $\mathbf{y}(t) = (y_1(t), y_2(t))^{\top}$ of length T from a bivariate normal distribution with mean zero and covariance matrix defined in equation (2.3) with the correlation term $\rho(t)$ varying over time. We achieved it by generating the random numbers using the statistical computing and graphics software R (http://www.r-project.org). We used the function mvrnorm() from the library "MASS" to generate the data from a multivariate normal distribution with the user-specified mean vectors and covariance matrices.

To investigate the empirical properties of the DCBootCB method, we considered five scenarios. In Scenarios 1, 4, and 5, we set the variance of time series $y_1(t), y_2(t)$ equal to one, whereas in Scenarios 2 and 3, we assumed that the variances were equal to 2 and 3, respectively. The values of the time-varying correlation term $\rho(t)$ and the length of the time series T were set as follows:

Scenarios

S1. The correlation is equal to zero for $t = 1, \ldots, T$, which implies that the two time series are uncorrelated across time. Here the total number of time points T was allowed to vary between the values 150, 300 and 600.

S2. The correlation changes according to the function $\frac{1}{\sqrt{6}} sin \frac{t}{\Delta}$ for $\Delta = \frac{1024}{2^k}$ and $k = 1, \ldots, 4$. This function represents a slowly varying periodic change in correlation. Here the total number of time points T equals 1000.

S3. The correlation changes according to a Gaussian kernel with mean $\mu = 300$ and standard deviation $\sigma = 25 * k$ for $k = 1, \ldots, 4$. This function represents a short-lived non-zero correlation. Here the total number of time points T equals 1000.

S4. The correlation changes in 0.1 increments from 0 to 0.5 and back to 0 at times $t = m * (l - 1) + 1, \ldots, m * l$, where $l = 1, \ldots, 11$ and $m = 50, 100, 200$. Here the total number of time points T was allowed to take the values 550, 1100, and 2200.

S5. The correlation changes from 0 to 0.6 and back to 0.2 at times $t = m*(l-1)+1, \ldots, m*l$, where $l = 1, \ldots, 3$ and $m = 50, 100, 200$. Here the total number of time points T was allowed to take the values 150, 300, and 600.

For each scenario and setting, the simulations were repeated 250 times. For each simulated data set, we generated $B = 1000$ bootstrap samples. The width of the adjacent

blocks for bootstrap samples was selected to equal 30 in order to increase the stability of the covariance matrix estimation. In each generated data set, we applied the sliding-window technique using two different window lengths, namely $w = 30$ and $w = 45$ time points. It allowed us to observe how sensitive our approach is to the selection of this parameter among commonly used window lengths. We based this choice on empirical studies, as well as analytical results presented in Leonardi et al. Leonardi and Van De Ville (2015) which showed that the choice of window lengths should be between 30 and 60 seconds. When selecting the length of the sliding-window, it is important to choose a window which is not too large because it might diminish true signal in the data and not too small because it might introduce spurious fluctuations as shown by Leonardi et al. Leonardi and Van De Ville (2015) and Lindquist et al. Lindquist et al. (2014). In the literature, there are other data-driven methods for selecting the length of the window, for example methods which are based on a time-frequency analysisHutchison et al. (2013), however, the price for data-driven selection is a higher computational cost. In this article, comparison of the length of the moving windows was not our main interest.

For each simulation, we calculated the proportion of time that the confidence interval contained the true value of correlation. We took an average over these proportions and obtained the average coverage of the true correlation function. We used this value as a summary of the results of each simulation scenario.

In addition, kernel smoothing is applied with a bandwidth equal to 30 to create functional estimates of the dynamic correlations. This choice of a bandwidth can be optimized, but in practice it has no major effect on the coverage probability.

To assess the uncertainty of the dynamic FC estimates obtained using the DCBootCB method, we created the empirical 95% confidence intervals and assessed their coverage of the true parameter across time for each simulation. In addition, we compared the performance

of the proposed algorithm to the Fisher z-transformation approach. To the best of our knowledge, confidence intervals based on the Fisher z-transformation have not been used in neuroimaging studies. Details of the Fisher z-transformation are presented in Section 2.4.2 and the results of the simulation study in Section 2.5.

Fisher z-transformation

Fisher z-transformation is used to transform the estimated correlation coefficient r, defined in Eq. 2.5, using function $f(\cdot)$ such that $f(r)$ is asymptotically normally distributed. We obtain the confidence intervals for the transformed quantity, $f(r)$, and use an inverse transformation to arrive at the confidence intervals for the true correlation coefficient ρ. Fisher z-transformation of a sample correlation coefficient r is expressed as:

$$z_r = \frac{1}{2} log\left(\frac{1+r}{1-r}\right). \tag{2.8}$$

Its asymptotic standard error is $SE_{z_r} = \frac{1}{\sqrt{N-3}}$, where N is the number of time points. Using this information, we can provide the 95% confidence interval for the transformed correlation coefficient z_ρ as $\left(z_r - 1.96 * SE_{z_r}, z_r + 1.96 * SE_{z_r}\right)$. Through simple calculations, we can convert the z_r estimate back to the correlation scale using the formula:

$$r = \frac{e^{2z_r} - 1}{e^{2z_r} + 1}. \tag{2.9}$$

As a result the confidence interval for the correlation coefficient is:

$$\left(\frac{e^{2(z_r - 1.96 * SE_{z_r})} - 1}{e^{2(z_r - 1.96 * SE_{z_r})} + 1}, \frac{e^{2(z_r + 1.96 * SE_{z_r})} - 1}{e^{2(z_r + 1.96 * SE_{z_r})} + 1}\right) \tag{2.10}$$

In our simulation study, we use the number of time points within each window to obtain standard errors for the pointwise confidence intervals of the estimated correlation coefficient, i.e. $N = w$.

Simulations results

Here we summarize the results for each of the simulation scenarios. These range from the null correlation assumption (Scenario 1), through the smoothly varying correlation function (Scenarios 2 and 3), to the correlation function with jumps (Scenarios 4 and 5).

Scenario 1: Time series were generated to be uncorrelated over time. As a consequence, the estimated dynamic correlation is expected to fluctuate around zero. The top left panel of Figure 2.1 shows a sample result for a single simulation run. The DCBootCB-estimated confidence bands cover zero for most of the domain. The average coverage of the true correlation function for 150, 300, and 600 time points is 95.57%, 95.1%, and 95.6%, respectively, for a window size 30; and 95.6%, 96.1%, and 96.08%, respectively, for window size 45 (Table 2.1). Fisher's approximation gives an average coverage of the true function of 99.4%, 99.7%, and 99.5% for window size 30; and 98.7%, 98.5%, and 98.8% for window size 45 (Table 2.1). Clearly, the average coverage estimated using the Fisher approximation is higher than the nominal level, indicating it is overly conservative in this setting. Thus, our results provide a lower bound.

SIM. 1	window	T=150 aveg. (Q1, Q2, Q3)	T=300 aveg. (Q1, Q2, Q3)	T=600 aveg. (Q1, Q2, Q3)
DCBootCB	30	95.57 (99.38, 100, 100)	95.10 (91.51, 100, 100)	95.60 (92.65, 96.76, 100)
	45	95.61 (100, 100, 100)	96.13 (95.12, 100, 100)	96.09 (93.52, 99.19, 100)
Fisher approx.	30	99.42 (100, 100, 100)	99.74 (100, 100, 100)	99.45 (100, 100, 100)
	45	98.69 (100, 100, 100)	99.01(100, 100, 100)	98.82 (100, 100, 100)

Table 2.1: Summary statistics of empirical coverage of the nominal 95% confidence interval for a true correlation coefficient for simulation study Scenario 1- correlation equal to zero across time.

Scenario 2: Time series were generated so that the correlation varied slowly in a periodic fashion at four different frequencies. The top middle panel and top right panel of Figure 2.1 show the results for a single simulation run for (1) a low frequency sine function ($k = 1$); and (2) a high frequency sine function ($k = 4$). The average coverage of the true correlation function for increasing frequencies is 95.1%, 95.1%, 94.2%, and 92.5% for window size 30; and 96%, 95.9%, 94.1%, and 88.9% for window size 45 (Table 2.2).The coverage for a high frequency sine function (k = 4) is lower than the nominal 95% for two reasons; first, fast-changing nature of the true association; and second, the oversmoothing caused by the length of the moving window. Fisher's approximation gives an average coverage of 99.4%, 99.4%, 99.2%, and 95.7% for a window size 30; 99%, 98.9%, 98.1%, and 95.7% for a window size 45 (Table 2.2). Average coverage calculated using Fisher's approximation is again much higher than the nominal level, showing that this method tends to be too conservative and thus, our results provide a lower bound. DCBootCB coverage is much closer to the nominal level.

ρ function	k	window size	Coverage in percent our method aveg. (Q1, Q2, Q3)	Coverage in percent Fisher aveg. (Q1, Q2, Q3)
sine	k=1	30	95.14 (92.99, 95.62, 97.58)	99.42 (99.28, 100, 100)
		45	96.02 (93.51, 96.65, 99.90)	99.03 (98.43, 100, 100)
	k=2	30	95.11 (92.89, 95.46, 98.14)	99.39 (99.59, 100, 100)
		45	95.91 (93.43, 96.75, 99.90)	98.92 (98.43, 100, 100)
	k=3	30	94.23 (91.78, 95.05, 97.32)	99.25(98.76, 100, 100)
		45	94.08 (90.99, 95.08, 98.19)	98.11 (96.47, 100, 100)
	k=4	30	92.55 (89.41, 93.09, 96.49)	98.76 (97.94, 100, 100)
		45	88.86 (84.50, 89.32, 94.24)	95.72 (93.32, 96.54, 99.63)
Gaussian	k=1	30	94.21 (91.48, 94.64, 97.19)	99.28 (98.87, 100, 100)
		45	94.16 (91.84, 94.87, 97.15)	97.92 (96.57, 98.33, 100)
	k=2	30	94.62 (92.38, 95.42, 97.43)	99.45 (99.38, 100, 100)
		45	95.02 (92.31, 95.61, 98.20)	98.54 (97.41, 100, 100)
	k=3	30	94.76 (92.74, 95.62, 97.53)	99.46 (99.38, 100, 100)
		45	95.47 (92.89, 95.97, 99.14)	98.80 (97.91, 100, 100)
	k=4	30	94.89 (92.69, 95.73, 97.84)	99.46 (99.38, 100, 100)
		45	95.60 (93.44, 96.18, 99.48)	98.89 (97.91, 100, 100)

Table 2.2: Summary statistics of empirical coverage of the nominal 95% confidence interval for a true correlation coefficient for simulation study Scenarios 2 and 3.

Scenario 3: Time series were generated with the correlation changing according to the shape of a Gaussian kernel with four different standard deviation values. The correlation coefficient is different from zero in an interval located within approximately $\pm$ 3 standard deviations of $t = 300$. The left bottom panel of Figure 2.1 shows the results for a single simulation run for Gaussian kernel with high standard deviation. The average coverage for increasing value of standard deviation is 94.2%, 94.6%, 94.8%, and 94.9% for window size 30; and 94.1%, 95%, 95.5%, and 95.6% for window size 45 (Table 2.2). The average coverage calculated using DCBootCB is very close to the nominal level. Fisher's approximation provides an average coverage of 99.3%, 99.4%, 99.5%, and 99.5% for window size 30; 97.9%, 98.5%, 98.8%, and 98.9% for window size 45 (Table 2.2). The average coverage calculated using Fisher's approximation is again significantly higher than the nominal level.

Scenario 4: Time series were generated with the correlation changing at each eleventh time point by 0.1 starting from $\rho = 0$ to 0.5 and back to 0, i.e. in a piecewise constant pyramid shape function. The bottom middle panel of Figure 2.1 shows the results for a single simulation run. Sudden jumps cause higher fluctuations around the jump's edges. As a result DCBootCB-generated confidence intervals cover the true correlation curve along the constant parts and lie away from it at the jump points. This is expected, as we are approximating a discontinuous function with a smooth estimate. The average coverage of a true correlation function for 550, 1100, and 2200 time points is 87.6%, 87%, and 85.6%, respectively, for window size 30; and 88.1%, 88.7%, and 86.2%, respectively, for window size 45 (Table 2.3). Fisher's approximation gives an average coverage of the true parameter of 94.4%, 92.5%, and 91% for window size 30; and 93.8%, 92.8%, and 90.4% for window size 45 (Table 2.3). The average coverage calculated using Fisher's approximation is closer to the nominal level, but the confidence intervals are significantly wider.

SIM. 4	window	T=550 aveg. (Q1, Q2, Q3)	T=1100 aveg. (Q1, Q2, Q3)	T=2200 aveg. (Q1, Q2, Q3)
DCBootCB	30	87.59 (89.30, 95.59, 95.97)	87.00 (85.74, 90.62, 93.37)	85.61 (83.53, 87.82, 90.64)
	45	88.11 (88.93, 98.72, 98.81)	88.66 (87.55, 92.95, 94.70)	86.20 (83.49, 88.75, 91.74)
Fisher approx.	30	94.39 (95.97, 95.97, 95.97)	92.54(93.37, 93.37, 93.37)	91.00 (91.02, 92.12, 92.12)
	45	93.83 (97.33, 98.81, 98.81)	92.86 (93.68, 94.7, 94.7)	90.38 (90.27, 92.53, 92.76)

Table 2.3: Summary statistics of empirical coverage of the nominal 95% confidence interval for a true correlation coefficient for simulation study Scenario 4.

Scenario 5: Time series were generated with the correlation function changing in a piecewise constant manner. The correlation was equal to zero for the first third of the signal, 0.6 for the middle third, and 0.2 for the last third. The bottom right panel of Figure 2.1 shows the results for a single simulation run. As in Scenario 4, the DCBootBC-generated confidence intervals covers the true correlation along the constant parts and performs worse at jump points. Again, this is expected as we are approximating discontinuous function with a smooth estimate. The average coverage for the setting consisting of 150, 300, and 600 time points is 69.6%, 84.4%, and 90.7%, respectively, for window size 30; and 45.3%, 77.5%, and 87.2%, respectively, for window size 45 (Table 2.4). The coverage is better for a longer time series, since the overlap of the discontinuity and the sliding-window is proportionally smaller than for the short time series. Fisher's approximation gives an average coverage of a true parameter of 83.8%, 93%, and 96.4% for window size 30; and 54.2%, 81.5%, and 91.4% for window size 45 (Table 2.4). The average coverage calculated using Fisher's approximation is closer to the nominal level, but again the confidence intervals are much wider.

Widths of the confidence intervals. Figure 2.2 displays the average width of DCBootCB confidence intervals (black curve) and Fisher's approximation confidence intervals (red curves) for Scenarios 1, 3, and 5, respectively. The shape of the average width is similar for all three scenarios. The main difference between the curves is the width of

SIM. 5	window	T=150 aveg. (Q1, Q2, Q3)	T=300 aveg. (Q1, Q2, Q3)	T=600 aveg. (Q1, Q2, Q3)
DCBootCB	30	69.58 (59.50,71.90, 80.17)	84.35 (80.90, 86.72, 90.41)	90.71 (88.79, 91.86, 94.40)
	45	45.33 (33.96, 45.28, 55.42)	75.45 (70.70, 77.73, 82.71)	87.21 (84.89, 88.85, 91.19)
Fisher approx.	30	83.78 (77.69, 85.54, 91.74)	92.97 (90.77, 93.36, 96.31)	96.44 (95.27, 96.85, 98.42)
	45	54.24 (45.28, 53.77, 64.15)	81.45 (77.34, 83.01, 87.11)	91.44 (89.97, 92.09, 94.24)

Table 2.4: Summary statistics of empirical coverage of the nominal 95% confidence interval for a true correlation coefficient for Scenario 5.

coverage. DCBootCB confidence intervals are on average narrower. It is worth noticing that the confidence intervals are wider at the beginning and at the end of the estimated dFC. This feature is not uncommon in kernel smoothing, as the number of points within a kernel window is smaller than in the middle of the interval. In the smoothing literature this effect is commonly known as a "boundary effect". The average width of the Fisher's approximation confidence intervals is approximately 25% greater than the width of the DCBootCB confidence intervals. For Scenario 3 (middle panel of Figure 2.2), the average width of the confidence interval decreases as the value of correlation function increases. This result is expected and follows the theoretical properties of the correlation coefficient. Similar dependency can be observed on the right panel of Figure 2.2.

Estimation Accuracy. To assess the estimation accuracy of the DCBootCB approach and the regular sliding-window method, we measured the mean square error (MSE) between estimated dynamically changing correlation and the true value of the correlation for both methods. Although the main interest of the paper is to provide an algorithm to estimate confidence intervals for the sliding-window estimate of dFC, the estimate of dFC which we get as a result of applying DCBootCB algorithm has a smaller MSE compared to the sliding-window method. Results for each scenario are presented in Figures 2.3 to 2.7.

Summary. For the majority of the simulation scenarios considered, the DCBootCB method provides appropriate coverage of the true correlation function. The empirical coverage is

very close to the nominal value. However, the proposed algorithm does not perform well in the case of step functions. This behavior was expected, as we are attempting to estimate the discontinuous function using smooth estimates. Fisher's approximation does a better job in terms of coverage in the discontinuous correlation function case, at the cost of a significant increase in the width of the confidence interval. In addition, in Scenarios 1, 2 and 3, Fisher's approximation gives an average coverage as great as 99.5%, illustrating that Fisher's approximation tends to be overtly conservative.

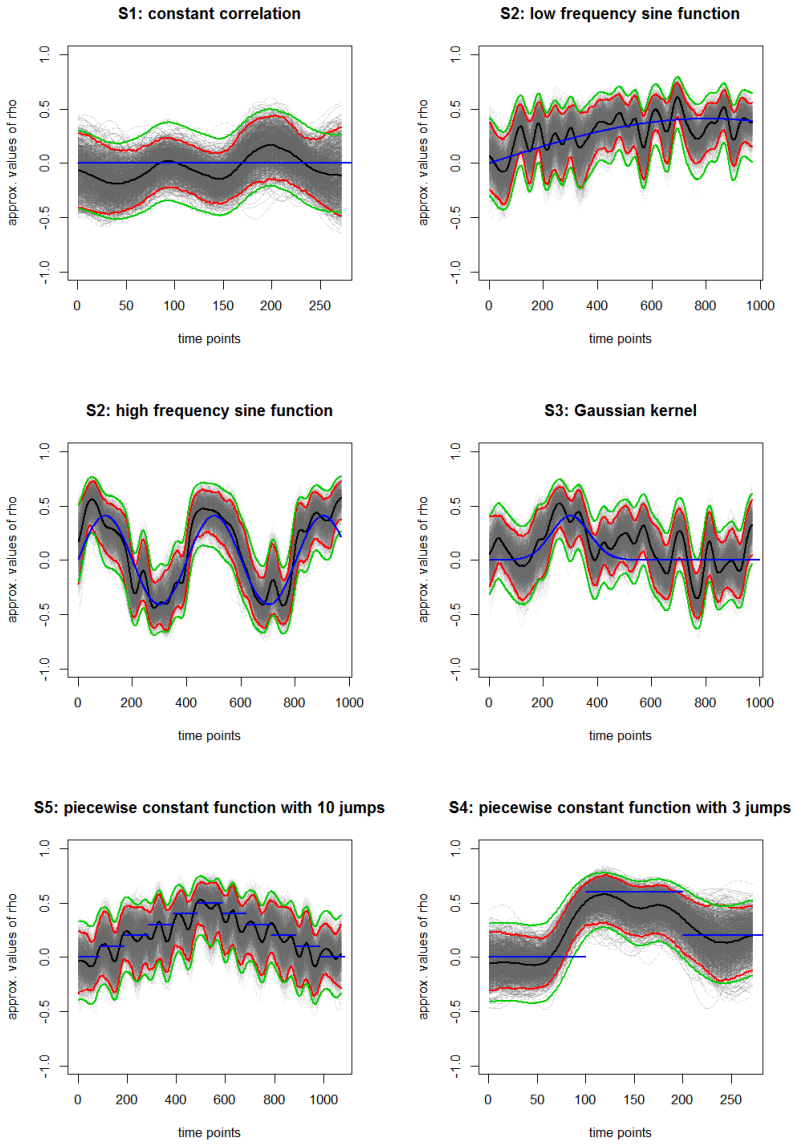

Figure 2.1: Results for a single simulation run of the time-varying functional connectivity for different scenarios. Blue line represents the true correlation between the two time series, black line the estimated correlation, the red lines the 95% confidence intervals based on the bootstrap samples (gray curves) and the green lines the 95% confidence intervals based on the Fisher approximation.

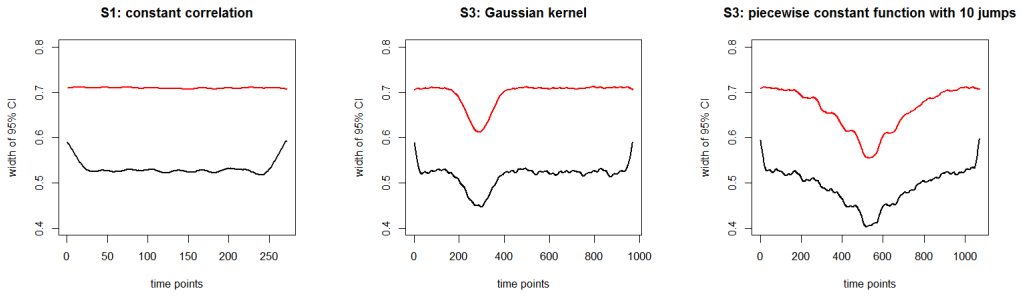

Figure 2.2: Average width of the time varying confidence interval for DCBootCB (black curve) and Fisher's approximation(red curve), when: the left panel - the true correlation coefficient equals zero(Scenario 1); the middle panel - the true correlation coefficient is Gaussian kernel–shaped (Scenario 3); the right panel - the true correlation coefficient is pyramid-shaped (Scenario 4).

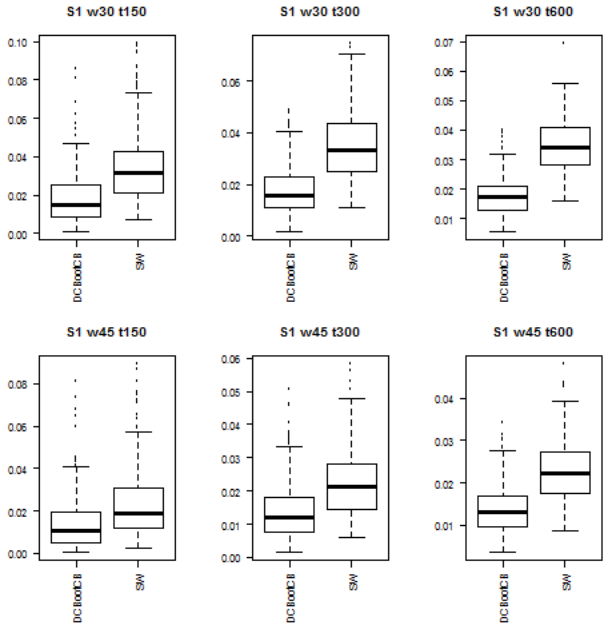

Figure 2.3: Boxplots of the MSE between estimated dFC and the true value of correlation for dFC calculated using DCBootCB algorithm and regular sliding-window technique for Scenario 1 - constant correlation across time.

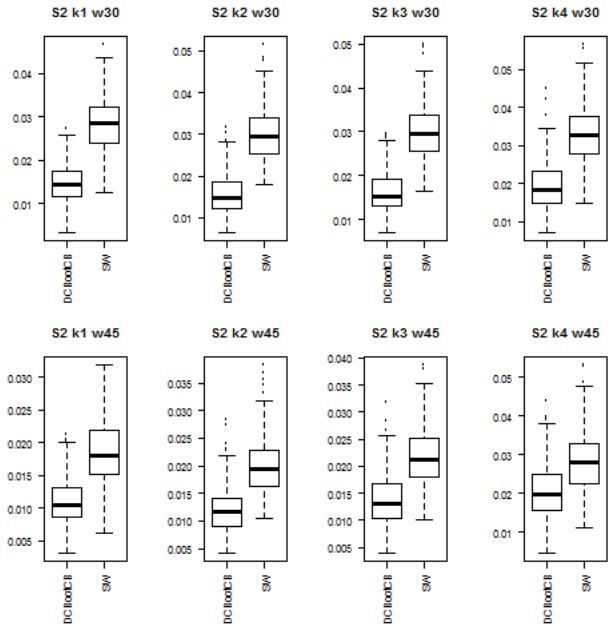

Figure 2.4: Boxplots of the MSE between estimated dFC and the true value of correlation for dFC calculated using DCBootCB algorithm and regular sliding-window technique for Scenario 2 - sine function.

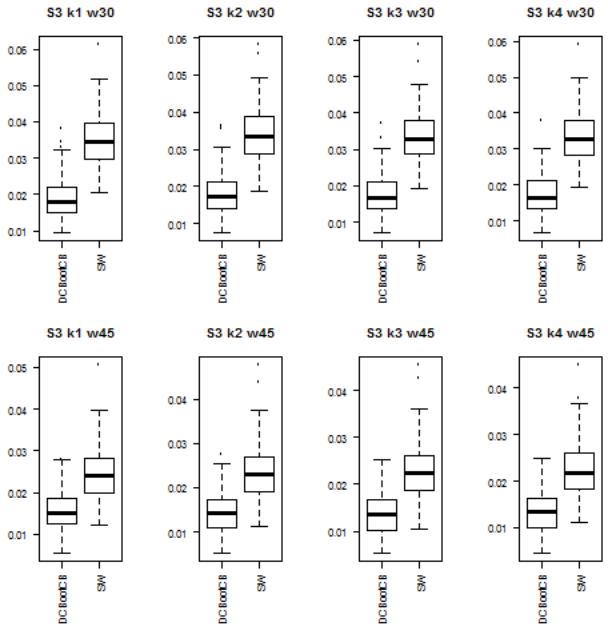

Figure 2.5: Boxplots of the MSE between estimated dFC and the true value of correlation for dFC calculated using DCBootCB algorithm and regular sliding-window technique for Scenario 3 - Gaussian kernel.

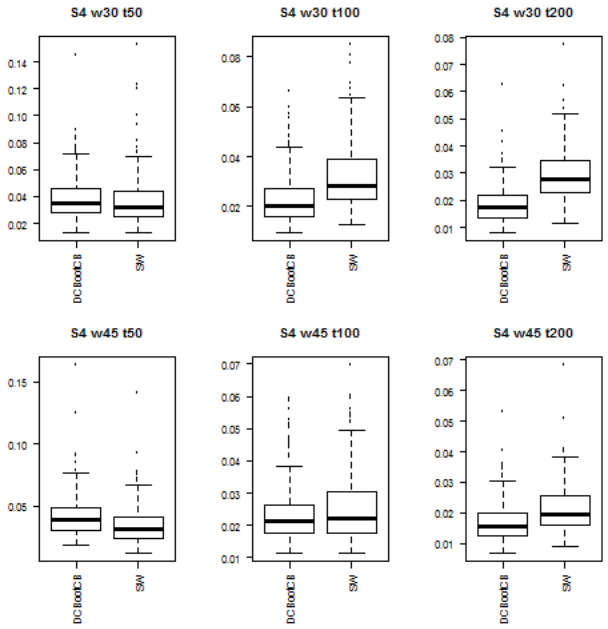

Figure 2.6: Boxplots of the MSE between estimated dFC and the true value of correlation for dFC calculated using DCBootCB algorithm and regular sliding-window technique for Scenario 4 - step-wise constant correlation across time.

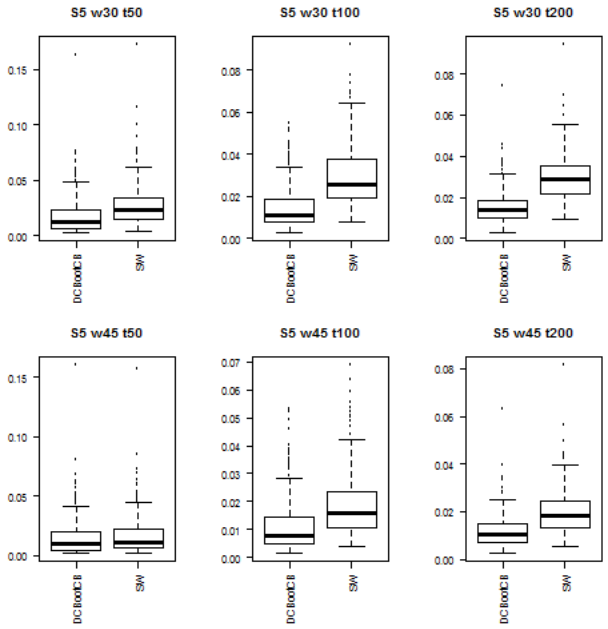

Figure 2.7: Boxplots of the MSE between estimated dFC and the true value of correlation for dFC calculated using DCBootCB algorithm and regular sliding-window technique for Scenario 5 - piecewise constant pyramid.

Kirby 21 data application

We applied the DCBootCB algorithm to the "Multimodal MRI Reproducibility Resource" study Landman, Huang, Gifford, Vikram, Lim, and et al. (Landman et al.), also known as the Kirby 21 dataset ($http://www.nitrc.org/projects/multimodal$). A detailed description of the study and data preprocessing steps can be found in Lindquist et al.Lindquist et al. (2014). Here, we use two repeated resting-state fMRI scans separated by a short break from 20 healthy adult volunteers. Each scan lasted 7 minutes resulting in 210 observations per subject per scanning session. Data was extracted from the six regions of interest defined in Chang and Glover Chang and Glover (2010), including the posterior cingulate cortex (PCC), the parietal cortex (Region 1), the frontal operculum (Region 2), the temporal cortex (Region 3), the orbitofrontal cortex (Region 4), and the anterior cingulate cortex (Region 5). The latter five regions were chosen due to the fact they showed high variability with the PCC during resting state. In Figure 2.8, we show examples of the original time series (left panels) and the dynamic connectivity estimates (right panels). The blue line depicts the estimate of dFC, the green line depicts the static correlation, and the red lines represent the confidence intervals. Specifically, we present the data from the PCC and the right interior frontal operculum for subject 2 during scan 2 and for subject 16 during scan 2, respectively. The dFC for subject 2 shows small changes across time, while the dFC for subject 16 shows higher variability across time.

To summarize the dynamic behavior of FC for each subject, region, and scan, we calculated the non-static coverage, which is the percentage of time when the confidence interval does not contain the static correlation. When the CI covers the static correlation there is less evidence that the correlation coefficient changes dynamically over time. The results are shown in Figure 2.9 for each subject, region, and scan. The non-static coverage in Figure 2.9

exhibits high variability across subjects, regions, and scans, indicating that the assumption of a static correlation is not viable.

In addition, we calculated the non-zero coverage(the proportion of the time points where the 95% CI does not contain zero), which indicates a significant association between two brain regions. Due to the dynamic nature of connectivity, the significance of association between two brain regions may vary across time. This property can be observed in Figure 2.10, where two heatmaps show the proportion of the non-zero coverage for each subject, region, and scan. For a number of pairwise associations, the value is high (dark blue) indicating that the assumption of a constant zero correlation is not appropriate. We also note high non-zero coverage variability across subjects, regions, and scans.

As a further illustration, we present results from the second scan for subjects 2 and 16 (see Figures 2.9 and 2.10). For subject 2, the non-static coverage between the PCC and each of the five other regions implied by a 95% CI is equal to 0%. This implies that a static correlation is sufficient to describe their associations. In contrast, the non-zero coverage is on average equal to 56% and varies between 22.10% and 98.9%. For example, the non-zero coverage between PCC and the right inferior frontal operculum (ROI2) is 47% and between PCC and the right inferior orbitofrontal cortex (ROI4) is 98.9%.

For subject 16, the results were quite different. Here the non-static coverage is on average equal to 18.3% and varies between 0% and 56.9%. For example, the non-static coverage between PCC and the right inferior frontal operculum (ROI2) is 56.9% and between PCC and the right inferior orbitofrontal cortex (ROI4) is 15.5%. Hence, a static correlation is not sufficient to describe the association between these two particular brain regions. The non-zero coverage is on average equal to 23.6% and varies between 0% and 48.6%. For example, the non-zero coverage between PCC and the right inferior frontal operculum (ROI2) is 47.5% and between PCC and the right inferior orbitofrontal cortex (ROI4) is 48.6%.

Application of DCBootCB to the Kirby 21 data set demonstrates that the estimated dynamic correlation is extremely variable and that providing only point estimates of the correlation can be misleading. Uncertainty estimation enables us to decrease the chance of making false positive statements about either non-zero association or static behavior of the connectivity.

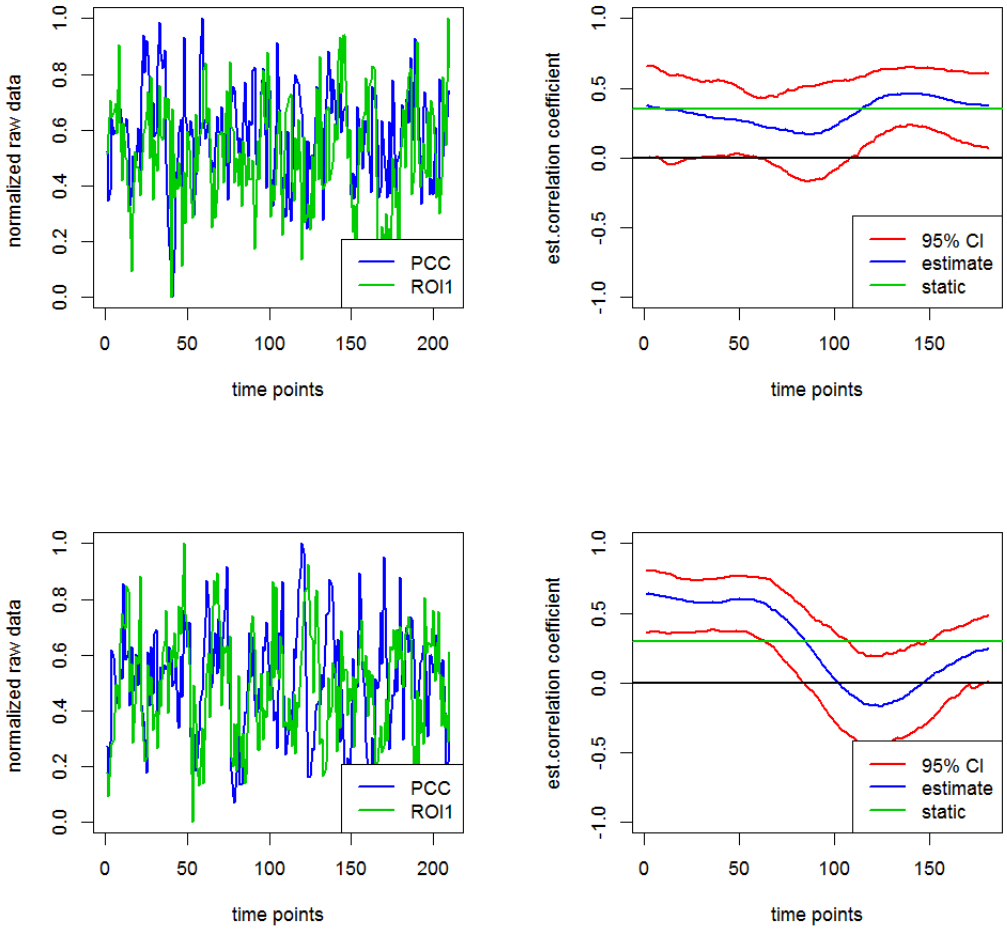

Figure 2.8: Left panels show raw time series and right panels estimated dynamic correlations between the PCC and the right interior parietal cortex for subject 2 undergoing scan 2 (small changes in FC) and for subject 16 undergoing scan 2 (large changes in FC). The green line on the right panel represents the static correlation.

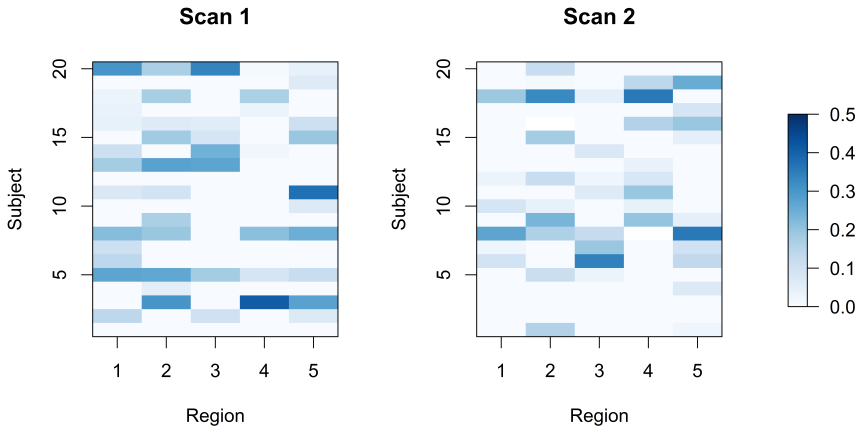

Figure 2.9: The proportion of the time interval where the dynamic correlation's 95% CI does not cover the static correlation between the PCC and 5 ROIs for each subject, region and scan.

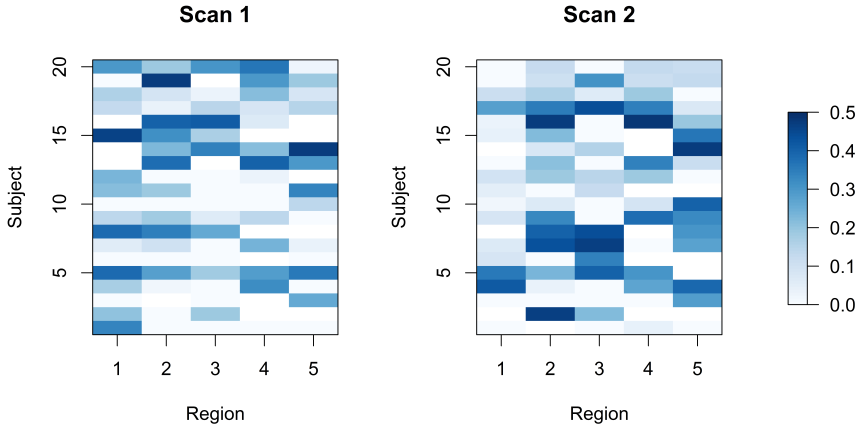

Figure 2.10: The proportion of the time interval where the dynamic correlation's 95% CI does not cover the zero correlation between the PCC and 5 ROIs for each subject, region and scan.

Discussion

The most common approach towards assessing the dynamic nature of FC has been the sliding-window technique. In this paper, we studied the properties of this method. Our main contribution was to introduce a method for obtaining non-parametric estimation of the confidence bands for the dynamically changing correlation coefficient. To do so, we utilized the MLPB method, which was designed specifically to generate valid bootstrap samples for multivariate correlated time series. We computed the confidence intervals to determine if there was evidence of a time-varying statistical association between two brain regions and to provide a summary measure of the degree to which it varies. To the best of our knowledge, such an approach has never been implemented in a study of connectivity using fMRI data.

The DCBootCB method requires specification of three tuning parameters: (1) the number of sampling points used for the correlation estimation; (2) the size of the smoothing window; and (3) the width of the adjacent blocks in the bootstrap algorithm. We based our choice of the sliding-window size on published empirical results. The most common width of the window was either 30 or 45 time points, and it has been shown that application of the much larger window length does not appropriately capture the dynamically changing signal. Similarly, the smoothing window size was selected to be 30 time points. The width of the adjacent blocks was equal to 30 time points in the bootstrap algorithm to guarantee the stability of the covariance matrix estimation. In future work, we will explore the effect of different block sizes.

In a series of simulation studies, we showed that the proposed confidence bands behave well. We considered situations of no association between the two time-series, gradually changing association, and step-wise constant association. Our simulation results lead us to conclude that the MLPB approach to bootstrapping correlated time series provides a valid

model-free, time-varying connectivity estimates together with associated confidence bands. We showed that point estimates for the correlation coefficient alone are not sufficient to assess connectivity, and it is necessary to also include uncertainty measures. In addition, our simulation studies show that the theoretical results are supported by empirical evidence. It is expected that when the correlation goes up, the width of confidence intervals will get narrower.

We compared confidence bands obtained by the DCBootCB algorithm with the Fisher asymptotic results. The precision of coverage of a true correlation coefficient was much better for the DCBootCB algorithm. We found that the Fisher asymptotic approximation tends to overestimate the coverage of confidence bands for dynamically changing correlation. The proposed algorithm has some difficulties with discontinuous functions. This is illustrated in simulation Scenarios 4 and 5. The main problem appears on the boundaries between the step-wise constant pieces. Even though this is a limitation of the DCBootCB algorithm, in practice, resting state dynamic correlation tends to change gradually, which was mimicked in simulation Scenarios 2 and 3.

We applied the DCBootCB algorithm to the Kirby-21 resting state data. We focused on assessing dynamic correlation between the PCC located in the default-mode network, and 5 ROIs known from the literature to display a high degree of variability with the PCC across time. On the one hand, results obtained in the analysis of the Kirby-21 data confirmed the high variability between regions and subjects in the same scan. On the other hand, we found high variability between scans performed on the same subject casting doubt on the reproducibility of the intra-subject dynamic correlation patterns.

In conclusion, we addressed one of the main issues associated with applying the sliding-window technique to estimate functional connectivity – the lack of assessment of uncertainty. Unfortunately, much of the functional connectivity research is focused exclusively

on the connectivity estimation without proper confidence band estimation. The introduced DCBootCB algorithm provides a mechanism to estimate the uncertainty using confidence bands that are not readily available in other cases. We also showed in a simulation study that the properties of the proposed algorithm are better in terms of coverage than Fisher's asymptotic approach.

Chapter 3

Semiparametric estimation of task-based dynamic functional connectivity on the population level

Dynamic functional connectivity (dFC) is a recent extension of static functional connectivity (FC) analyses. dFC permits time-dependent associations between time series of two brain regions typically acquired with functional MRI. dFC changes are most commonly quantified by the pairwise correlation coefficients between the time series within a sliding window of 30-60 measurements. Here, we apply a recently developed bootstrap-based technique (Kudela et al. (2017)) to robustly estimate subject-level dFC with its confidence intervals in a task-based fMRI study (24 subjects tasting their preferred beer and Gatorade as an appetitive control). Semiparametric mixed models combined information across subjects and scans to obtain a population-level dFC estimate for each pair of brain regions, flavor, and difference of flavors. As a summary dFC metric, we used the proportion of time points when associations were either significantly positive or negative. For both flavors, dFC analysis yielded regional associations closely resembling the resting state networks. Reward-related ventral striatal (VST), lateral orbitofrontal, and ventral anterior insula (vAI) regions were positively associated during beer. The enhancement of right VST-vAI association by beer independently validated the main activation-based finding (Oberlin et al. (2016)). Most notably, dFC uncovered numerous associations undetected by the traditional static FC analysis.

Introduction

One of the recent interests in functional magnetic resonance imaging (fMRI) is the assessment of dynamic functional connectivity (dFC), estimated by finding the time-varying association between time series of two brain regions, most often using functional magnetic resonance imaging (fMRI). Recently, a growing consensus in the neuroimaging field is that

summarizing FC as a constant measure over time (i.e., a static metric) is not sufficient to gain an understanding of brain networks properties Calhoun et al. (2013).). It has been demonstrated that brain activity changes are non-stationary regardless whether the study is task-based or task-free (Allen et al. (2012); Cribben et al. (2012); Debener et al. (2006); Doucet et al. (2012); Sadaghiani et al. (2009)). This interest in dFC is primarily driven by the idea that many psychiatric and behavioral disorders as well as neurodegenerative diseases might impact the time dependence of functional connectivity. The strength of association between brain regions might be higher or lower amongst different subject groups, return to the resting baseline at different rates, and differ in the extent to which some networks (de)-synchronize. A number of studies describe associations between the changes in connectivity and various diseases (see e.g. Filippini et al. (2009)),) including Alzheimer's disease (Jones et al. (2012))) and autism (Starck et al. (2013)). For example, disease-specific changes in dFC were found for patients with schizophrenia, a disease which lacks a straightforward diagnostic test (Jones et al. (2012); Sakoğlu et al. (2010)). As noted by Calhoun et al. (2013), such results pose an interesting prospect for a future interpretation of time-varying characteristics of dFC as a disease biomarker. Many studies focus solely on estimating dFC in a resting state where subjects are imaged while lying still and not performing any tasks (Turk-Browne (2013)). These experiments laid the groundwork for describing how brain regions group into distinct functional networks Beckmann et al. (2005); Fox et al. (2005); Greicius et al. (2003). However, the results from resting state studies only partially answer the question of how networks communicate (Turk-Browne (2013)). In a task-based study, dFC offers unique insights into a behavior of the brain networks during a stimulation targeted to probe a specific disorder or disease. Our current research is motivated by an interest in alcoholism risk. With that in mind, we selected a task-based fMRI sample of social-to-heavy alcohol drinkers during stimulation with beer and Gatorade®

flavor. The goal of this work is to estimate the time-varying FC and its confidence intervals for each flavor and their difference. Unlike other approaches, our implementation is performed from the whole brain perspective and on the group-level. Here, we propose a two-step approach . In the first step, we apply a recently developed bootstrap-based approach (Kudela et al. (2017)), which utilizes multivariate linear process bootstrap and the sliding window technique, to obtain the time-varying association among 278 functionally defined brain regions (Shen et al. (2013)) at a subject level. As a result, we obtain a smooth trajectory and its confidence interval for 38,503 pairwise time-varying associations for each subject and scan. Then, in the second step, these subject specific estimates of dFC are used as an outcome in the semiparametric additive mixed model (Ruppert et al. (2003)) to estimate a flavor-specific population-level dFC for each pairwise combination of brain regions. Such an approach can handle the complex correlation structure of the data and allows us to combine the information across subjects to obtain a population level estimate of time-varying association and its confidence intervals for each flavor and flavor difference. In addition, we propose steps to summarize the result from 38,503 population level pairwise associations for each flavor and difference between flavors by calculating the positive and negative non-zero coverage, which is the proportion of time the 95% confidence interval (CI) of a dFC curve does not contain zero and is greater or less than zero. The proposed approach is applicable to different types of time series data. In the literature, the methods to analyze dFC were primarily validated and are most commonly implemented in resting state studies. One of the most popular methods is based on the sliding window approach, in which the window of pre-selected size is slid across time to calculate the FC measure based on the observations contained within the window, but as shown in Kudela et al. 2017Kudela et al. (2017), such an approach does not provide confidence intervals. Measures such as a time-frequency coherence analysis with wavelet transforms (Chang and Glover

(2010)), an independent component analysis (Kiviniemi et al. (2011)), and a correlation analysis (Hutchison et al. (2013)) have also been used to study the properties of dynamic resting-state connectivity.

A number of recently published studies considered a whole-brain network analysis. For example, a data-driven method based on a higher-order singular value decomposition was proposed by Leonardi and Van De Ville (2015) to estimate whole brain networks from a group-level time-varying FC. Another popular approach is utilizing a group independent component analysis (Calhoun et al. (2001)). This method allows assigning multi-subject resting-state data into functional brain regions and then applies the sliding-window and k-means clustering methods to study whole brain time-varying networks (Allen et al. (2012); Handwerker et al. (2012); Jones et al. (2012); Sakoğlu et al. (2010)). Another popular class of methods is based on change-point detection (Cribben and Yu (2016)). Advantages of the proposed approach, compared to other methods, is that it allows accounting for multiple repeated observations per subject, experimental design , as well as subject-specific variability. It is a completely data-driven approach within a simple computational framework for complex data. In addition, the proposed approach yields condition-specific dFC and confidence intervals for the whole brain at the group level. The remainder of this work is organized as follows. Section 3.2 describes the fMRI study sample, experimental design, and image acquisition preprocessing steps. Statistical methods to estimate subject–specific and population level dFC are detailed in Section 3.3. The results are presented in Section 3.4 while Section 3.5 offers a discussion.

Study description

Experimental design

Subjects. All subjects who participated in the study were recruited from the local community. All experimental procedures were approved by the Indiana University Institutional

Review Board, and all subjects signed an informed consent prior to the study. All 24 subjects were male beer drinkers with a range of recent drinking ranging from social to heavy. They were right-handed and in good self-reported physical and mental health. The beer was reported as one of their two most-often consumed alcoholic beverages. Demographic and study-specific characteristics of the participants are summarized in Table 3.1. Specific exclusion criteria and a more detailed description of the study is provided in Oberlin et al. (2016).

	Mean ± (SD)	Range	N(%)
Age	24 (2.3)	21-28	
Caucasian	–	–	24 (100%)
Education	15.8	(1.4)	12-19
% with at least one first degree relative w/AUD			7 (29%)
Drinks per week	14.9 (9.9)	2-33	
Drinks per drinking day	4.9 (3.0)	1-10	
Heavy drinking days per week	1.6 (1.4)	0-6	
AUDIT	10.2 (6.3)	3-26	

Table 3.1: Subject Characteristics.

Experimental design. The design of this task-based fMRI study is illustrated in 3.1. Specifically, cue reactivity of reward regions to the flavors of each subject's most commonly consumed brand of beer ("B") and Gatorade®("**G**") were assessed. Gatorade was chosen as the appetitive flavor control as its flavor intensity is similar to beer (see Oberlin et al. (2013, 2015)) were assessed. These flavors were delivered in ∼1-sec sprays (trials) on subjects' tongues, and were interspersed with neutral water ("**w**"; flavorless sensory baseline). Subjects completed six fMRI scans, with beer and Gatorade scans alternating (see Figure 3.1). In each scan, three flavor epochs (4 trials each) were interspersed with 4 water epochs (3 trials each) resulting in 12 flavor and 12 water trials with a fixed 11-sec inter-trial interval.

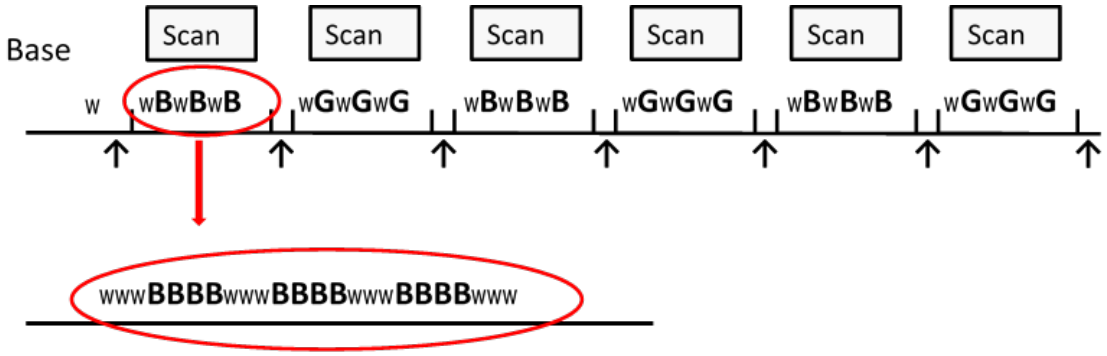

Figure 3.1: Experimental design. **B** denotes beer, **G** denotes Gatorade and **w** denotes water. Detailed sequence of stimulation trials during one scan is denoted by red ellipses.

Imaging Procedures and Analysis

Image Acquisition. Imaging was performed on a Siemens 3T Magnetom Trio-Tim (Erlangen, Germany) scanner using a 12-channel head coil array. Functional imaging volumes were positioned on a high resolution ($1.0 \times 1.0 \times 1.2$ mm^3 voxels) anatomic volume acquired with a 3D magnetization prepared rapid gradient echo (MPRAGE) sequence. Functional data were acquired with a blood oxygenation level dependent (BOLD) contrast sensitive pulse sequence (echo planar imaging, gradient echo, 125 volumes, repetition/echo time 2250/29 ms, flip angle 78°, field of view 220 × 220 mm, 39 interleaved 3-mm thick axial slices, $2.5 \times 2.5 \times 3.0$ mm^3 voxels, GRAPPA acceleration factor 2). Head movement and motion-related artifacts were minimized using deformable foam pads on both sides of the participant's head and a real-time three-dimensional prospective acquisition correction algorithm Thesen et al. (2000).

Imaging Processing. An FSL-based preprocessing pipeline implemented within Matlab generally followed the Human Connectome Project guidelines (Smith et al. (2013)) as detailed in (Amico et al. (2016); Contreras et al. (2016)). Templates and atlases included with FSL as well as cortical and subcortical parcellations of interest were brought from

Montreal Neurological Institute (MNI) space and resliced to match the native BOLD EPI space resolution. T1-weighted MPRAGE volumes were denoised (Coupé et al. (2010, 2008)), prior to brain masking and extraction (FSL "bet") and then nonlinearly transformed (FSL's FLIRT and FNIRT) to the MNI brain template, which also yielded tissue segmentation. The inverse MNI-to-native transformation then allowed cortical (Shen et al. (2013)) and subcortical (Patenaude et al. (2011)) parcellations to be applied in native BOLD data space. Pre-processing included slice timing correction, motion correction, registration to T1, detrending, band pass filtering (0.009-0.08 Hz), and normalization to mode 1000 (Smith et al. (2013)). Head motion systematically alters correlations in functional connectivity (FC) data so following the methodology proposed by Power et al. (Power et al. (2014, 2015)), motion regressors from the realignment and their derivatives were regressed out. We also used three image quality control measures (framewise displacement, DVARS and whole-brain standard deviation) to tag and scrub outlier FC data. Of the initial 29 subjects, 5 were excluded because one or more of their six BOLD scans contained excessive ($> 40\%$) fraction of BOLD volume outliers, resulting in the final 24 subject sample. Finally, we also addressed confounding effects of physiologic noise and residual head motion by regressing out signals in various tissue compartments. This procedure relied on eroded masks in the whole-brain gray matter, white matter, cerebrospinal fluid of the third ventricle and included global signal regression. Commonly, the tissue regressor step uses only the mean signal from each tissue type, but in our experience, regressing 3 to 5 PCA components in a later step (Chai et al. (2012); Power et al. (2015))), better accounts for various noise sources and generates cleaner single scan connectivity matrices. The PCA regression step was performed after the band-pass filtering so that all principal components regressed out would be within the frequency range of interest.

FC Data Analysis.The FC pipeline automatically parcellated cortical and subcortical gray matter of each subject into 278 regions of interest (ROI), as defined by a meta-analysis of resting state fMRI data (Shen et al. (2013)). Each cortical ROI was assigned to one of the seven resting state networks (RSNs) reported by (Yeo et al. (2011)) as based on the resting state fMRI study of 1000 healthy volunteers (see Figure 3.2, top). To better visualize network organization of all 278 regions, we assigned non-cortical brain regions to either a subcortical or cerebellar network. However, the BOLD volume coverage was optimized for the cortex and excluded the most inferior aspects of the cerebellum in many subjects. Therefore, no statistical inferences were made for the cerebellar regions.

Regions of Interest. The investigations of the whole brain, pairwise associations allow a comprehensive and unique perspective on the brain's response during resting-state and task -based experiments (Bolt et al. (2017)). In this study, we applied a whole-brain approach to first evaluate whether dFC in the gustatory task fMRI comported with the canonical RSNs of (Yeo et al. (2011)). In the next step, we focused on a subset of a *priori* selected regions from (Oberlin et al. (2016)) that: 1) responded to the flavors of beer and Gatorade and, 2) showed differential flavor responses. Despite large methodological differences, data-driven dFC and general linear model (GLM)-based "activation" approach should both show flavor responses in a large network of sensorimotor regions, gustatory cortex (area "G" in the insula/opercular areas), amygdala and caudate nucleus. It should be noted that GLM-based flavor effects are relative to the water baseline (Tables S1 and S2, Oberlin et al. (2016)), while dFC results incorporate water trials and would be more analogous to the "implicit baseline" (i.e., resting brain) comparison. Regardless of the methodology, it is reasonable to hypothesize differential flavor responses in frontal and striatal areas implicated in the alcohol cue response (Table 2, Oberlin et al. (2016)). While reward and associative regions such as ventral striatum (VST) and orbitofrontal cortex

(OFC) are our primary focus, areas assigning stimulus salience such as dorsal anterior cingulate cortex (dACC) and insula (Uddin (2015)) are also expected to differentiate beer and Gatorade stimuli. The lateral frontal regions involved in inhibitory control (Congdon et al. (2010))and known to be affected in a population at risk for alcohol abuse (Kareken et al. (2013)) are also of interest. Finally, when individuals are at quiet "rest", the default mode network (DMN; Greicius et al. (2003)) becomes more prominent (Buckner et al. (2008)), while networks active during cognitive/attentional engagement (e.g., the fronto-parietal (FP) network) become less active. The DMN and FP networks tend to be negatively correlated in the healthy brain, while hyper-connectivity of the DMN and networks serving attention and working memory is reported in other types of psychopathology, including depression and schizophrenia (Whitfield-Gabrieli and Ford (2012)).The increased interaction of the DMN and FP networks during beer flavor stimulation would suggest an increased risk for alcoholism.

In order to investigate the whole brain associations as well as the association between our regions of interest and resting state networks, in the following sections, we present a detailed overview of the statistical approach and summarize our dFC results.

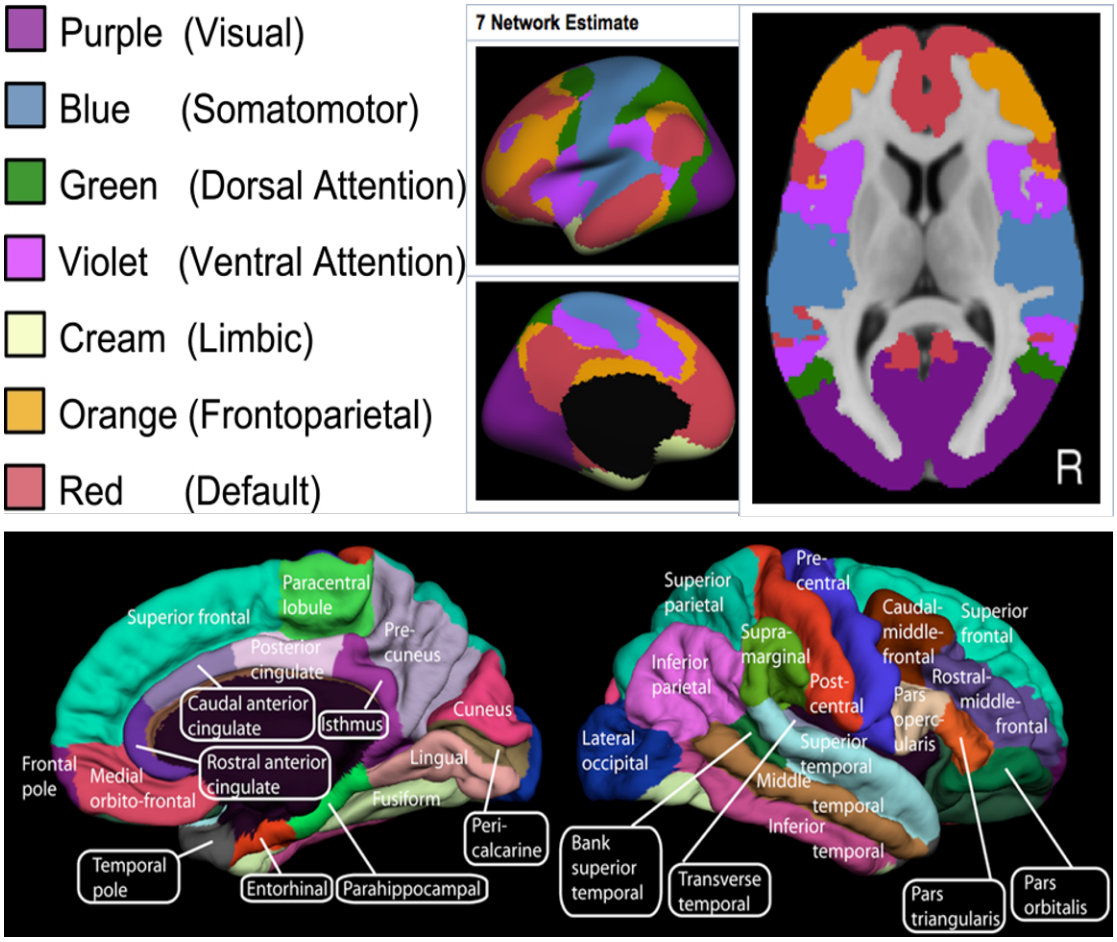

Figure 3.2: Upper panel: Visualization of the seven cortical resting state networks proposed by Yeo et al. (2011)(source: Yeo et al. (2011)). Lower panel: Visualization of the major medial and lateral anatomical subregions. The left and right insula are not depicted (source: Hagmann et al. (2008)).

Statistical methods

The goal of this work was to estimate the population level dFC across time for both flavors and their difference for all pairwise ROI associations. We implemented this by: 1) estimating pairwise ROIs associations at a subject level and, 2) combining the information across subjects and flavor-specific scans to model a population-averaged dynamically changing association for each flavor and a pair of regions. Below we present each step in more detail.

Subject-level pairwise estimation

The dFC and its confidence intervals between all pairs of brain regions for each scan were estimated at a subject level by applying a recently established technique (Kudela et al. (2017)) using: 1) the Multivariate Linear Process Bootstrap (MLPB) - a specialized bootstrap method applicable to bootstrapping time series data (Jentsch et al. (2015)), and 2) the sliding window correlation estimate. We briefly describe the approach here. For each subject and pair of regions, we divided the time-series into adjacent blocks and used the data within each block to generate bivariate time series bootstrap samples by using the MLPB. We then combined the bootstrap samples across adjacent blocks to create a bootstrap realization of a bivariate time series. Next, for a given sliding window and bootstrap realization of time series for a given pair of regions, we used the data within the window to calculate the Pearson's correlation coefficient. The sliding window was moved by one time point at a time and the correlation coefficient was calculated within each such window. The whole procedure was repeated 250 times creating a set of bootstrap samples and time-varying estimates of FC for each pair of regions. By using the quantiles of a set of time-varying estimates of correlation, we estimated dFC using the median and its confidence interval via $\frac{\alpha}{2}$ and $(1-\frac{\alpha}{2})$ quantiles for the $(1-\alpha)*100\%$ CI for all pairs of regions in each subject and scan. Further details can be found in Kudela et al. (2017).

Population-level estimation

We treated scan-specific realizations for a selected flavor as repeated measurements. The most common method to analyze such data is a linear mixed model approach. Such models work well when the linearity assumption is satisfied. However, when the response variable is a non-linear function of time, more flexible non-parametric approaches such as penalized splines should be considered. Figure 3.3 depicts an example of an estimated dFC for a pair of regions for each subject and scan illustrating high within- as well as between-subject variability. In this example, a simple linear mixed model approach describes the association poorly. Assuming any parametric shape, common across all scans, is not appropriate. Rather, we need to model the population level dFC in a smooth, nonparametric way. There are many applicable nonparametric methods, but only some can account for multiple repeated observations per subject and the experimental design to properly address the variability and complex correlation structure of the data. Therefore, we applied the penalized splines within the framework of semiparametric additive mixed effects models. One of the advantages of this approach is that it is easily extendable and can accommodate the study design by taking into account scan-, subject-, and task-specific variability. This method also successfully addresses the implementation in a large data sample with a population level estimate of 38,503 curves ($278 * 279/2 - 278$) for each flavor and the difference between flavors. the penalized splines estimator of the model and the best linear unbiased estimator of mixed models (Brumback et al. (1999); Durbán et al. (2005))), we can use software already developed for mixed model analysis that provides a simple implementation for complex problems.

Application of this approach allows us to combine the information across subjects and obtain a population level estimate of time-varying association and its confidence intervals for each flavor and a pair of regions. As a byproduct of this approach, we also obtain a

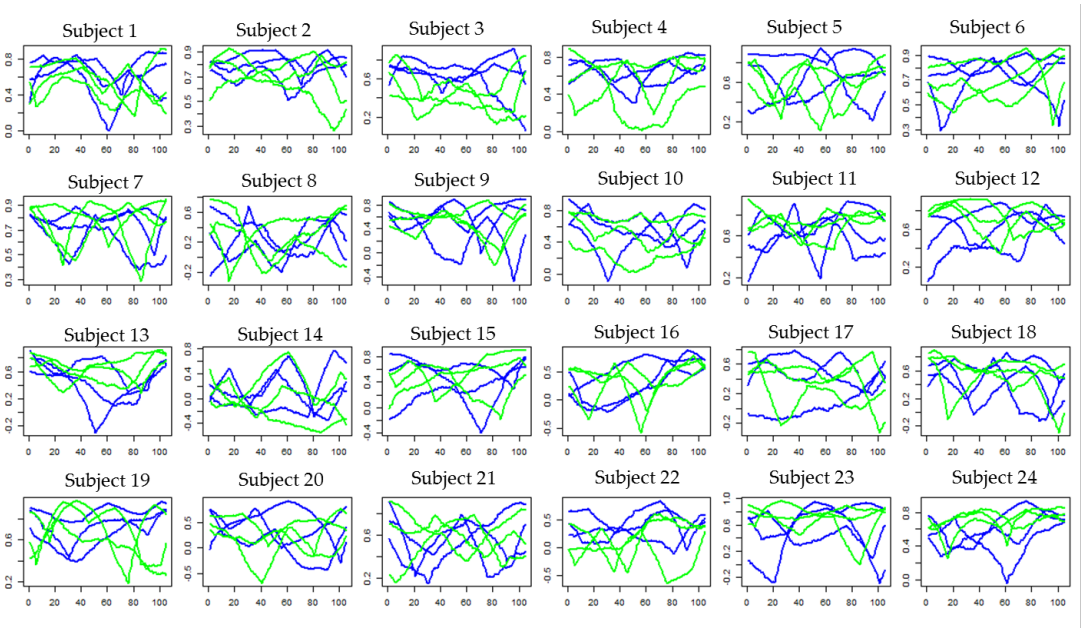

Figure 3.3: Dynamic functional connectivity between the left and the right somatomotor cortical (Shen ROI IDs roi 34 and 154) regions for three beer scans (blue curves) and three Gatorade scans (green curves) in 24 subjects.

population level time-varying difference between two flavors and its confidence intervals. The details of our statistical model are presented below.

The general form of the proposed model can be expressed as: $dFC_{ijd} = f_d(t_j) + g_{id} + \varepsilon_{ijd}$, where a response variable dFC_{ijd} is the estimated dynamic FC for each subject i ($i = 1, \ldots, 24$); time point j denoted by $t_j = 1, \ldots, 105$ (identical for all subjects, with the first 10 and the last 10 time points dropped to accommodate the sliding window approach); and flavor d (d=B or G;for beer or Gatorade, respectively). We assume that the measurement error, ε_{ijd}, is normally distributed $N(0, \sigma_\varepsilon^2)$; $f_d\ (t_j\ )$ is the group-average curve representing the shape of dFC for flavor d; g_{id} is the subject-specific deviation from the group-average curve for flavor d. Informed by the study design, we assumed that g_{id} is a sum of two random effects: subject-specific intercept, b_{i0} and nested within-subject random scan effect,

a_{iS0} where b_{i0} $N(0, \sigma^2_{(b_0)})$, a_{iS0} $N(0, \sigma^2_{(a_0)})$ and S denotes a scan number. The inclusion of the nested within-subject random scan effect accounts for the study design.

We started with a simple model where the association between a pair of brain regions is assumed to be constant across time. The assumption of a static association is most commonly used in functional connectivity studies. In such a case, the flavor specific population level estimates are modeled as: 1) $f_B(t) = \beta_0$ for beer, 2) $f_G(t) = \beta_0 + \gamma_0$ for Gatorade. As a byproduct of this approach, we obtain the difference between flavors as $c(t) = f_G(t) - f_B(t) = \gamma_0$.

In the second model, we assumed that the dFC can vary non-linearly across time by using the aforementioned penalized splines approach within the framework of semiparametric additive mixed effects models. In a penalized spline approach, the outcome variable is modeled as a linear combination of basis functions $z_k(t)$ that can be expressed as $y = f(t) + \epsilon = \beta_0 + \beta_1 t + \sum_{k=1}^{K} u_k z_k(t) + \epsilon$. The parameters are then estimated by minimizing the criterion $min \sum_{i=1}^{n} (y_i - f(t_i))^2 + \lambda \sum_{k=1}^{K} u_k^2$ Ruppert et al. (2003). The design matrix for penalized splines is expressed as $\mathbf{X}_i = \begin{bmatrix} 1 & t_1 & z_1(t_1) & \dots & z_k(t_1) \\ \vdots & \vdots & \vdots & \ddots & \vdots \\ 1 & t_{105} & z_1(t_{105}) & \dots & z_k(t_{105}) \end{bmatrix}$. After decomposing the design matrix into $\mathbf{X}_i = \begin{bmatrix} 1 & t_1 \\ \vdots & \vdots \\ 1 & t_{105} \end{bmatrix}$ and $\mathbf{X}_i = \begin{bmatrix} z_1(t_1) & \dots & z_k(t_1) \\ \vdots & \ddots & \vdots \\ z_1(t_{105}) & \dots & z_k(t_{105}) \end{bmatrix}$, one can represent the penalized splines in terms of mixed models as follows: $\mathbf{y}_i = \mathbf{X}_i\beta + \mathbf{Z}\mathbf{u} + \epsilon_i$, where $\mathbf{u} = [u_1, \dots, u_k]^\top$ are treated as random effects that follow normal distribution $N(0, \sigma^2_u)$. The smoothing parameter λ is then estimated as $\frac{\sigma^2_\epsilon}{\sigma^2_u}$. The use of penalized splines within the framework of mixed models is detailed in Ruppert et al. (2003).

In our analysis, we use penalized splines to estimate flavor-specific population level dFC and as a byproduct also obtain the difference between flavors. We define a set of knots $\kappa_1, \dots, \kappa_K$ according to quantiles across the time domain and set the number of knots K to 40 to allow the dFC function to change non-linearly. Main advantage of penalized splines is that due to a penalty imposed on spline basis coefficients, it is less sensitive to the

choice of location and the number of knots (Ruppert et al. (2003)). If there are too many knots (risk of overfitting), the unnecessary coefficients will be shrunk towards zero. Here, we used O'Sullivan penalized splines (Wand and Ormerod (2008)) due to their appealing properties including smoothness, numerical stability, natural boundary properties, and a direct generalization of smoothing splines.

By using methods defined above, we can now model the population-level estimate of dFC as: 1) $f_B(t) = \beta_0 + \beta_1 t + \sum_{k=1}^{K} u_k z_k(t)$ for beer, 2) $f_G(t) = \beta_0 + \gamma_0 + (\beta_1 + \gamma_1)t + \sum_{k=1}^{K} u_k z_k(t) + \sum_{k=1}^{K} w_k z_k(t)$ for Gatorade. With this flavor-specific function representation, the difference between the flavors can be expressed as $c(t) = f_G(t) - f_B(t) = \gamma_0 + \gamma_1 t + \sum_{k=1}^{K^\star} w_k z_k(t)$, where $z_k(t)$ are the O'Sullivan spline basis functions. By treating β_0,β_1,γ_0,γ_1 as parameters for a fixed design matrix and by inserting the value of O'Sullivan basis functions into a random design matrix, it becomes possible to use linear mixed models to estimate the coefficients in the penalized spline model. u_k,w_k are then treated as random effects, which follow $N(0, \sigma_u^2)$ and $N(0, \sigma_w^2)$, respectively. Both models are summarized in Table 3.2.

	beer $f_{w=B}(t)$	Gatorade $f_{w=G}(t)$	g_{iw}
Model 1	β_0	$\beta_0 + \gamma_0$	$b_{i0} + a_{is0}$
Model 2	$\beta_0 + \beta_1 t + \sum_{k=1}^{K} u_k z_k(t)$	$\beta_0 + \gamma_0 + (\beta_1 + \gamma_1)t + \sum_{k=1}^{K} u_k z_k(t) + \sum_{k=1}^{K^\star} w_k z_k(t)$	$b_{i0} + a_{is0}$

Table 3.2: Models estimating dFC for the two flavors and their difference.

Multiple comparison correction

In our study, we calculated population-level pairwise correlations between 278 brain regions, yielding $38,503 (= 278 \star \frac{279}{2} - 278)$ estimates and confidence intervals for flavor specific curves and differences between flavors. We also investigated if the pairwise associations are statistically significant. To account for multiple comparison, we applied a commonly used false discovery rate (FDR) correction developed by Benjamini and Yekutieli (2001). FDR controls the proportion of false positives among all significant tests. We compared our results with a more stringent family-wise error rate (FWER) correction, which controls

the probability of any false positives appearing in results (Bretz et al. (2011)). As shown in the results section, the number of significant associations is similar for both methods.

Results

In the following section, we summarize the results for each model.

Model 1

Since the number of pairwise associations is large, we applied FDR-based t-statistic threshold for model parameters β_0 and γ_0 and presented the result in the form of a matrix, where rows and columns represent brain regions and each matrix element is a thresholded t-statistic value. β_0 can be interpreted as a mean dFC across time for beer flavor and γ_0 as a mean dFC across time for a difference between Gatorade and beer flavors.

Figure 3.4 illustrates mean dFC across time for the beer flavor, with brain regions organized according to the seven cortical networks from (Yeo et al. (2011)), with two additional network blocks comprised of subcortical and cerebellar regions. The lower triangular matrix elements include thresholded negative or positive t-statistic values for dFC estimates between pairs of regions. The upper triangular elements summarize the percentage of significant associations within each pair of networks. The diagonal elements illustrate dFC between regions from the same network ("within-network"), while non-diagonal elements represent interactions of regions from different brain networks ("between-network"). For clarity, we separated the summary matrix into negative-only (Figure 3.5, left) and positive-only parts (Figure 3.5, rightleft); i.e., positive mean dFC across time and negative mean dFC across time, respectively. Most of the significant negative associations occur between networks. Such patterns of interactions between the default mode, somatomotor, dorsal and ventral attention networks is less evident in the resting state networks (RSN), whether using 7 or 17 cortical network solutions reported in the Yeo study. Positive significant associations tended to be between regions in the same network. For example 80% of associations

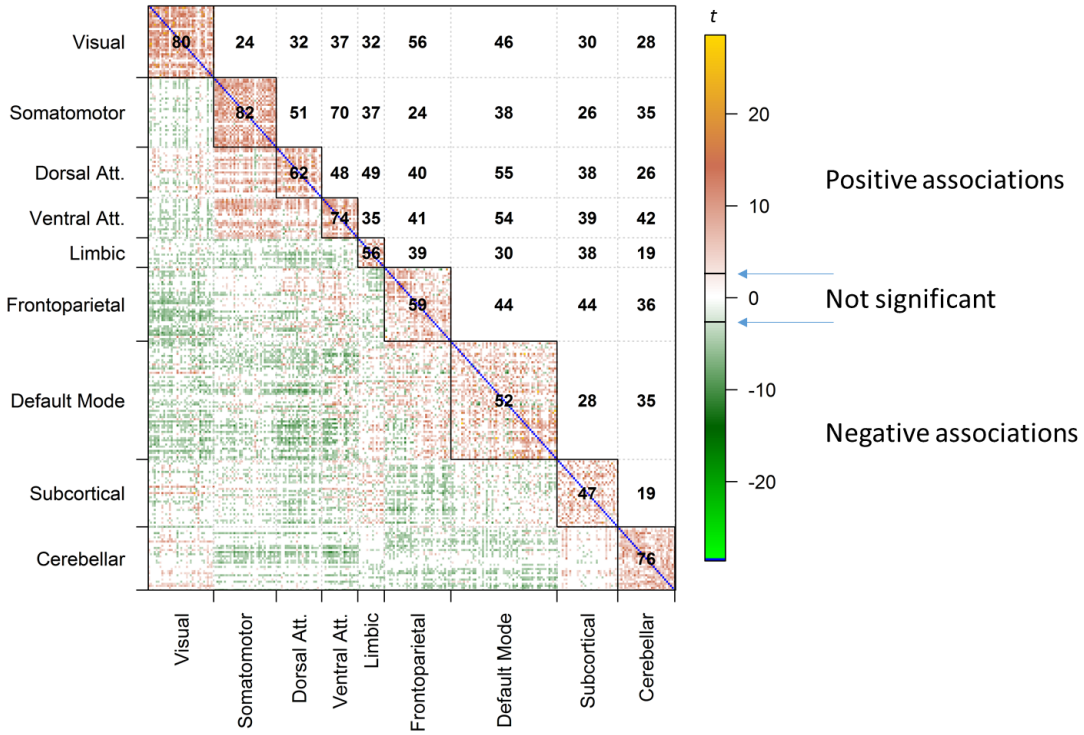

Figure 3.4: A matrix of significant associations for beer assuming static FC. FDR-corrected t-statistic values for β_0 in the simple model (model 1) are shown for all pairwise correlations (below diagonal) and percentage of significant pairwise ROI correlations within- and between- each network (on and above diagonal, respectively). Color bars denote the values of the t statistic.

for pairs of regions from the visual network were significant, indicating positive dFC across time within that network. In fact, these averaged dFC patterns of within-network regions comport with the resting state networks previously observed by (Yeo et al. (2011)) suggesting functionally based brain organization common to resting and task-based data. Figure 3.6 depicts the mean dFC across time of pairwise associations for the flavor difference (γ_0 in the model) with positive and a negative parts shown in Figure 3.7. No associations were significant after adjusting for multiple comparisons. The values presented in Figure 3.6 and Figure 3.7 are uncorrected (i.e., thresholded using a single test assumption). Unlike dFC

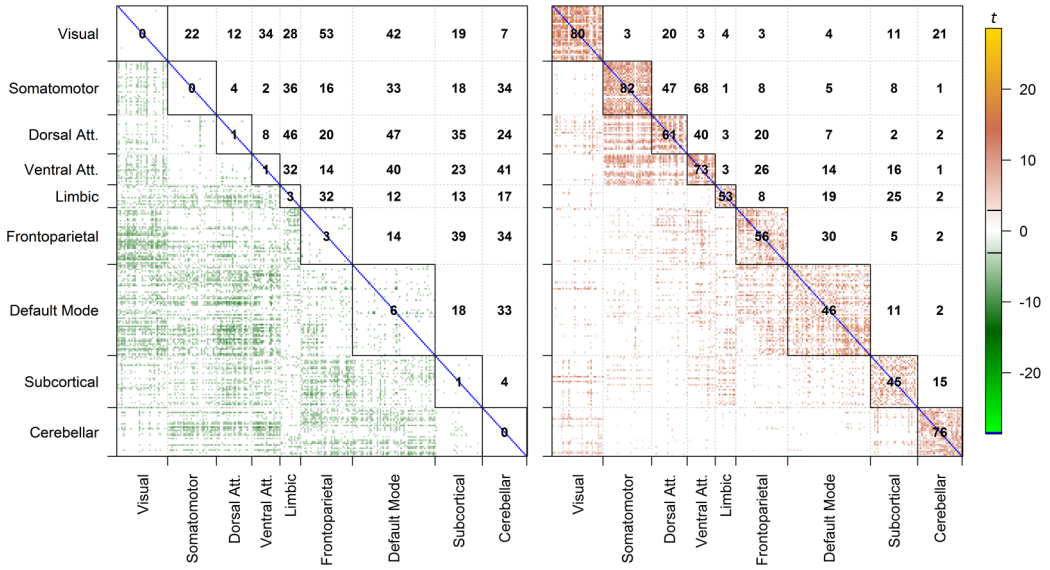

Figure 3.5: A matrix of significant associations for beer assuming static FC. FDR-corrected t-statistic values for β_0 in the simple model (model 1) are shown for negative- and positive-only correlations (below diagonal) and percentage of significant pairwise ROI correlations within- and between- each network (on and above diagonal, respectively). Color bars denote the values of the t statistics.

patterns for the beer flavor condition in Figures 3.4 and 3.5, the patterns are less clear. For associations that were greater during beer than Gatorade scans, ($t - statistic < 0$), the highest percentage was between frontoparietal and default mode networks (7%) and between somatomotor and dorsal attention (7%). For associations that were greater during Gatorade than beer scans (t-statistic> 0), the highest percentage was 10% between somatomotor and limbic networks (which largely consist of the orbitofrontal cortical regions), and between dorsal attention and frontoparietal networks (12%).

Figure 3.8 shows pairwise associations of a priori regions of interest during beer scans modeled with a static FC (β_0 in model 1) after adjusting for multiple comparisons ($p_{FDR} < 0.05$; lower triangular matrix elements). The two Figure 3.8 panels illustrate associations of

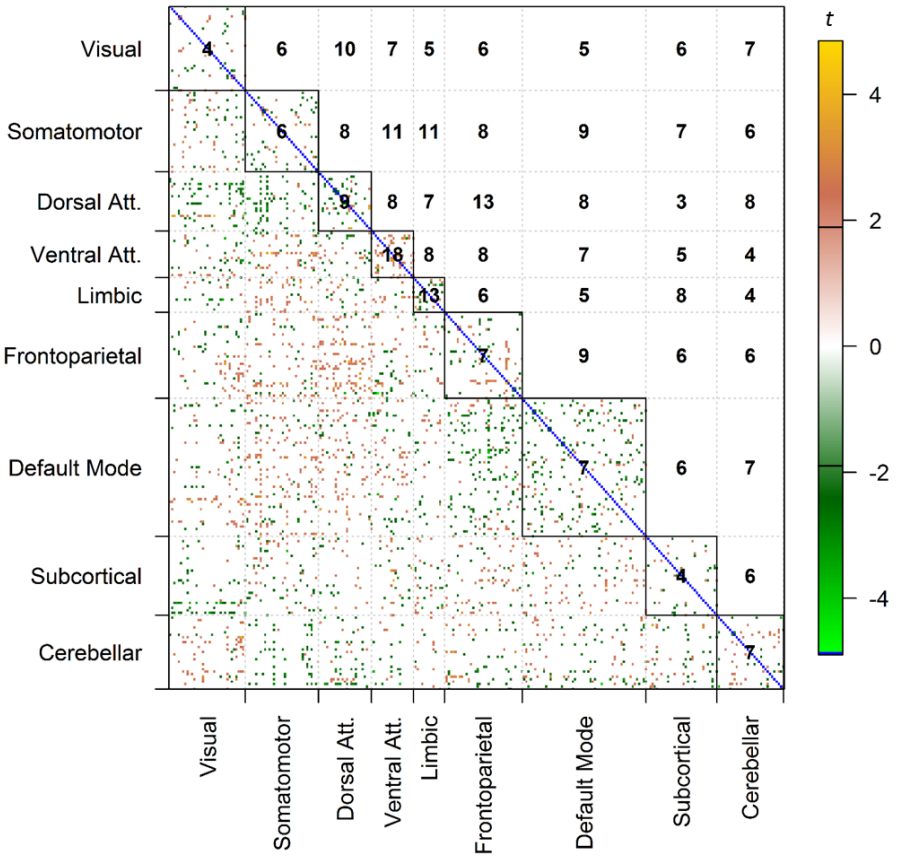

Figure 3.6: Matrix of pairwise associations for the flavor differences assuming static FC. t-statistic values for γ_0 in model 1 are shown at $p < 0.05$ (two-tailed, uncorrected for multiple comparisons) and presented similarly as in Figure 3.3.

brain regions that responded in the GLM-based analysis when contrasting [*Beer* > *water*] and [*beer* > *Gatorade*] as reported in the Supplementary Tables S1 (left) and Table 2 (right) in Oberlin et al. (2016). For completeness, the unthresholded associations are presented in the upper triangular matrix elements. As anticipated, most regions activated in the [*Beer* > *water*] contrast showed significant positive associations (Figure 3.8, left). A subset of the regions from the [*beer* > *Gatorade*] contrast showed significant positive associations that were most prominent between two right ventral and dorsal anterior insula

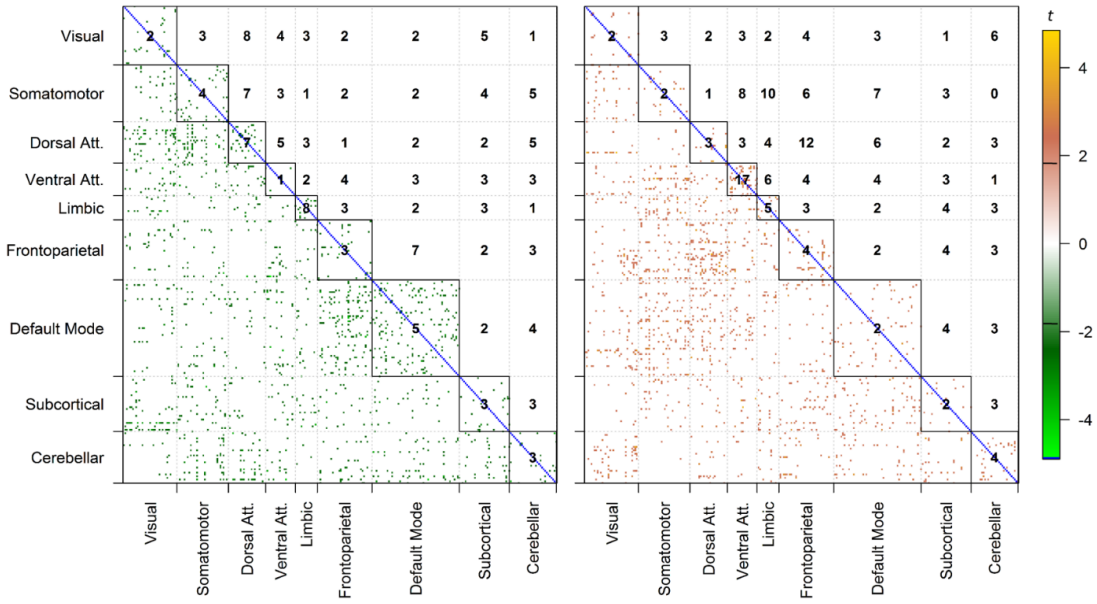

Figure 3.7: Matrix of pairwise associations for the flavor differences assuming static FC. t-statistic values for γ_0 in the model 1 are shown at $p < 0.05$ (two-tailed, uncorrected for multiple comparisons) with negative values indicating (*beer* > *Gatorade*; left) and positive (*Gatorade* > *beer*; right) associations.

cortical regions (R-vAIC and R-dAIC, respectively) and the right anterior cingulate (R-ACC) (Figure 3.8, right). Slightly weaker but still significant positive associations were also present between the right ventral striatum (R-VST), right ventral AIC (R-vAIC), and right rostrolateral orbitofrontal cortex (R-rostOFC). These results indicate that enhanced beer activation in the striatal and OFC reward regions was indeed accompanied by significant positive associations of salience and reward-dedicated regions during beer scans. Similarly, Figure 3.9 depicts pairwise associations of a priori regions of interest for the difference between Gatorade and beer (γ_0) modeled as a static FC and without a multiple comparison adjustment. It is notable that even at an uncorrected p ¡ 0.05 threshold (lower triangular matrix elements), the associations are sparse. The unthresholded t-statistic values shown in the upper triangular elements illustrate the magnitude and direction of observed associa-

tions. For example, associations of R-VST, R-vAIC, and R-rostOFC are negative, indicating enhanced association during beer as compared to Gatorade scans. While directionality of these relationships is consistent with Oberlin et al. (2016), none are significant, raising a legitimate question whether FC can be better modeled.

Model 2

This model included non-linearly changing time-dependent association between the time series of two different brain regions, with several examples presented in Figure 3.10. The blue line and associated shaded area depict time-varying estimate of dFC for beer and its confidence interval (CI), respectively. Similarly, green color indicates Gatorade and red denotes the difference between Gatorade and beer dFC estimates. Several different scenarios are captured by the respective Figure 3.10 panels. In the left panel, dFC estimates for beer and Gatorade are both positive across time, indicating a positive association between Right ventral AIC/Frontal Operculum (FO) and Left Inferior Frontal Gyrus (IFG) across the full scan time period. The Gatorade dFC initially increases and then decreases, and increases again, stabilizing for the remaining time points while the beer dFC first increases and then decreases over time. The difference of Gatorade and beer estimates is initially around zero (when associations for Gatorade and beer are equal) and then decreases as the association during beer stimulation becomes greater than the association during Gatorade. The middle and right panels of Figure 3.10 illustrate some of the other time-varying scenarios for the population-level dFC curves. These are only three examples out of 38,503 pairwise comparisons. To identify dFC curves of interest, we propose to use an objective metric that quantifies the proportion of time that the confidence intervals around the dFC curve excludes zero. This metric gives more comprehensive, whole-brain view of the results. In addition, it is relevant whether the confidence intervals are above or below zero (i.e., association or a difference between associations is significantly positive or negative across

time). Informed by the study design, where flavor and water trials are equally represented (i.e., 50%; see Figure 3.1), we performed a hypothesis test for the proportion of time that the confidence intervals around the curves excluded zero. As the null hypothesis, the proportion is equal to 0.5 and tested against the alternative that proportion is greater than 0.5. Figure 3.11 presents the matrix of the FDR-corrected proportions for non-zero coverage across time for beer flavor. The brain regions are organized as in Figure 3.4, with the upper triangular and diagonal elements showing the percentage of significant proportions within and between each network, respectively. For example, 75% of pairwise associations between somatomotor and ventral attention network regions are significant. On the lower triangular, each dot represents the value of the proportion for a specific pair of brain regions. Figure 3.11 middle and right panels show a matrix representing a proportion of significant non-zero dFC across time for beer flavor when the confidence interval for beer is below zero and above zero, respectively. Similarly as before, many significant positive associations of dFC across time are observed within the RSNs. The majority of the negative associations occur between regions from different networks. For example, 56% of time-varying associations between limbic and dorsal attention network regions have a significant negative non-zero coverage. The difference between flavors is summarized by the matrix of significant proportions in Figure 3.12. When the difference is significant and below zero, dFC for beer is significantly greater than Gatorade during at least 50% of the time (Figure 3.12, middle panel) and when the difference is significant and above zero, dFC for Gatorade is significantly greater than for beer during at least 50% of time points (Figure 3.12, right panel). For beer being significantly greater than Gatorade, the highest percentage of significant associations is between somatomotor and dorsal attention networks and for Gatorade being significantly greater than beer, the highest percentage of significant associations is between frontoparietal and dorsal attention networks.

Figures 3.13 presents the significant results for non-zero coverage for a priori selected regions of interest for beer flavor (lower triangular elements) and difference in dFC between flavors (upper triangular elements). For beer, we tested if the confidence interval excluded zero at least 50% of the time. For the flavor difference, we tested if the confidence interval was at least 10%, 16% and 33% of the time different than zero. Here, for the flavor difference (upper triangular elements) we present only the results when the proportion parameter was equal to 0.1. The results for beer and the flavor difference are adjusted for multiple comparisons.

The non-zero coverage dFC metric (Figure 3.13) discovered more pairwise associations between a priori regions than detected by the constant across time dFC model (Figure 3.8). Specifically, for beer scans, we found 25 more significant associations between a priori regions shown in Figure 3.8 (left). For differences between flavors, the non-zero coverage metric discovered four significant associations while none were present in the static dFC model (Figure 3.8, right). Utilizing only the standard (static) FC approach, these differences of dFC between flavors in our a priori regions of interest would go undetected.

The association for beer is significant and positive across all time points. The association for Gatorade does not differ from zero for about half of the time. The difference between Gatorade and beer (red curve) and its confidence interval show that for later time points (peak about time point 65) the associations for beer is greater than for Gatorade. The non-zero coverage of 0.36 for the flavor difference is significantly different than the 0.1 proportion. The R-rostrolateral OFC region reported in Oberlin et al 2016, also showed significant beer-potentiated association to both R-VST and R-vAIC (Figure 3.14, middle and right, respectively). The difference between flavors occurred only for the early time points and it was not significantly different from the 0.1 proportion.

For homologous regions, like the right precentral gyrus (R-PreCG) of the sensorimotor cortex (SMC) and three sensorimotor network (SMN) regions presented in Figure 3.15, we found that dFC shows an expected, high, nearly constant, positive association for both flavors but no difference between flavors (left panel). Slightly lower positive association is seen between ipsilateral R-PreCG and R-Rolandic Operculum (RO)/Insula, area "G" of the primary gustatory cortex (center panel). For both flavors, the associations of the R-PreCG and R-Putamen (subcortical part of the SMN) are much lower, slowly increase but remain positive (right panel).

Another interesting behavior is presented in Figure 3.16 between the right precentral gyrus (R-PreCG) of the sensorimotor cortex (SMC) and striatal and orbital reward-related regions. Unlike positive associations to other SMN regions for both flavors, during Gatorade stimulation dFC of the R-PreCG is not associated to the right ventral striatal (R-VST), right rostrolateral OFC, and left rostrolateral OFC (left, center and right panels, respectively). During beer scans, however, dFC curves of the R-PreCG and all three reward areas are negatively associated, with the magnitude of these associations diminishing during the last 20 time points. This beer result drives a significant positive association of the Gatorade-beer difference dFC curve, especially for the R-VST and R-rostrolateral OFC areas.

Figure 3.17 interestingly shows that by using our approach we can detect significant associations where the standard methods fails. Here, we can observe dFC curves indicating time series associations of the R-dAIC with the left caudate (includes both head and body H&B) and right medial superior frontal gyrus (R-mdSFG) (left and center panels). Similarly, an interesting dFC pattern is present for the R-rostrolateral OFC and left IFG p.T (pars triangularis), with the region extending into the middle frontal gyrus (L-IFG p.T./MFG). In these examples, dFC curves often change sign during the scan, for example

mid-way through. By averaging across time, this information is lost in the standard (static) FC approach.

Here, we focused on a subset of a priori regions of interest. More detailed investigation to discover novel associations will be performed in the future study. In the above examples, we used experimental design-based proportion of 0.5 as our null hypothesis proportion for beer flavor. We also investigated how the number of significant associations depends on the value of proportion and type of multiple comparison adjustment. The number of significant associations as a function of the value of proportion is calculated using FDR and Bonferroni criteria. Figure 3.18 shows the number of significant associations for beer flavor while Figure 3.19 depicts the number of significant associations for the difference between flavors. For both multiple comparison adjustment methods, the number of significant association decreases with increasing value of proportion, and takes a similar value.

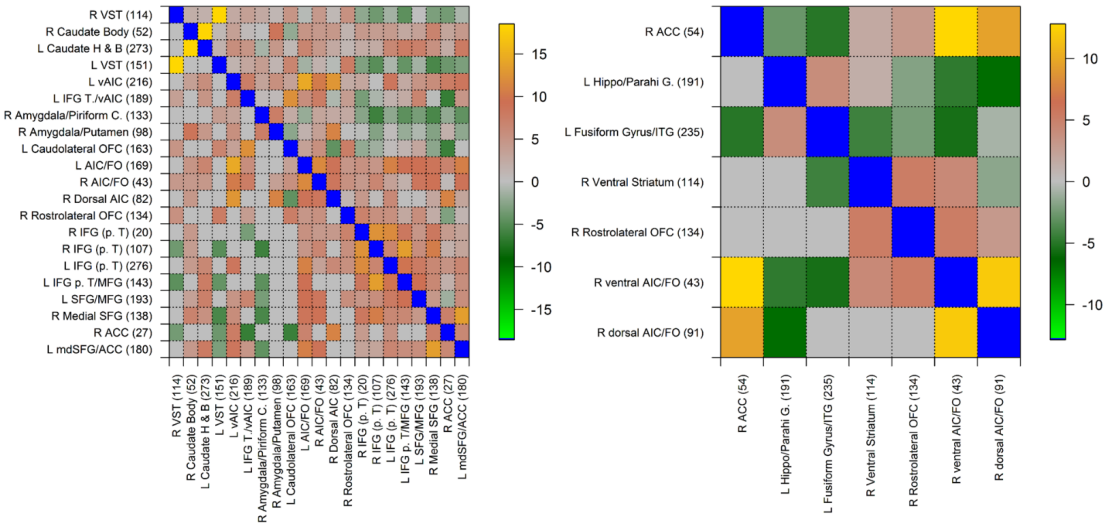

Figure 3.8: Matrix of pairwise associations for beer in selected a priori regions of interest assuming static FC. These regions responded in $[Beer > water]$ (left) and $[Beer > Gatorade]$ (right) contrasts ($p < 0.001$, detailed in Oberlin et al. (2016)). t-statistic values for β_0 below the diagonal are displayed at $p_{FDR} < 0.05$ (FDR-adjusted for multiple comparisons), while upper triangular values are not thresholded. Brain region indices from Shen et al. (2013) are in parentheses. Abbreviations: L-left, R-right, md – medial , VST – Ventral Striatum, ACC – Anterior Cingulate Cortex , H & B – Head and Body, vAIC – ventral Anterior Insular Cortex, FO – Frontal Operculum, IFG p.T. – Inferior Frontal Gyrus (Pars Triangularis), OFC – Orbitofrontal Cortex, SFG – Superior Frontal Gyrus, MFG – Middle Frontal Gyrus, Hippo/Parahi – Hippocampus/Parahippocampal Gyrus.

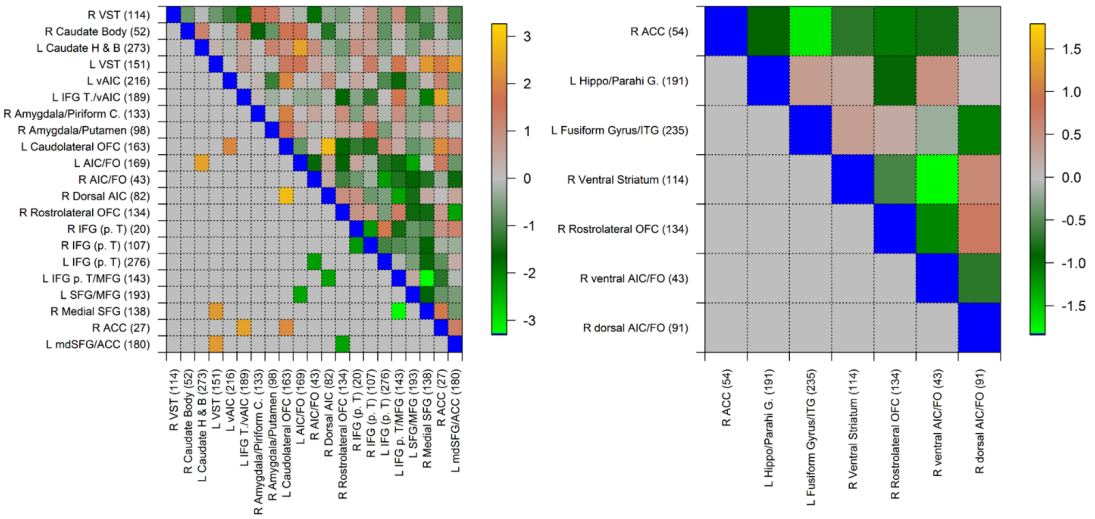

Figure 3.9: Matrix of pairwise associations for difference between flavors in selected a priori regions of interest assuming static FC. t-statistic values for γ_0 in the lower triangular are shown at $p < 0.05$ (not adjusted for multiple comparisons), while the upper triangular values are not thresholded to illustrate magnitude and sign of the associations. It is notable that no associations are significant after correcting for multiple comparisons and are sparse even at a low $p < 0.05$, uncorrected threshold. The color bar scales indicate t-statistic values.

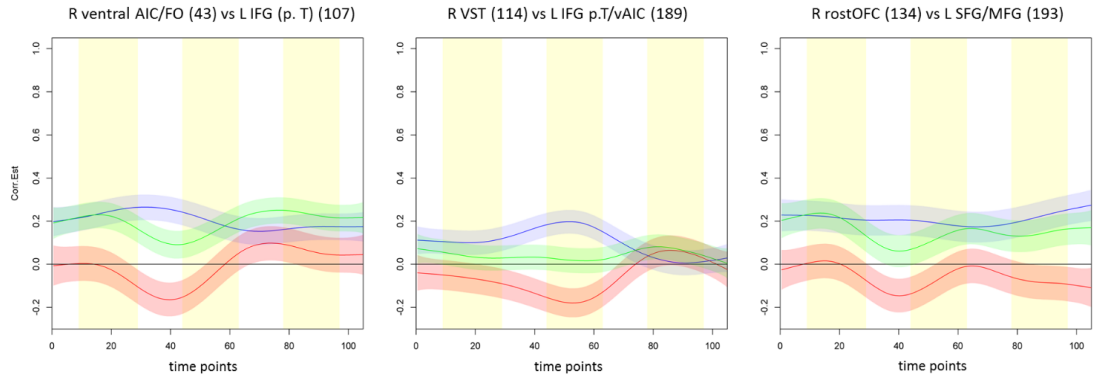

Figure 3.10: dFC examples. Blue, green and red lines and shaded areas represent estimated dFC with pointwise 95% CIs for beer, Gatorade and Gatorade-beer difference, respectively. Left: both flavors differ significantly from 0 for all time points (TP), with their difference changing sign as a function of time. Center: dFC for beer is significantly positive across time up TP=70, Gatorade is not significant across time and difference between flavors is significant up to TP=70. Right: dFC for beer differs significantly from zero and is changing very little across time, while Gatorade is significantly different than zero for almost all time points. The difference between flavors is significant only during a short time window between 30 and 50 TP.

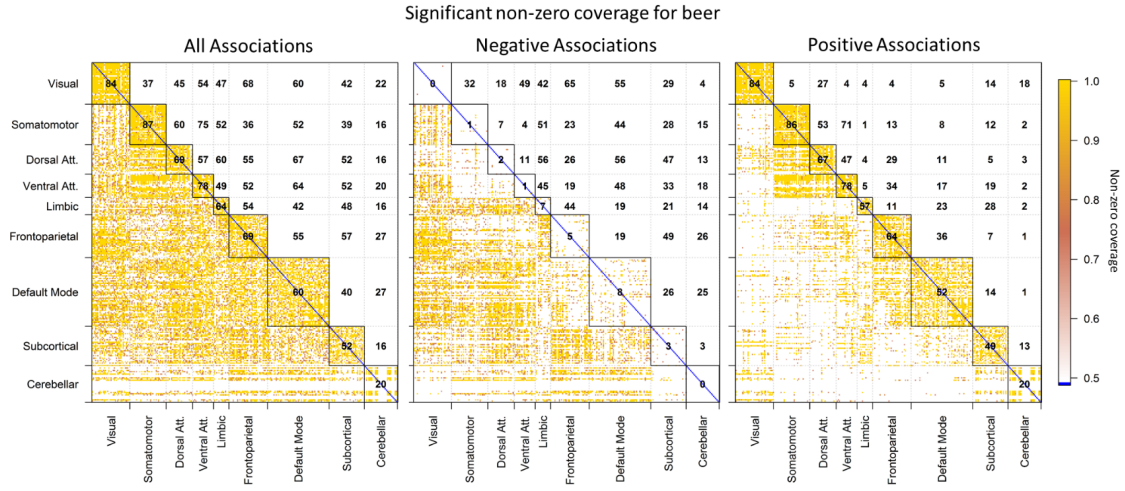

Figure 3.11: Matrices representing a proportion of significant non-zero dFC across time for beer flavor (left). Middle: A matrix representing a proportion of significant non-zero dFC across time for beer flavor when the confidence interval for beer is below zero (middle) and above zero (right). The upper triangle shows a percentage of significant non-zero dFC for all network pairs.

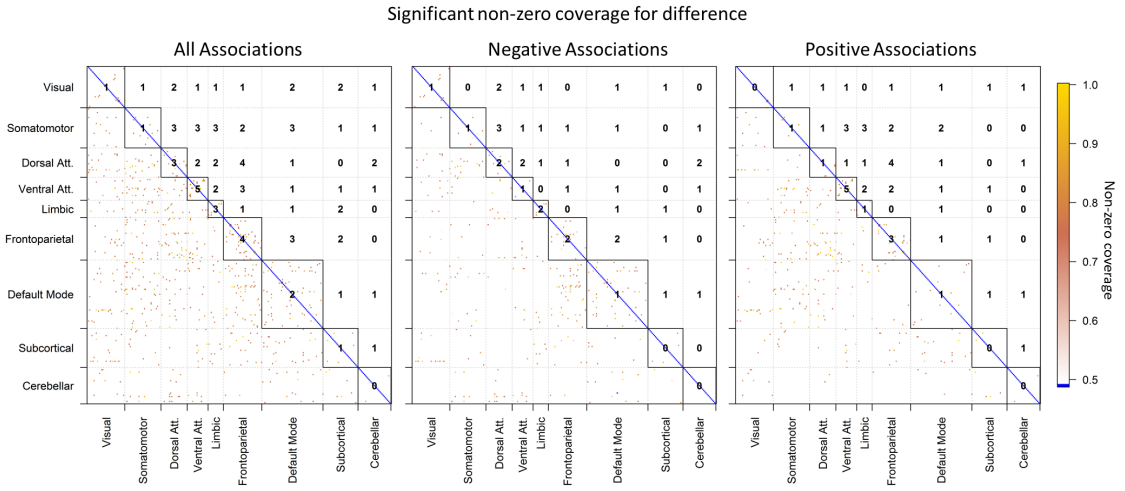

Figure 3.12: Left: A matrix representing a proportion of significant non-zero dFC across time for the difference between flavors. Middle: Decomposition of left panel into *beer* > *Gatorade* difference. Right: Decomposition of a left panel into *Gatorade* > *beer* difference. The upper triangle shows a percentage of significant non-zero dFC for all network pairs.

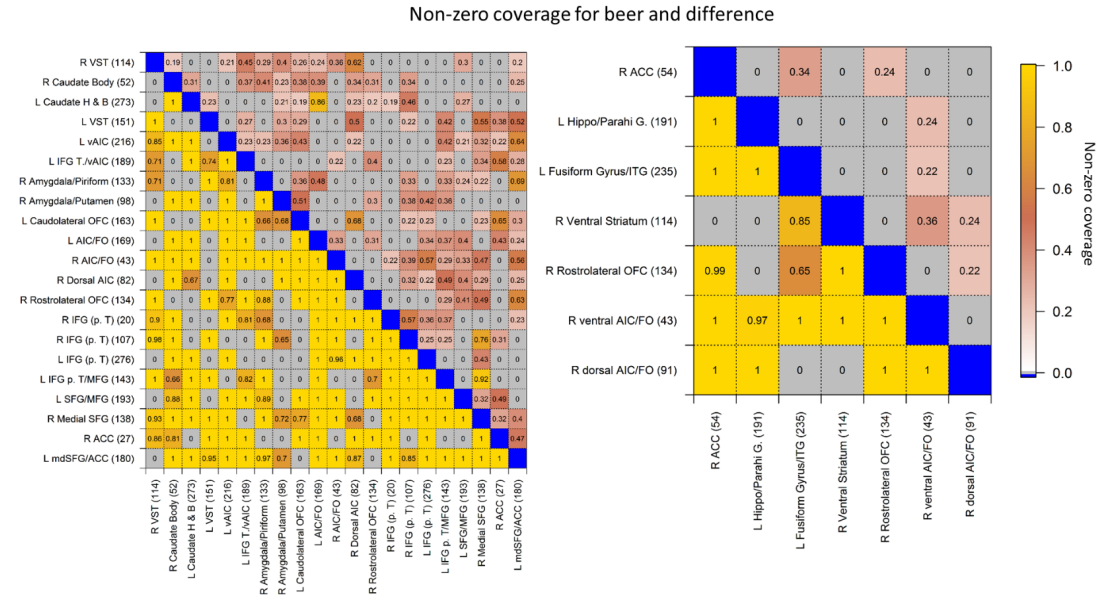

Figure 3.13: Non-zero coverage for selected a priori regions of interest. Lower triangular elements show the beer results while upper triangular elements indicate the difference between flavors . N on-zero coverage for beer was tested for 0.5 and presented difference was tested for 0.1. The significant findings adjusted for multiple comparisons ($p_{FDR} < 0.05$) are indicated by the color bar (nonsignificant results are in gray).

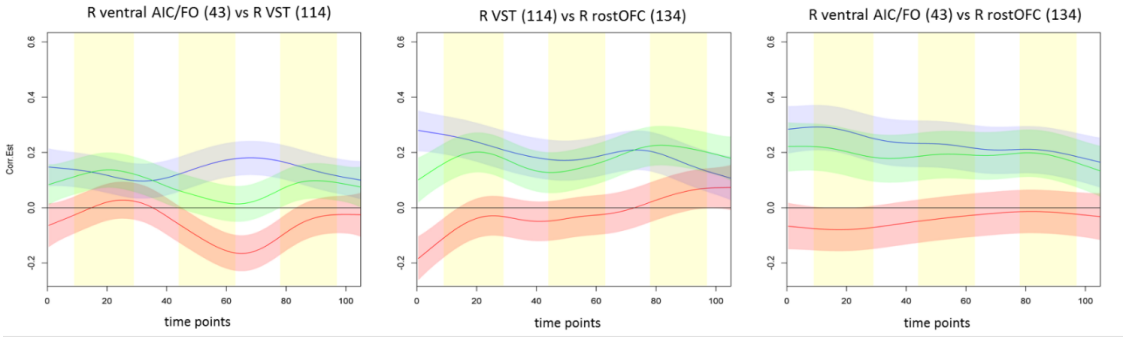

Figure 3.14: dFC curves for several reward-related a priori regions of interest where the activation-based analysis reported [*beer* > *Gatorade*] effects (Oberlin et al. (2016)). Blue, green and red lines and shaded areas represent estimated dFC with pointwise 95% CIs for beer, Gatorade and Gatorade-beer difference, respectively.

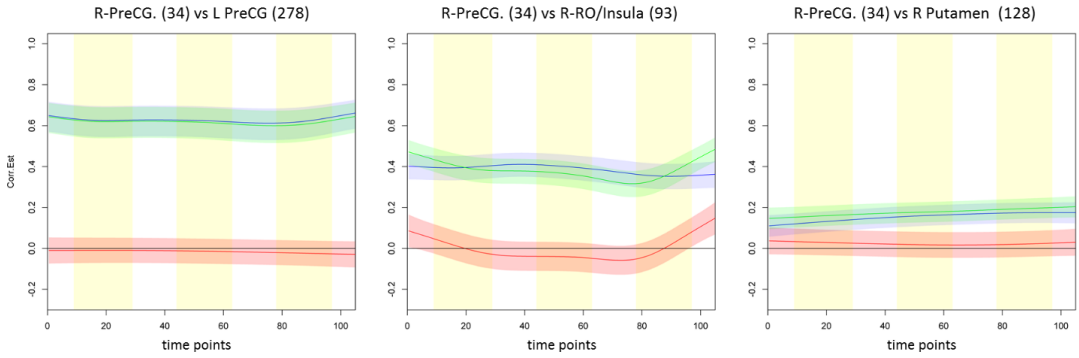

Figure 3.15: dFC curves indicating time series associations between the right precentral gyrus (R-PreCG) of the sensorimotor cortex (SMC) and three sensorimotor network (SMN) regions. Blue, green and red lines and shaded areas represent estimated dFC with pointwise 95% CIs for beer, Gatorade and Gatorade-beer, respectively. A homologous, left precentral gyrus area shows an expected, high, nearly constant, positive association for both flavors but no flavor difference (left panel). Slightly lower positive association is seen between ipsilateral R-PreCG and R-Rolandic Operculum (RO)/Insula, area "G" of the primary gustatory cortex (center panel). For both flavors, the associations of the R-PreCG and R-Putamen (subcortical part of the SMN) are much lower, slowly increase but remain positive (right panel).

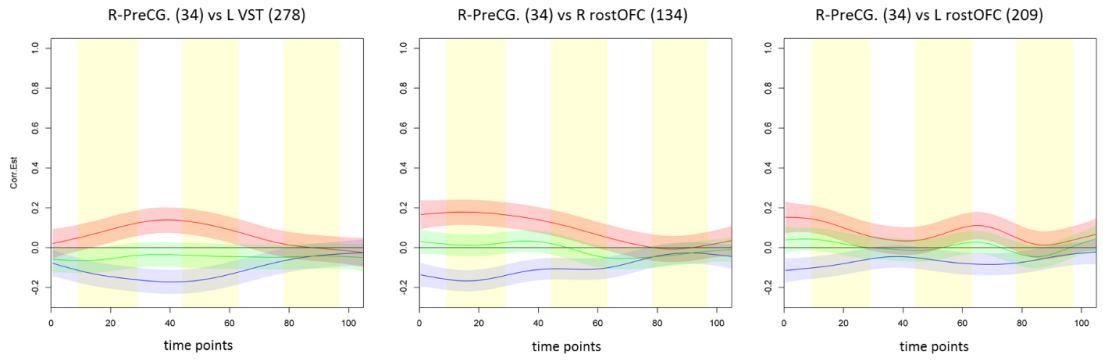

Figure 3.16: dFC curves indicating time series associations between the right precentral gyrus (R-PreCG) of the sensorimotor cortex (SMC) and striatal and orbital reward-related regions. Unlike positive associations to other SMN regions for either flavor, dFC of the R-PreCG for Gatorade is not associated to the right ventral striatal (R-VST), right rostrolateral OFC, and left rostrolateral OFC (left, center and right panels, respectively). During beer, however, dFC curves of the R-PreCG and all three reward areas are negatively associated, with the magnitude of these associations diminishing during the last 25 time points. This beer result drives a significant positive association of the Gatorade-beer dFC curve, especially for the R-VST and R-rostrolateral OFC areas.

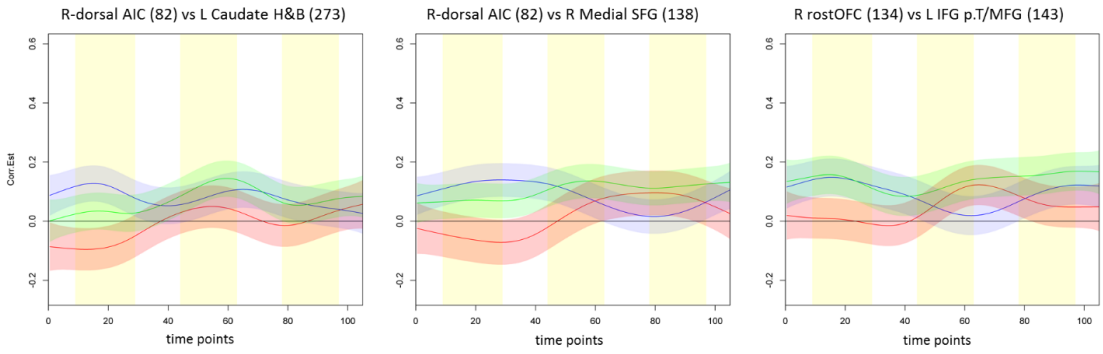

Figure 3.17: An example of dFC curves for which we do not detect any significant association for beer flavor in the standard, constant over time dFC analysis because these effects often change a sign canceling out the association (change a phase mid-way). Blue, green and red lines and shaded areas represent estimated dFC with pointwise 95% CIs for beer, Gatorade and Gatorade-beer difference, respectively.

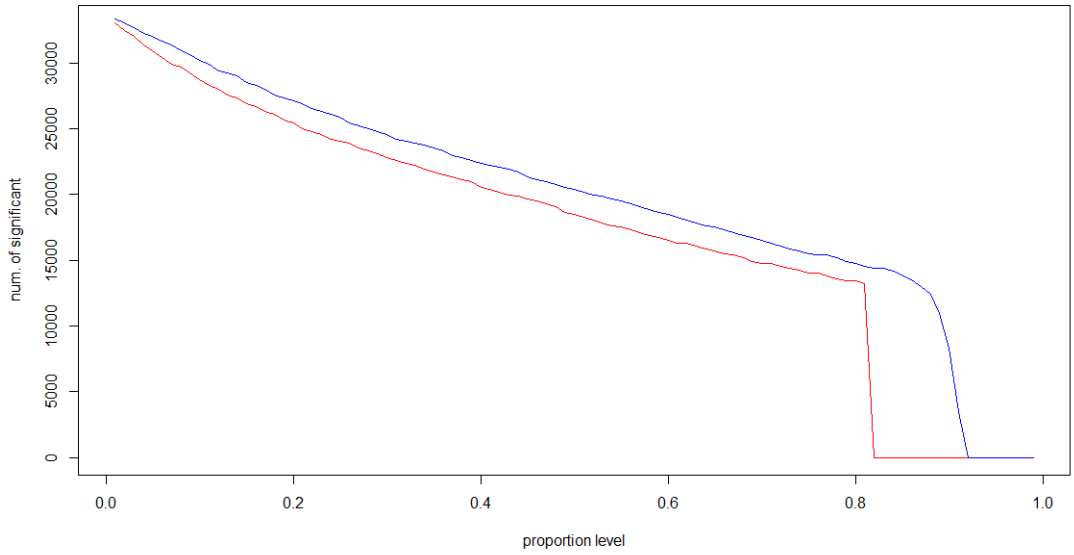

Figure 3.18: A number of significant associations for beer flavor versus a level of proportion for FDR and FWER corrections (blue and red line, respectively).

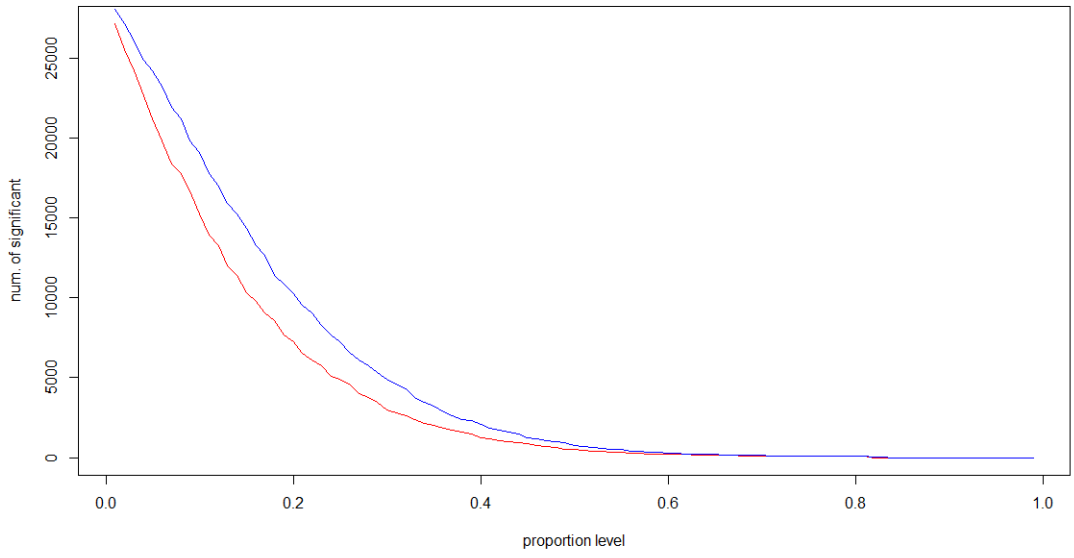

Figure 3.19: A number of significant associations for a difference between flavors versus a level of proportion for FDR and FWER corrections (blue and red line, respectively).

Discussion

The methods presented in this work provide a novel application of statistical methods for the analysis of task-based dynamic FC data. Our approach examines the population–level dFC for a large number of associations between pairs of time-varying processes with complex correlation structure. We first estimated the time-varying association among 278 functionally defined brain regions (Shen et al. (2013)) at a subject level using the recently developed algorithm (Kudela et al. (2017)). As a result, we obtained a smooth trajectory and its confidence interval for 38,503 pairwise time-varying associations for each subject and scan. Then, these subject-specific estimates were used to model a population-averaged dynamically changing association for each stimulus.

In the second step, we applied the semiparametric additive mixed effects models to estimate the population level time-varying associations between 278 brain regions. This approach allowed us to incorporate the study design by taking into account scan effects as well as subject- and task-specific variability. As a result, we were able to combine the information across subjects and scans to obtain a population-level estimate of time-varying association and its confidence intervals for each flavor and the difference between flavors.

We also compared the performance of two popular procedures for multiple testing; FDR- and FWER- based correction. The FDR correction for strongly correlated fMRI data was slightly less conservative than the Bonferroni correction but the number of significant associations was very similar. We proposed a novel metric to summarize the results from 38,503 population-level pairwise associations for each flavor and difference between flavors by using a non-zero coverage of confidence bands and the location/sign of dFC curves. As a result, we showed that the dynamic functional connectivity analysis of the gustatory task fMRI data yielded a pattern closely resembling the resting state networks (the networks found when subjects do not perform any task) reflecting a common functionally-based brain

organization. Our dFC approach reproduced known averaged FC between homologous areas (Figure 3.15) and revealed differences in dFC patterns some of which standard approaches would likely miss. The non-zero coverage for the difference revealed beer and Gatorade differentiation in visual, somatomotor and attentional networks as well as frontoparietal and default mode networks.

For the simplest model (assuming constant association across time), the intercepts interpreted as the mean dFC across time for each flavor also yielded FC patterns similar to the RSNs. We observed that the flavor stimulation potentiated dFC between limbic-subcortical, somatomotor-attentional, and frontoparietal-default mode networks. However, the average difference between flavors was not significant after adjusting for multiple comparisons. More focused review of a priori regions of interest largely reproduced previously reported results (Oberlin et al. (2016)), with reward-related ventral striatal, lateral orbitofrontal and insular regions showing positive associations during beer scans. These associations were also potentiated by beer (as compared to Gatorade) confirming their importance in the alcohol cue response. Our dFC analysis showed patterns and time dependence of associations that would not be detectable with standard approaches.

One of the limitations of the proposed approach is that temporal smoothing introduced by the sliding window application precludes a disentangling of flavor and water stimulus contributions. In other words, all reported flavor results might be reduced by the inclusion of water trials. One of the solutions would be finer sampling with multiband acquisitions, which would increase the number of measurements by approximately 2-3 times. The second limitation is that our approach considers only associations between two brain regions at a time and further extension is needed for more than two regions. In order to fully benefit from the large sample of estimated dFC curves, an application of clustering algorithms would allow a comprehensive investigation of different classes of dFC curves. Consequently,

one could uncover and test specific time dependence scenarios not easily modeled in the standard FC or GLM-based approaches. In the future study, we plan to extend our dFC analysis to these exciting new domains. The results presented here should be regarded as preliminary because of the modest data sample. Hence, more detailed interpretation of presented associations should be left for the follow-up investigations. The methods presented here can be extended to other fMRI designs.

The outlined methodology can be implemented with statistical significance criteria applicable at different spatial resolutions- from the whole-brain, to the network level, or even a subset of a priori regions. The proposed approach is data-driven, applicable to both task and resting state time series data, and provides flexible methodology to investigate associations between brain regions.

Chapter 4

Task-based differentiation of functional networks during a gustatory task

Modularity analysis provides the division of brain regions into communities with intra-connectivity greater than obtained by chance. Here, we used dynamic Functional Connectivity (dFC) to extract communities. dFC quantified time-dependent associations between time series of brain regions in a task-based fMRI study (24 subjects tasting their preferred beer and Gatorade as an appetitive control). We first estimated dFC by applying recently developed bootstrap-based technique and generalized additive mixed models. To study the system's modularity and incorporate the dFC information, we then optimized the quality function (Mucha et al. (2010)) by using the Louvain algorithm. The dynamic modularity was summarized on the population and subject levels by calculating network- and region-based entropy (a measure of uncertainty of group assignment) for each flavor. At a network level, three predominant communities emerged for both flavors involving: 1) visual-subcortical, 2) somatomotor-attentional, and 3) frontoparietal-default mode network regions. The entropy was significantly greater for Gatorade than beer in orbitofrontal, somatomotor, and default mode networks. This finding was reproduced regionally, with reward-related orbitofrontal and ventrostriatal regions also implicated in the alcohol cue response (Oberlin et al. (2016)). For both flavors, the entropy in orbitofrontal, paracentral lobule, left precentral/middle frontal gyri was positively associated with drinking-related variables.

Introduction

Modularity is one of the network structure metrics. It represents the connectivity information within a system by using versatile network communities and aims to find organized structures in the network. This is accomplished by using Graph Theory, where graphs are mathematical structures describing pairwise relations between objects. A system of asso-

ciated units is then modeled as graphs with nodes (vertices) that are connected by edges (lines). Graphs provide relatively simple method to analyze very complicated structures and enable the characterization of general properties of network organization. One of the main graph theory findings, highly relevant in the field of brain imaging, was a discovery of modular network decomposition. It was noted that many networks contain groups of a smaller number of highly intra-connected nodes called modules or communities, which are sparsely connected with outside nodes (Simon (1962)). Modular architecture emerges in the systems that perform many jobs at once, under changing conditions, and at the same time aim to optimize their whole performance (Kashtan and Alon (2005)).

In the brain imaging context, each community can operate simultaneously without much influence from other brain areas. As noted by Fornito et al. (2015), one of the plausible reasons for such organization is that it protects the brain from extending and disrupting the operation of other modules if any pathological changes occur in the local center of a particular community. This enables increased diversity and consistency of network activation design (Robinson et al. (2009); Shanahan (2010)). The high connectivity between the brain regions in any given module implies that their role in the brain might be similar (Fornito et al. (2016)). On the other hand, higher-order functions performed by the brain possibly rely on boosted between-module interactions (Fornito et al. (2016)). Consequently, it is reasonable to assume that the differences in network community structure between healthy and diseased subjects reveal another perspective on development and roots of brain diseases with the quantification of network sub-organization becoming a rapidly growing area of research (Fortunato (2010); Newman (2006)).

In this manuscript, we propose a methodology to find the local network communities in a task-based fMRI study of beer drinkers stimulated with beer and Gatorade flavors. The communities are detected using the information provided by the dynamic functional

connectivity (dFC), namely dynamically changing association between two time series from different brain regions. We are interested in finding communities of brain regions with a specific property, i.e. high intrinsic and weaker extrinsic dFC. Since the appropriate number of communities or how different brain regions should be grouped into communities is unknown, we rely on the data-driven techniques to discover the hidden features.

Here, we propose a two-step procedure to detect the communities. First, we estimate dFC at a subject- and group-level. Secondly, we apply the modularity analysis to find local network communities based on obtained dFC information. Specifically, we use a recently proposed bootstrap-based technique (Kudela et al. (2017)) to estimate a subject level dFC and its confidence intervals. Next, we apply generalized additive mixed models (GAMM) to combine information across subjects and scans accounting for the experimental design. As a result, we obtain both subject- and group-level estimates of dFC for the two flavor stimuli. We further use this dFC estimates in modularity analyses to find the time varying community assignment for each network and brain region at a subject- and group-level using a method of Mucha et al. (2010). To find the optimal partitioning, we use a Louvain algorithm which is fast, works well for large networks, and was demonstrated to be more accurate in a community assignment for networks with known community structure Lancichinetti and Fortunato (2009). Our group-level modularity analyses allow us to summarize the results from the whole brain perspective, while subject-specific modularity analyses enable us to investigate differences in the module assignments between flavors by utilizing entropy, a measure of module assignment uncertainty (Wakefield (2013)). Entropy allows us to summarize dynamic module assignment on a region and network basis. In addition, we present how the proposed approach can test an association between modularity (as summarized by entropy) and variables of interest (e.g., drinking frequency) for any arbitrary brain region or network.

Many methods have been proposed to describe a partition of the network into communities (detailed overview can be found in Sporns and Betzel (2016)). In the proposed approach we: 1) search for a partition that groups the brain regions that tend to work together, creating densely connected communities with the number of connections higher than expected by chance and, 2) propose a way to summarize and compare the results between flavors. Methods well known in statistical data analysis, such as hierarchical clustering (Hastie et al. (2009)), can be considered to discover the hidden communities in the data. However, they tend to overlook the peripheral nodes (Girvan and Newman (2002)). For example, hierarchical clustering starts by grouping the nodes with the strongest similarity, nodes with weak similarity to other members of the same group tend not to be classified correctly, which does not fulfill the definition of communities of interest.

The main advantage of proposed methodology is that it allows us to detect communities of interest in a data-driven, flexible way. It also enables us to assess associations between brain regions and networks from the different perspective and gain insights that other methods would likely miss. The remaining sections are organized as follows: Section 4.2 describes the experimental design and image preprocessing, Section 4.3 presents our approach for estimating functional connectivity, Section 4.4 covers a brief summary of the static and dynamic modularity estimation, Section 4.5 summarizes the analyses results and Section 4.6 contains a discussion.

Experimental design and Image preprocessing

Experimental design

Subjects. The fMRI data were acquired in a sample of 24 male beer drinkers with a recent drinking history ranging from social to heavy. All subjects were right-handed, reported a good physical and mental health and listed beer as one of their two typically consumed alcoholic beverages. Participants' main demographic characteristics are presented in Table

4.1. Prior to participating in the study, each subject signed a consent form approved by the Indiana University Institutional Review Board. Further details, exclusion, and inclusion criteria are detailed in Oberlin et al. (2016).

	Mean ± (SD)	Range	N(%)
Age	24 (2.3)	21-28	
Caucasian	–	–	24 (100%)
Education	15.8	(1.4)	12-19
% with at least one first degree relative w/AUD			7 (29%)
Drinks per week	14.9 (9.9)	2-33	
Drinks per drinking day	4.9 (3.0)	1-10	
Heavy drinking days per week	1.6 (1.4)	0-6	
AUDIT	10.2 (6.3)	3-26	

Table 4.1: Subject Characteristics (AUD - Alcohol Use Disorder; AUDIT - Alcohol Use Disorders Identification Test)

Experimental design. The fMRI experimental procedure is illustrated in Figure 4.1. Each subject underwent six fMRI scans. During each scan, small quantities of beer or Gatorade were delivered on subject's tongue in 1-sec sprays (trials) with beer or Gatorade flavor interspersed with water trials. In each scan, subject experienced three flavor epochs with four trials each, which were interspersed with four water epochs consisting of 3 trials each. In summary, 12 flavor and 12 water trials were delivered with an inter-trial interval fixed at 11 seconds. The study was designed to evaluate the response of reward regions to the taste of most-often consumed beer ("B") and Gatorade®("G"; an appetitive flavor control). In addition, each subject participated in computerized rating assessment just before imaging and between each fMRI scan. As described in Oberlin et al. (2016)four drinking-related characteristics were assessed: 1) flavor pleasantness (1 = "Least Pleasant Ever", 7 = "Most Pleasant Ever"); 2) flavor intensity (measured by Green's Labeled Magnitude Scale (Green et al. (1996)))]; 3) "wanting" defined as the number of beers subject had a craving for at the moment (a standard 12 oz. beer was a unit; 4) "desire" to drink alcohol defined as a mean score from 4 items from the Alcohol Craving Questionnaire (Singleton et al. (2000))

on a 7-point visual analog scale (VAS; 1 = strongly disagree, 7 = strongly agree). Mean ratings of four characteristics were further tested to see if there is a difference between beer, Gatorade, and water. We used a simple mixed model for repeated-measures design. The significant results were corrected for multiple comparisons. In addition, we investigated associations between mean ratings of the four above-listed characteristics and entropy value for brain regions that were found to be significant as detailed later. More details about experimental design and measures can be found in Oberlin et al. (2016, 2013, 2015).

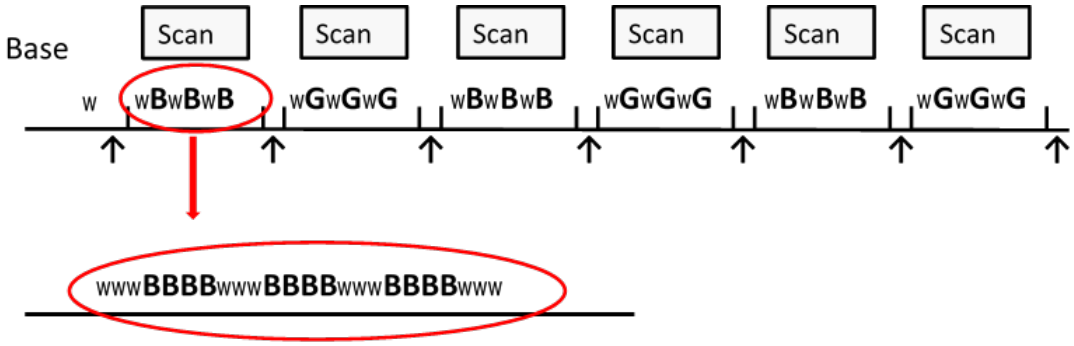

Figure 4.1: Experimental design. **B**, **G** and **w** indicate beer flavor, Gatorade flavor and water, respectively. After water sprays at baseline, 6 fMRI scans are performed with scans consisting of beer or Gatorade flavor stimulation interspersed with within-scan water trials (Oberlin et al. (2016)). Red ellipses depict zoomed in view per one scan.

Imaging Procedures and Analysis

Image Acquisition: 125 Blood Oxygenation Level Dependent (BOLD) contrast-sensitive volumes per scan were acquired with a 12-channel head coil array on a 3T Siemens Trio-Tim MRI scanner. These functional BOLD data were obtained with an echo planar imaging (EPI) sequence (gradient echo, 125 volumes, TR/TE= 2250/29 ms, flip angle of 78°, acquisition matrix 88×88, 39 interleaved 3-mm thick axial slices, $2.5 \times 2.5 \times 3.0\ mm^3$ voxels, GRAPPA acceleration factor was equal to 2).

Deformable foam pads on both sides of the participant's head were used to diminish the influence of head movement and motion associated artifacts. Also, a real-time three-dimensional prospective acquisition correction algorithm was applied (Thesen et al. (2000)).

Image Processing: An FSL-based image (Jenkinson et al. (2012)) processing pipeline generally followed the Human Connectome Project guidelines (Smith et al. (2013)) and was implemented in Matlab 2013b (The Mathworks, Inc). Each of six functional scans was preprocessed using FSL (version 5.0.8) with mode 1000 normalization; z-scoring; detrending (6 motion regressors, brain global signal (GS), deep white matter (WM) and ventricular cerebral spinal fluid (CSF) signals, and their 9 derivatives); band-pass filtering (0.009 - 0.08 Hz); and regressing out 5 principal components of GS, WM and ventricular CSF signal (Power et al. (2012, 2014); Siegel et al. (2014)). A functionally-based whole brain parcellation into 278 brain regions of interest (ROIs) (Shen et al. (2013)) was applied to each subject's native space using nonlinear FSL registration separately for each BOLD scan. The voxel-wise time series were averaged for each of the 278 brain regions. Further analysis is performed using data from these time series. Each ROI was assigned to one of the resting-state networks (RSNs), with the division into 7 or 17 brain networks determined from the sample of 1000 healthy volunteers who took part in resting state fMRI scans (Yeo et al. (2011)). These networks were consistently observed within individuals. BOLD signals from brain regions located within the same network were found to be highly correlated, while the association between BOLD signals from brain regions located in different networks was low.

Estimation of functional connectivity

In this section, we give more detail introduction to estimation of dynamic functional connectivity. dFC assesses the dynamically changing association between two or more anatomically distinct time series. Correlation is the most popular FC metric and most commonly

characterized by an averaged over time pair-wise association referred to as "static" FC. To estimate modularity of the system, we use information from the estimated population-level correlation representation of dFC. Here dFC matrices are obtained in two steps. In the first step, subject- and scan-specific dFC is evaluated for each pair-wise combination of 278 brain regions. This was accomplished by applying recently developed bootstrap based technique (Kudela et al. (2017)) that implements multivariate linear process bootstrap (MLPB) (Jentsch et al. (2015)) and the sliding window technique. MLPB allows bootstrapping of the time series data, which is not possible with regular bootstrap methods. The sliding window technique enables calculation of dFC by sliding the window of pre-specified length and calculating Pearson correlation for observations from two time series which fall within a window. The combination of these two methods by first bootstrapping time series within adjacent blocks and then combining bootstrap samples into one realization and applying a sliding window technique, allows us to obtain a time-varying correlation estimate. This procedure is repeated 250 times. These subject-specific estimates of dFC and confidence intervals around it are calculated for each scan and each pair of brain regions by using the empirical quantiles of the distribution.

Details of this approach can be found in (Kudela et al. (2017)) with described procedure performed for each subject. Since the brain was parcellated into 278 regions, we obtain 38,503 ($= \frac{278*279}{2} - 278$) estimates of dynamic FC for each subject.

In the second step, we use generalized additive mixed models (GAMM) to combine information across subjects and scans, and to account for the experimental design. We use a GAMM implementation based on a correspondence between the penalized splines models and the best linear unbiased estimation of the random effects' parameters in the mixed models (Brumback et al. (1999); Durbán et al. (2005)).]. This correspondence enables estimation of highly complex models within a simple computational framework. Also, this

approach takes into account the experimental design by separately modeling subject- and scan-specific variability. As a result, we obtain an estimate of a population level dFC for each pair of regions and flavor. The details about penalized splines expressed in the form of semiparametric additive mixed models can be found in (Ruppert et al. (2003)).

Here, we considered three models. First, we investigated functional connectivity as a static measure across time (i.e., over the full scan period). Second, we modeled functional connectivity as a dynamically changing process. Third, we modeled functional connectivity allowing more variability on a subject-specific level. Proposed models can be represented as $dFC_{ijd} = f_d(t_j) + g_{id} + \varepsilon_{ijd}$, where a response variable dFC_{ijd} is the estimated dynamic FC for each subject i ($i = 1, \ldots, 24$); time point j denoted by $t_j = 1, \ldots, 105$ (identical for all subjects, with first 10 and last 10 time points dropped to accommodate the sliding window approach); and flavor d (d=B or G;for beer or Gatorade scans, respectively)). The population-level estimate for specific flavor d is expressed as function $f_d(t_j)$ and the subject-specific deviation from this estimate is expressed as g_{id}. Here, g_{id} is a sum of a subject-specific random intercept b_{i0} and nested within subject random scan effect a_{iS0}, where b_{i0} $N(0, \sigma^2_{(b_0)})$ and a_{iS0} $N(0, \sigma^2_{(a_0)})$ and $S = 1, 2, 3$ denotes a scan number for specific flavor. The measurement error is represented by ϵ_{ijd} $N(0, \sigma^2_\epsilon)$. The exact forms of these functions for each model as well as a population level form of the estimates for each flavor are listed in Table 4.2.

	beer $f_{w=B}(t)$	Gatorade $f_{w=G}(t)$	g_{iw}
M1	β_0	$\beta_0 + \gamma_0$	$b_{i0} + a_{is0}$
M2	$\beta_0 + \beta_1 t + \sum_{k=1}^{K} u_k z_k(t)$	$\beta_0 + \gamma_0 + (\beta_1 + \gamma_1)t + \sum_{k=1}^{K} u_k z_k(t) + \sum_{k=1}^{K^\star} w_k z_k(t)$	$b_{i0} + a_{is0}$
M3	$\beta_0 + \beta_1 t + \sum_{k=1}^{K} u_k z_k(t)$	$\beta_0 + \gamma_0 + (\beta_1 + \gamma_1)t + \sum_{k=1}^{K} u_k z_k(t) + \sum_{k=1}^{K^\star} w_k z_k(t)$	$b_{i0} + a_{is0} + \sum_{k=1}^{K} \nu_k z_k(t)$

Table 4.2: Models M1, M2, M3 for estimating dFC for each flavor and their difference.

$z_k(t)$ in Table 4.2 denotes basis function for penalized splines. In our approach, we used O'Sullivan penalized splines, which exhibit good properties such as numerical stability, a

generalization of smoothing splines and good boundary properties (Wand and Ormerod (2008)). Similar to the conventional splines method, we defined a set of knots $\kappa_1, \ldots, \kappa_K$ corresponding to the quantiles of time point distribution. The penalty controls the effect of too many nodes by shrinking the excessive coefficients towards zero (Ruppert et al. (2003)). In addition, this approach provides population- as well as subject-level estimates of dFC for each flavor.

Modularity

The dFC matrices calculated from penalized regression spline models can be equivalently represented in terms of graphs, with each graph comprised of nodes and edges. Here, nodes represent brain regions while edges indicate associations between pairs of brain regions. The larger FC between brain regions, the stronger is the edge between them. Here, we work with undirected graphs as the direction of an edge is not specified. First, we provide a brief summary of the terminology used in the modularity literature.

The degree of the node is the number of edges a particular node has with other nodes.

An adjacency matrix, A,, is used to represent a graph as a square matrix. Rows and columns represent graph nodes, while each matrix value indicates either the strength of an edge (a weighted adjacency matrix) or its existence (a binary adjacency matrix).

Modularity is a measure to quantify the partition into communities. It assesses a chance that particular division has a greater number of node-to-node connections within its communities than expected in a random null model (Fornito et al. (2016)). In a random null model, it is assumed that the same information about the number of nodes and degree of each node is available, but edges are linked to other nodes by chance.

In the binary case, modularity is defined as the observed proportion of the edges that fall within the given group of nodes minus the expected value of such a proportions if edges were randomly assigned. In our approach, we are using a signed FC matrix as an adjacency

matrix. Signed FC means that we allow FC to take positive and negative values. Therefore, we apply adapted version of modularity measure proposed Mucha et al. (2010), where the weighted adjacency matrix has a positive and a negative part. The observed edges and expected proportion of edges are calculated separately for both parts. The formal definition of the quality function,Q_{signed} proposed by Mucha et al. (2010) is:

$$Q_{signed} = \frac{1}{2m}\sum_{ij}(A_{ij}^{+} - A_{ij}^{-} - (\gamma^{+}\frac{k_i^{+}k_j^{+}}{2m^{+}} - \gamma^{-}\frac{k_i^{-}k_j^{-}}{2m^{-}}))\delta(g_i, g_j), \tag{4.1}$$

where A_{ij}^{+} and A_{ij}^{-} are parts of the network's adjacency matrix that contain only positive and negative value of dFC , respectively. k_i^{+} and k_i^{-} are positively and negatively associated node's degrees ($k = k^{+} + k^{-}$) and $2m = \sum_j k_j$; $\delta(g_i, g_j)$,is the Kronecker delta function that is equal to one when nodes come from the same community ($g_i = g_j$) and zero otherwise. γ^{+} and γ^{-} are two resolution parameters, which allow the importance of a random null model to be scaled separately for positive and negative associations. It should be noted that originally proposed quality function did not allow a detection of the communities of different sizes and that the inclusion of the resolution parameter γ was suggested by Arenas et al. (2006). By tuning the values of γ, we can detect communities of different sizes. Large modules are detected when $\gamma < 1$ while the modules with smaller number of nodes are detected when $\gamma > 1$. However, the resolution limitation still exists, and detection of modules of a specified size is unobtainable. The inclusion of γ^{+} and γ^{-} in Mucha et al. (2010) approach enabled generalization of the quality function to the case of weighted signed networks. In our case, we evaluated a wide range of gamma parameters from coarse- to fine-grained $\gamma = 0.1, 0.2, \ldots, 3$. As noted by Sporns and Betzel (2016), this approach gives a broader view of the modular network organization.

The division into modules that reaches the highest value of a quality function is considered to be the best estimate of network's community representation. The mechanism of

optimizing quality function Q_{signed} to obtain the best partition is called modularity maximization. Unfortunately, an analytical solution to this problem does not exist. However, different heuristic algorithms were proposed to uncover a partition with the highest value of a quality function. We use a Louvain algorithm introduced by Blondel et al. (2008), which optimizes modularity by implementing a hierarchical approach. It consists of two main steps. First, it divides the network into small communities that maximize modularity within the local groups of nodes. When modularity cannot be improved, the nodes assigned to the same community are aggregated and treated as vertices of a new smaller weighted graph. The procedure is repeated iteratively until the quality function reaches a maximum. This algorithm is popular due to its simplicity and speed, and it is appropriate for large graphs.

One of the drawbacks of the Louvain algorithm is its dependence on the order in which nodes are assigned to communities. As a consequence, one might obtain slightly different results from one run to the next. Consensus clustering is one of the methods proposed to give an accurate and stable solution out of all obtained partitions. In the solution proposed by Lancichinetti and Fortunato (2012), modularity maximization algorithm is run many times. For each pair of nodes a relative frequency of two particular nodes belonging to the same module is calculated. The result for each pair of nodes can be expressed as a consensus matrix. Also, the authors proposed to discard all entries of consensus matrix that fall below pre-specified threshold τ, , as those might be induced by a presence of very noisy vertices. Here, we used $\tau = 0.2$ following the author's guidance for Louvain method. Finally, the Louvain algorithm is run on the obtained consensus matrix. The whole algorithm is repeated until the final consensus matrix consists of only zeros and ones. Such results are more stable and give more accurate partition.

Dynamic modularity The methods discussed so far describe the static modularity structure of a network. As was pointed out in Section 3, assessing FC as a stationary measure across time provides only partial information about underlying changes in associations occurring in the brain (Chang and Glover (2010); Hutchison et al. (2013)). Therefore, we further applied the extension proposed by Mucha et al. (2010) to a time-varying estimate of dFC to characterize the community structure across time. The idea is similar to the static modularity case but now we introduce a new parameter C_{jrs}, which allows linking together equivalent nodes across the time points. The modularity quality function is now defined as (Mucha et al. (2010)):

$$Q_{signed} = \frac{1}{2\mu}\sum_{ijsr}\{(A^{+}_{ijs} - A^{-}_{ijs} - (\gamma^{+}\frac{k^{+}_{is}k^{+}_{js}}{2m^{+}_{s}} - \gamma^{-}\frac{k^{-}_{is}k^{-}_{js}}{2m^{-}_{s}}))\delta_{sr} + \delta_{ij}C_{jsr}\}\delta(g_{is}, g_{jr}), \quad (4.2)$$

where $(A^{+}_{ijs} - A^{-}_{ijs} - (\gamma^{+}\frac{k^{+}_{is}k^{+}_{js}}{2m^{+}_{s}} - \gamma^{-}\frac{k^{-}_{is}k^{-}_{js}}{2m^{-}_{s}}))\delta_{sr}$ is related to the static version of modularity for a given time point s. A^{+}_{ijs} and A^{-}_{ijs} are respectively positive and negative part of an adjacency matrix at time point s between brain regions i and j. k^{+}_{is} and k^{-}_{is} are positively and negatively associated nodes degree at a time point s. γ^{+} and γ^{-} are the resolution parameters corresponding to the positive and negative connections, respectively. Similar to the static modularity case, we investigated various gamma values and found that the resolution parameter value of two for positive and negative connections gave the partition that was the closest match to the commonly reported number of RSNs. The new term in the formula $\delta_i jC_{jsr}$ determines the level of coupling of brain regions i and j between adjacent time points s and r, keeping community labels across time consistent. At this time, there is no specific guideline to set the coupling parameter value. In our dFC application, we decided to keep it at the minimum level of 0.01 in order to minimally constrain the modularity changes in this task-based fMRI study. Preliminary investigation showed that higher

coupling values result in higher constraints on possibility of module change for consecutive time points. In the future research, we will seek to investigate this dependence in more details. Another new parameter is the strength of each node for each time point defined as $k_{js} = \sum_i (A^+_{ijs} + A^-_{ijs})$; where the strength of nodes across time points is $c_{js} = \sum_r C_{jsr}$ and the total strength of nodes $2\mu = \sum_{js}(k_{js} + c_{js})$. To compare the results and quantify the dynamic modularity both on the group- and subject-specific level for brain regions and networks, we implement a measure called cross-entropy or deviance. This metric is often used in the modern statistical methods to measure an error for classification problems and is defined as negative log-likelihood of a multinomial distribution (Wakefield (2013)):

$$H(X) = -\sum_x (p(x)\log(p(x)). \tag{4.3}$$

The cross-entropy provides a measure of module assignment uncertainty that was normalized to range between 0 and 1. It gives a single number summary for dynamic modularity and enable us to test for differences between flavors on a region and network basis by taking advantage of modularity analyses performed on the subject-specific estimates of dFC obtained from Model 2 (see Table 4.2). Specifically, subject- and flavor-specific dFC matrices are first extracted from Model 2 and used as a signed matrices in modularity analysis. As a result we obtain dynamic module assignment, which enable us to calculate cross-entropy for each subject, region and network. This single numerical summary for each subject and flavor is further used in statistical testing to see if there are significant differences between flavors and if an association with drinking-related variables exists. To adjust for multiple comparisons, we used false discovery rate correction (Bretz et al. (2011)). In the following section, we present a results of proposed analysis.

Results

In this section, we present the results of modularity analysis performed using static and dynamic FC. We start by summarizing the network level results for static modularity and then present the dynamic modularity results for networks and regions. Finally, we present the summary for associations with drink related variables. In both static and dynamic approaches, we assume that γ^+ and γ^- takes the same value.

Static modularity

We perform modularity analysis based on a population–level static estimate of FC. We first analyzed the behavior of the partition as a function of the resolution parameter γ, ranging from 0.1 to 3 in increments of 0.1. To facilitate the comparison of static and dynamic modularity findings, we assume that γ^+ and γ^- take the same value in both approaches.

Figure 4.2 depicts how the number of modules changes for each flavor (left panel) and how module assignment changes for brain regions (right panel) when the gamma parameter increases. For γ values in the range $0.2 - 1.5$ for beer (black curve) and $0.2 - 1.4$ for Gatorade (red curve), the number of modules is the same for both conditions. Interestingly, for a large range of gamma values $(0.2 - 1.4)$, there are three modules for both flavors, reminiscent of the three blocks of brain networks obtained for the same data set using a semiparametric estimation of dynamic functional connectivity on the population level presented in Section 4.3. For middle range of gamma values (γ is equal $1.6 - 2.3$ for beer and $1.5 - 2.2$ for Gatorade), the number of modules gradually increases and reaches 7 for beer and 6 for Gatorade. The brain region assignment remains consistent across a wide range of the γ values. However, for γ greater than 2.2, the number of modules increases quickly and differentially across flavors, making the division into modules less useful for the between-flavor comparisons. For gamma greater than 2.6 and 2.4 for beer and Gatorade,

respectively, the number of modules is almost equal to the number of brain regions, which does not provide any valuable information about communities of brain regions.

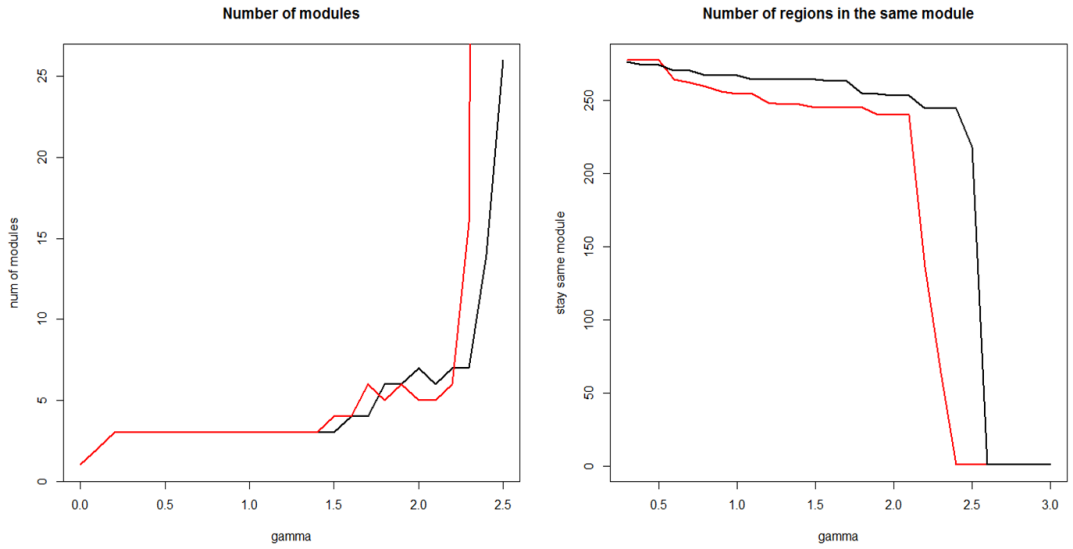

Figure 4.2: Community assignment as a function of the resolution parameter γ for static modularity. It is notable that a number of brain regions remaining within the same module stay fairly constant for a larger range of gamma values (up to 2.5) during beer scans while during Gatorade variability in the module assignments starts sooner ($\gamma > 2.2$). Black and red curves indicate beer and Gatorade scans, respectively.

We further investigated the $\gamma = 2.2$ result for both flavors. Here, we focused on a partition with a number of modules similar to a number of the known resting state networks and with the smallest number of sparse modules (modules containing only 1 or two regions). Due to limited cerebellar coverage that varied from subject to subject, the results for cerebellar regions are not further discussed in this work. Figure 4.3 illustrates the modular organization of brain regions for beer (left panel) and Gatorade (right panel) at a resolution parameter, $\gamma = 2.2$. Three main communities can be distinguished with a limited number of regions organized into small modules visible in the bottom right corners of both panels in Figure 4.3. Similar community structure is present for both flavors and includes: 1)

visual-subcortical, 2) somatomotor-attentional, and 3) frontoparietal-default mode network regions (shown in Figure 4.3 from top-left to bottom-right). The somatomotor-attentional network block of regions elicited by beer scans is split into two modules for Gatorade scans.

In Table 4.3, we present how selected partition relates to the 17 cortical network solutions from Yeo et al. (2011). Most of the brain regions were assigned into one of three (beer) and one of four modules (Gatorade). It should be noted that our approach is fully data-driven and uses the resting state networks only to relate the estimated task-based modularity to the known, biologically-meaningful brain organization.

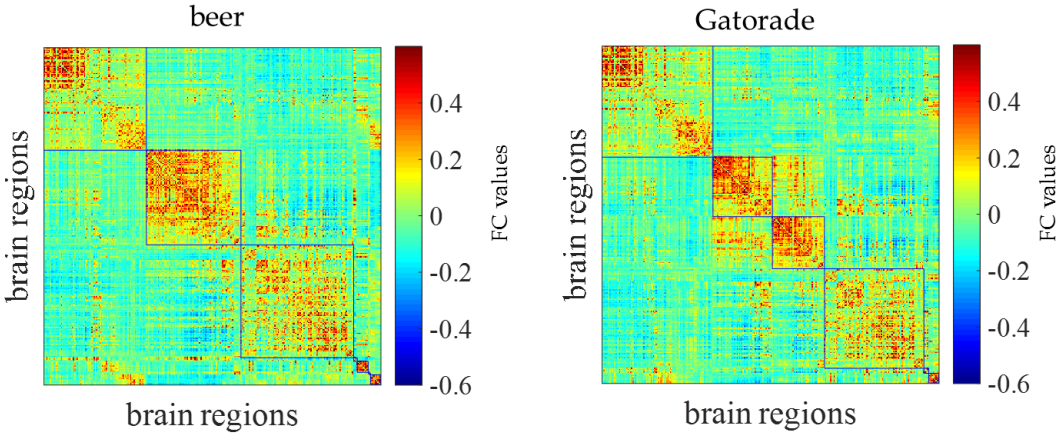

Figure 4.3: Modular organization of brain regions for the static FC for beer (left) and Gatorade (right) flavors using resolution parameter, $\gamma = 2.2$. The modules are denoted by rectangles, with 3 (out of 7 total) communities prominent during beer scans. Similarly, there are 4 (out of 6 total) prominent communities during Gatorade scans. The color bar indicates the Pearson's correlation coefficient value.

In summary, the static modularity yielded three predominant communities of brain regions that reflected pairing of known RSNs. The visual network module may reflect the visual cues of upcoming flavor stimulation, with somatomotor-attentional networks engaged during the task execution and the frontoparietal-default mode networks (FP-DMN) implicated in switching between task execution (i.e., flavor and water stimuli) and rest

	beer							Gatorade						
Network	1	2	3	4	5	6	7	1	2	3	4	5	6	Sum
Visual Associative	18	0	0	0	0	0	0	18	0	0	0	0	0	18
Visual Primary	13	0	0	0	0	0	0	13	0	0	0	0	0	13
SM Dorsal	0	18	0	0	0	0	0	0	17	1	0	0	0	18
SM Anteroventral	0	11	0	0	0	0	0	0	0	11	0	0	0	11
Posterior Attention	6	4	0	3	0	0	0	5	6	1	0	1	0	13
Dorsal Attention	0	10	0	0	0	0	0	0	8	2	0	0	0	10
Salience	0	14	1	0	0	0	0	0	3	12	0	0	0	15
Ventral Attention	0	3	6	0	0	0	0	0	2	2	5	0	0	9
Inferior Temporal	1	0	2	0	4	0	0	1	0	0	2	0	4	7
Orbitofrontal Cortex	0	0	9	0	0	0	0	0	0	0	9	0	0	9
Precuneus	3	1	1	0	0	0	0	3	1	0	1	0	0	5
Frontoparietal 1	3	3	11	0	0	0	0	3	4	2	8	0	0	17
Frontoparietal 2	0	2	12	0	0	0	0	0	5	0	9	0	0	14
Auditory	1	5	3	0	0	0	0	0	0	5	3	1	0	9
PCC/Parahippocampal	3	0	0	0	0	0	0	3	0	0	0	0	0	3
DMN 1	0	1	23	0	0	0	0	0	2	0	20	2	0	24
DMN 2	0	1	20	0	0	0	0	0	1	2	18	0	0	21
Subcortical	15	5	6	0	5	1	0	16	0	5	7	0	4	32
Cerebellar	22	0	0	0	0	0	8	30	0	0	0	0	0	30
Total	85	78	94	3	9	1	8	92	49	43	82	4	8	278

Table 4.3: Assignment of 278 brain regions from Shen et al. (2013) during beer and Gatorade scans across modules and brain networks (17 cortical networks from Yeo et al. (2011), as well as subcortical and cerebellar regions for completeness). PCC = Posterior Cingulate Cortex, SM = Somatomotor, DMN = Default Mode Network.

periods. Table 2 illustrates that participation of brain networks in given modules is similar for both flavors. For example, module 1 engages the same number of visual networks regions and very similar number of regions from the other networks. This similarity is also observed for the somatomotor-attention related block (module 2 for beer and modules 2 and 3 for Gatorade). Module 3 for beer and module 4 for Gatorade involve the frontoparietal and default mode networks with a notable presence of reward-related orbitofrontal and subcortical areas. This finding suggests an association of gustatory stimuli to brain systems known to deactivate during the tasks and to be involved in autobiographical memory (DMN) as well as the selection of sensory contents by attention (FP network) (Ptak (2012)).

Dynamic modularity

We used a population-level time-varying estimate of dFC, defined in Section 3, and the modularity quality function, $Q_{multislice}$" to characterize the community structure across time on a population level. Similarly to the static modularity case, for gamma values exceeding 2.2, the number of modules quickly increases as a function of γ reaching the number of brain regions. Here, we use a resolution parameter $\gamma = 2.0$ facilitating flavor comparison while maintaining desired spatial resolution.

Figure 4.4 illustrates the modularity as a function of time during the beer and Gatorade scans (left and right panels, respectively) that was estimated using dFC obtained on a population level. The number of time points corresponds to 105 BOLD volume acquisitions, with the first and last 10 volumes (out of 125 acquired for each scan) excluded to accommodate the sliding window approach. The brain regions are ordered according to the 17 RSNs solution of Yeo et al. (2011), with subcortical and cerebellar networks included for completeness. We found five modules for beer and seven for Gatorade condition, with the module membership indicated by a color bar. It is evident that many regions stay in the same module across time during the scans, while for others the module assignment varies across time.

For each of the resting state networks and flavor, we calculated the entropy, the longest and shortest number of consecutive time points that region stayed in the module, and the most dominant module (i.e., module present for most time points within a scan). Similarly to the static modularity solution, we found three main communities consisting of: 1) visual-subcortical, 2) somatomotor-attentional, and 3) frontoparietal and default mode networks. The results presented in Table 4.4 reflect large scale population and network-level effects during gustatory task performance. The biggest difference in entropy between flavors can be found in the posterior attention, inferior temporal, frontoparietal, default

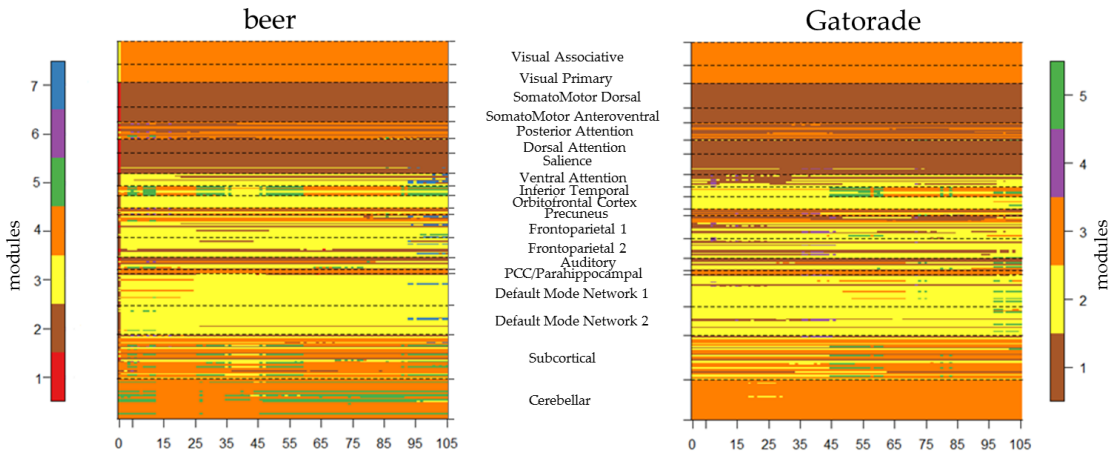

Figure 4.4: Dynamic modularity for beer flavor and Gatorade scans (left and right panels, respectively), with the resolution parameter, $\gamma = 2.0$ and organized according to the resting state networks (Yeo et al. (2011)).

mode, and subcortical networks. These findings likely reflect task-related network activity in a visually-cued paradigm with salient flavor stimuli dynamically affecting somatosensory, visual-association and reward-related areas, with the task-rest switching evident in the frontoparietal and default mode networks .

Table 4.5 presents the number of brain regions by number of unique modules encountered by region through time for beer and Gatorade flavor. For beer flavor, some regions change module only between the first and the second time point, remaining at the same module through all other time points. In such a case we classified these time series as staying in one module across time. We have noticed that for both flavors 75% of all regions stay in the same module across time. Of these regions, 67% are common between flavors.

	beer				Gatorade			
Brain Networks	min	max	main	Ent.	min	max	main	Ent.
Visual Associative	2	2	4	0.08	1	1	3	0
Visual Primary	2	2	4	0.08	1	1	3	0
SomatoMotor Dorsal	2	2	2	0.08	1	1	1	0
SomatoMotor Anteroventral	2	2	2	0.08	1	1	1	0
Posterior Attention	1	5	4	0.47	1	3	1	0.62
Dorsal Attention	2	2	2	0.08	1	1	1	0
Salience	2	4	2	0.18	1	3	1	0.17
Ventral Attention	2	3	3	0.65	1	3	2	0.68
Inferior Temporal	1	3	4	0.98	1	3	2	0.9
Orbitofrontal Cortex	2	2	3	0.08	1	2	2	0.07
Precuneus	2	4	4	0.6	1	4	3	0.63
Frontoparietal 1	2	5	3	0.57	1	3	2	0.67
Frontoparietal 2	1	3	3	0.38	1	3	2	0.51
Auditory	2	4	2	0.58	1	3	1	0.68
PCC/Parahippocampal	1	2	4	0.03	1	1	3	0
Default Mode Network 1	1	3	3	0.18	1	3	2	0.31
Default Mode Network 2	1	3	3	0.17	1	3	2	0.3
Subcortical	1	5	4	0.59	1	3	3	0.67
Cerebellar	1	3	4	0.48	1	2	3	0.05

Table 4.4: Summary of population level dynamic modularity across 17 cortical brain networks (Yeo et al. (2011)), subcortical and cerebellar regions. Ent. = Entropy, PCC = Posterior Cingulate Cortex.

Testing dynamic modularity

In order to perform statistical testing, for each subject we calculated the entropy of the dynamic modularity at the network and region of interest levels. To reduce high between-subject variability at a finer spatial resolution ($\gamma = 2$), we set the resolution parameter to $\gamma = 1$ resulting in more stable dFC estimates, analogous to the spatial smoothing procedure often performed in fMRI. Table 4.6 presents the between flavor results at the network level using the paired t-statistic test after adjusting for multiple comparisons. We found a significant ($p_{FDR} < 0.05$) between-flavor difference in entropy in the orbitofrontal cortex (OFC), somatomotor and lateral default mode networks, The results for the dorsal attention network are just above the boundary of significance. Similarly to static modularity case, we did not consider cerebellar regions due to the limited fMRI acquisition coverage. Networks

♯ of modules per time series	Gatorade	beer
1	209	208
2	29	42
3	39	24
4	1	4
Sum	278	278

Table 4.5: Number of distinct modules which were assigned for brain region across time for each flavor.

with significant findings in Table 4.6 are visualized on Figure 4.5. All presented networks had higher entropy for Gatorade compared to beer.

Network	t-statistic	p_{FDR}
Visual Associative	1.85	0.133
Visual Primary	2.15	0.089
SomatoMotor Dorsal	-3.18	0.038
SomatoMotor Anteroventral	-2.91	0.038
Posterior Attention	-1.87	0.133
Dorsal Attention	-2.65	0.053
Salience	-0.87	0.438
Ventral Attention	1.19	0.333
Inferior Temporal	-2.29	0.084
Orbitofrontal Cortex	-3.68	0.019
Precuneus	-1.22	0.333
Frontoparietal 1	-0.97	0.404
Frontoparietal 2	-2.2	0.089
Auditory	-0.63	0.567
PCC/Parahippocampal	0.31	0.758
Default Mode Network 1	-1.43	0.261
Default Mode Network 2	-2.88	0.038
Subcortical	-1.14	0.336
Cerebellar	2.56	0.054

Table 4.6: Difference in entropy between beer and Gatorade for the resting state networks. Paired t-statistic test values (negative sign indicate higher entropy for Gatorade) and associated significance using the FDR-adjusted correction for multiple comparisons are provided.

In addition to these network-level results, we also performed statistical testing on the entropy values of all 278 brain regions. Figure 4.6 and Table 4.7 show regions that responded differentially to flavors using a paired t-test and adjusting for multiple comparisons. The

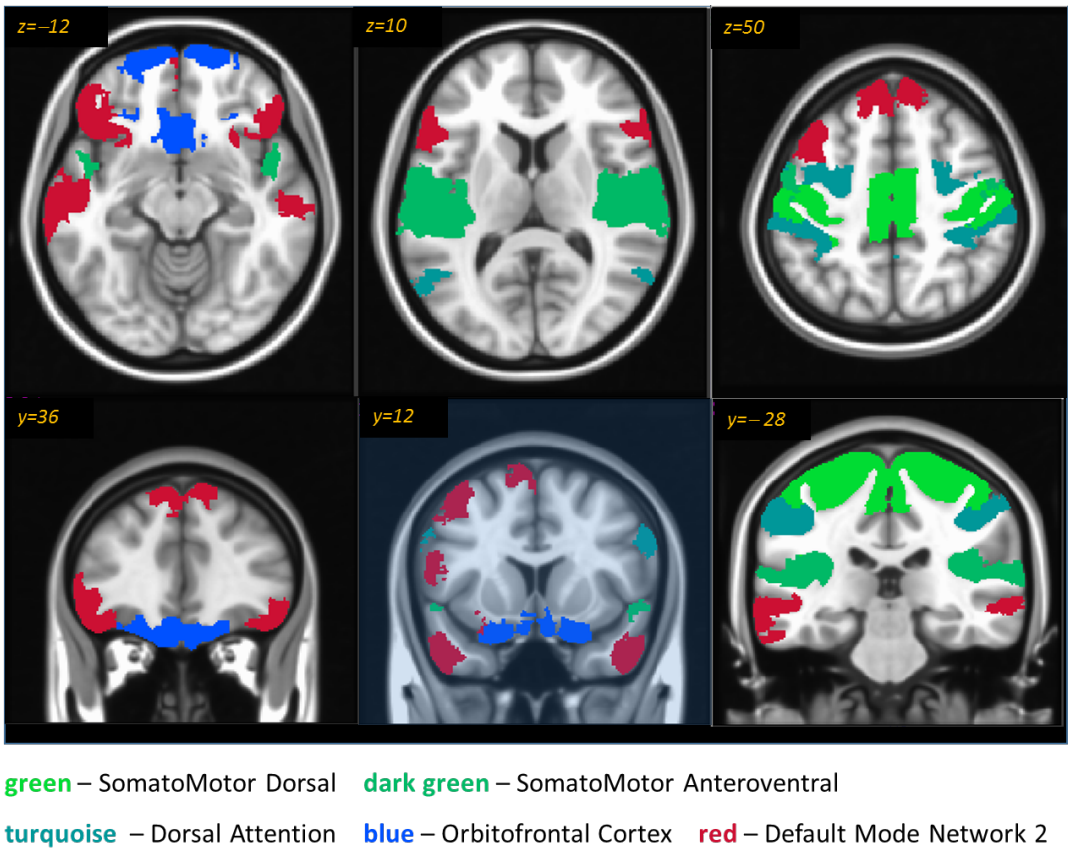

Figure 4.5: Visualization of the cortical networks (Yeo et al. (2011)) with entropy significantly higher during the Gatorade than beer scans. MNI coordinates of axial and coronal slices (top and bottom rows, respectively) are indicated in the top left corners of each panel.

t-statistic values are negative, which indicates higher entropy during the Gatorade scans compared to beer scans. Some of the significant regions are consistent with the regions found in previous study. Figure 4.7 presents side-by-side comparison of these findings and brain activations reported in an earlier study (Oberlin et al. (2016), included with permission).

Subjective Ratings

We also tested associations between the entropy values for significant regions under both flavors and subjective ratings, and two drinking measures: total number of drinks per drinking day within 35 days, and total number of heavy drinking days within 35 days.

region number	Brain region	Lobe	Network	t-statistic	p_{FDR}
3	Right Medial Frontopolar OFC	Frontal	Orbitofrontal	-3.41	0.043
4	Right Postcentral Gyrus	Frontal	Somatomotor	-4.14	< 0.001
45	Right Paracentral Lobule	Parietal	Somatomotor	-3.57	0.043
74	Right Caudolateral OFC	Frontal	Orbitofrontal	-3.6	0.035
134	Right Rostrolateral OFC	Frontal	Frontoparietal	-3.89	0.035
145	Left Inferior Frontal Gyrus p. T	Frontal	Frontoparietal	-5.59	< 0.001
154	Left Pre- and Post-central Gyrus	Frontal/Parietal	Somatomotor	-3.9	0.035
161	Left Dorsal ACC/BA24 & 32	Frontal	Default Mode	-3.51	0.043
187	Left Superior Medial Gyrus	Frontal	Frontoparietal	-3.87	0.035
209	Left Lateral OFC	Frontal	Frontoparietal	-3.99	0.035
242	Left Precentral Gyrus/MFG	Frontal	Dorsal Attention	-3.4	0.043
255	Left Dorsal Paracentral Lobule	Parietal	Somatomotor	-3.84	0.035
263	Left Caudate Head	Subcortical	Subcortical	-3.49	0.043

Table 4.7: Brain regions (Shen et al. (2013)) differentially responding to beer and Gatorade. The significance was established using a paired $t-test$, with p values adjusted for multiple comparisons using FDR-based correction. ACC - Anterior Cingulate Cortex, MFG - Middle Frontal Gyrus, BA - Brodmann Area.

First, we investigated if there were any differences between flavors for subjective ratings. Similarly to Oberlin et al. (2016), the flavors of Gatorade and beer were rated as more intense than water in our sample of 24 subjects (middle panel Figure 4.8, results adjusted for multiple comparisons). Gatorade was rated as more pleasant than water, while differences in pleasantness of beer and water were not significant (Figure 4.8, left). As compared to water, beer scans resulted in significantly higher wanting of beer and desire to drink (Figure 4.8, right). Also, compared to Gatorade beer scans resulted in significantly greater wanting of beer.

For beer scans, we found associations of the entropy with: 1) intensity of beer flavor in the right postcentral gyrus (Shen ID=4, $t = 2.99$, $p = 0.007$), right paracentral lobule (ID=45, $t = 2.67$, $p = 0.014$), left precentral/middle frontal gyri (ID=242, $t = 3.11$, $p = 0.005$), left dorsal paracentral lobule (ID=255, $t = 2.49$,$p = 0.021$), 2) total drinks in the left dorsal paracentral lobule (ID=255, $t = 2.49$, $p = 0.016$), and 3) total drinks per drinking day in the right rostrolateral OFC (ID=134, $t = 2.22$, $p = 0.037$). For Gatorade scans,

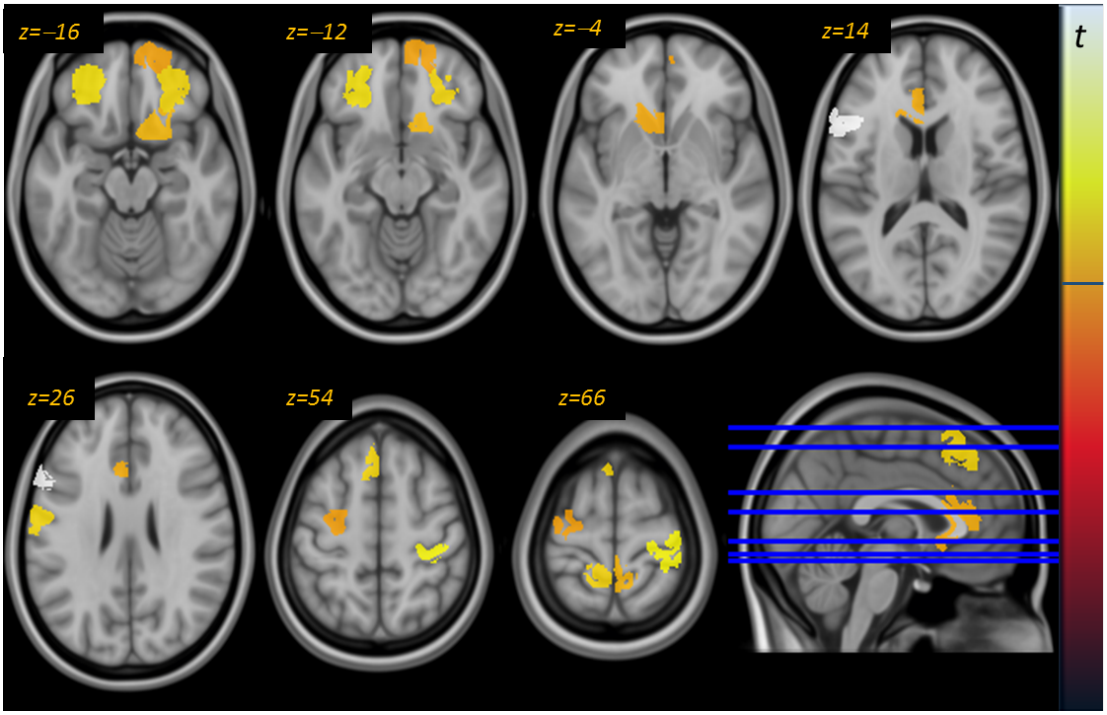

Figure 4.6: Regions with significantly higher entropy for Gatorade than beer (Table 6, $p < 0.05$, FDR-corrected for multiple comparisons). Reward-sensitive orbitofrontal and striatal regions are prominent for $z < 0$ slices. There were no significant regions in the *beer* > *Gatorade* comparison. MNI coordinates are indicated in the top left corners of each panel. Color bar indicates t-statistic value, with horizontal line indicating value corresponding to $p_{FDR} = 0.05$.

the associations of the entropy were observed with: 1) pleasantness in the right medial frontopolar OFC (ID=3, $t = 2.83$, $p = 0.01$), 2) total drinks in the right postcentral gyrus (ID=4, $t = 2.26$, $p = 0.034$), right rostrolateral OFC (ID=134, $t = 2.21$, $p = 0.038$), left dorsal paracentral lobule (ID=255, $t = 3.40$, $p = 0.003$), 3) total drinks per drinking days in the right caudolateral and rostrolateral OFC (ID=74 and 134, $t = 2.45$, $p = 0.023$ and $t = 3.82$, $p = 0.001$, respectively), left dorsal paracentral lobule (ID=255, $t = 2.83$, $p = 0.01$), and 4) total heavy drinking days in the left dorsal paracentral lobule (ID=255,

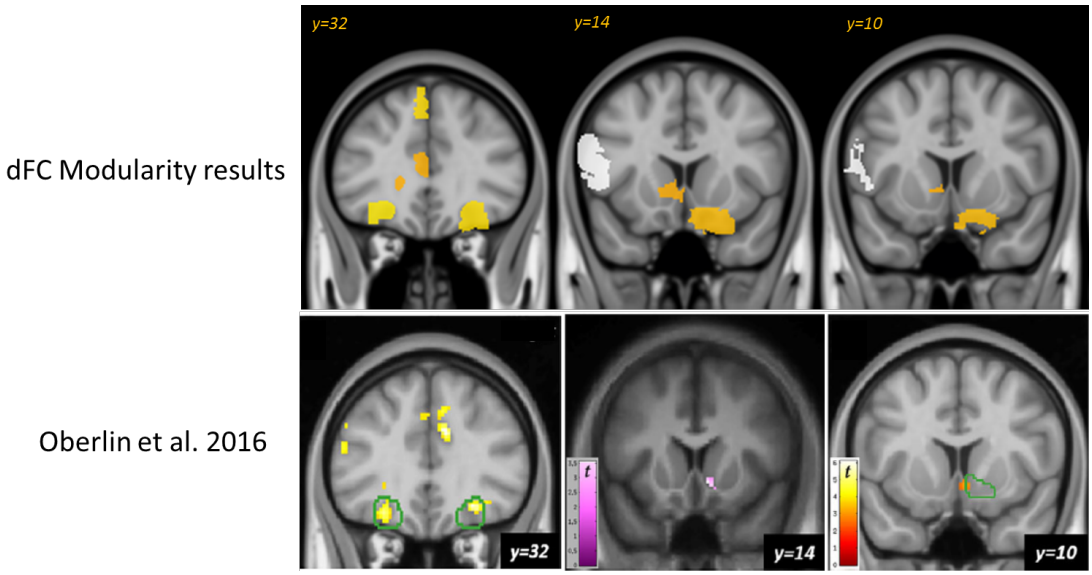

Figure 4.7: Regions with significant difference in entropy (top row) compared to published results by Oberlin et al. (2016). MNI coordinates of coronal slices are indicated in the top left corners of first row and lower right corner in the bottom row.

$t = 2.44$, $p = 0.023$). Due to a limited sample size, p-values for these associations were not adjusted for multiple comparisons.

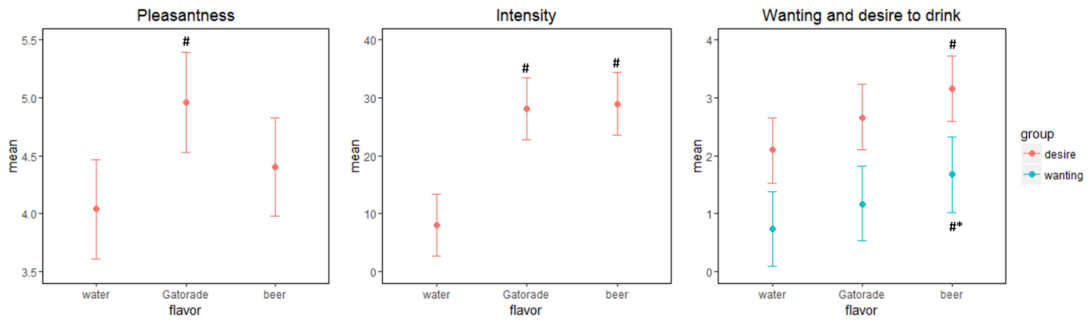

Figure 4.8: Subjective ratings with confidence intervals for pleasantness, intensity, wanting and desire to drink averaged across scans of the same flavor (detailed in Oberlin et al. (2016)). Beer pleasantness was lower than for Gatorade and higher than for water but neither of these effects was significant (left panel). Beer and Gatorade were regarded as similarly intense and both were significantly different from water (middle panel). The flavor of beer increased wanting for beer and desire to drink. Beer wanting was significantly greater than wanting water and Gatorade. The desire to drink was significantly greater for beer as compared to water but not Gatorade. Subjects rated water before scanning. $\sharp p < 0.05$ compared to water, $\star p < 0.05$ compared to Gatorade.

Discussion

Modularity is one of the measures to characterize networks. In this work, we proposed a novel combination of the statistical, network and brain imaging methods to analyze modularity in task–based experiments. We combined: 1) a recently developed bootstrap-based technique to assess dFC on subject level; 2) penalized splines within the framework of additive mixed models to obtain population-level estimate of dFC and account for the experimental design; and finally 3) Mucha et al. (2010) quality function and Louvain algorithm. We applied this strategy to the dFC matrices to obtain gray matter partitions into communities that are tightly connected inside of the community and sparsely outside of it.

We related our findings with the known resting state networks (RSN). The static and dynamic modularity analysis yielded functional modules that were generally comprised of

2-3 known resting state networks contained within each of the derived modules. The brain regions' grouping derived from this task-based study of only 24 subjects to a large extent comported with the resting state network organization. It should be noted that our approach is fully data-driven and uses the RSNs only to relate the estimated task-based modularity to the known brain organization. The resemblance suggests that modularity analysis using dFC can uncover similar brain architecture in a modest sample of subjects performing the gustatory task fMRI.

The three main communities in both statically and dynamically-derived modularity approaches consisted of 1) visual and subcortical, 2) somatomotor-attentional, and 3) frontoparietal and default mode networks. However, some of these modules, such as the visual-subcortical do not change much and are well described within the static modularity. For some of the regions located within frontoparietal, default mode, and attentional networks we do observe module assignment changes as one would expect in a task-based gustatory fMRI study, where task execution is accompanied by the attentional shifts that engage executive function and induce switching between the resting and active time periods.

To summarize the between-flavor differences, for each region and network we calculated the entropy and used information from all subjects to perform the statistical testing. Our results suggest that flavor differences were present in many regions dedicated to gustatory stimulation and involved somatomotor areas that were also associated with subjective ratings and drinking measures. In addition, frontal lobe and orbitofrontal regions implicated in executive control, attention and reward (such as lateral OFC) were also prominent and similarly exhibited associations with the drinking measures. Due to the modest data sample, these results should be viewed as preliminary and need to be reproduced in a larger cohort that would better accommodate the testing of multiple associations. Therefore, more

detailed interpretation of presented associations should be left for the follow-up investigations.

Most notably, flavor-specific involvement of reward-related orbitofrontal regions that was observed using our methodology does comport with a subset of the previously published results in Oberlin et al. (2016). This latter study used very different methodology, with a general linear model (GLM) deconvolving responses of beer and Gatorade from neutral water baseline. Such an approach detects "activation" of segregated brain areas rather than changes of the dynamic functional connectivity throughout the whole gustatory scan. Therefore, comparing these two methods is not straightforward. Another difference is that the GLM is run on the voxel-wise level, while this work was performed by averaging time series over predefined brain regions. The GLM findings reported in subcortical areas would be harder to detect because the selected brain parcellation is too coarse and reduces our sensitivity in the ventral striatal areas reported in the study by Oberlin et al. (2016). Finally, the sliding window approach used in estimating dFC effectively smoothed the time series preventing beer and Gatorade flavor comparisons to the water baseline. Thus, all our results incorporate water trials, potentially diminishing the reported flavor differences.

Nevertheless, our findings indicate the importance of several networks and regions implicated in the alcohol cue response. Interestingly, we found that significant regions show higher values of entropy for Gatorade compared to beer. In other words, brain regions tend to stay at the same modules more often for the beer scans than for the Gatorade scans. While somewhat unexpected, this result could be driven by several factors. It is feasible that the reward-related regions such as orbitofrontal cortex and ventral-striatal areas would exhibit more sustained response in these social-to-heavy drinkers as indicated by their ratings of wanting for beer and desire to drink. The latter observation could not be tested in the GLM framework where responses to each trial are modeled using a standard hemodynamic

response function. It is also feasible that sensory properties of the two flavors, while rated as equally intense, are not completely matched. For example, differences in acidity could explain more variability during Gatorade scans, where Gatorade-to-water contrast would be stronger than beer-to-water contrast during beer scans. Such effect would presumably mostly affect the sensorimotor areas but could conceivably also impact other networks. Gatorade was also slightly more pleasant than beer and water but effects of pleasantness would more likely be focused in a smaller number of regions separate from those observed in Oberlin et al. (2016).

Both, the dynamic and static modularity analysis require a specification of resolution parameter, γ . Here we investigated how module assignments change for different values of γ to get a broader insight into a modular organization of the brain function. Currently, there is no "prescription" to select an optimal value of γ. However, we determined that over a large range of γ values, a solution does not change considerably. The second parameter that needs to be specified, but only in the dynamic modularity analysis is the coupling parameter C_{jsr}. We used a single small value of the coupling parameter to best preserve information about modules across all time points. It is reasonable to assume that this parameter might depend on the study design (task vs. rest), desired spatial resolution (larger or smaller modules), as well as the sample studied (clinical population vs. healthy control). To the best of our knowledge , there is no formal procedure to specify this parameter value - rather one might need to perform a multi-parameter optimization. In the future work, we will investigate the coupling parameter values that are most appropriate for the functional connectivity of the brain. In summary, we quantified changes in functional connectivity during the gustatory task fMRI using state-of-the-art brain network modularity approach in combination with applications of modern statistical methodology. The techniques developed here provide a novel analytical framework to discover both task-based and resting state FC properties.

Chapter 5

Summary

One of the most widely used, non-invasive techniques to study brain activity is functional magnetic resonance imaging (fMRI). Such data are frequently used to study functional connectivity (FC), a statistical association among two or more anatomically distinct fMRI signals (Friston (1994)). FC has emerged in recent years as a valuable tool for providing a deeper understanding of neurodegenerative diseases, neuropsychiatric and substance abuse disorders. Information about complex association structure in high-dimensional fMRI data is often discarded by a calculating an average across complex spatiotemporal processes without providing its uncertainty measure.

In the first part of the dissertation, a nonparametric approach to quantify the uncertainty of dynamic FC (dFC) estimates was proposed. Currently, the most common strategy for estimating dFC is to use the sliding-window technique. However, its greatest shortcoming is the inherent variation present in the estimate, even for null data, which is easily confused with true time-varying changes in connectivity Lindquist et al. (2014). This can have serious consequences as even spurious, noise-induced fluctuations can be easily confused with a signal of interest. For these reasons, assessment of uncertainty in the sliding-window correlation estimates is of critical importance. Here, we proposed a new approach to assess the uncertainty of a dynamic FC estimate by providing its confidence bands. Our method is based on three components: an extension of a bootstrapping method for multivariate time series, introduced by Jentsch et al. (2015); sliding window correlation estimation; and kernel smoothing. Through series of simulation studies and an application to resting state fMRI data we showed the efficacy of the proposed method.

In the second part of the dissertation, we proposed a two-step approach to analyze and summarize dFC estimates from a task-based fMRI study of social-to-heavy alcohol drinkers

during a stimulation with beer and Gatorade flavors. In the first step, we applied the method proposed in Section 3 to estimate dFC for each region-subject combination. In the second step, we used semiparametric additive mixed models to account for the complex correlation structure and model dFC on a population level taking into account the study's experimental design. We proposed to use a proportion of the time points during a scan when the confidence intervals exclude zero (positive and negative non-zero coverage) as a summary measure for a large number of pairwise comparisons. Our dFC analysis of the gustatory task fMRI data yielded functional modules closely resembling known resting state networks (Yeo et al. (2011)), reflecting a common functionally-based brain organization. We found increased positive association in reward-related regions of interest: ventral striatum (VST), lateral orbitofrontal cortex, and ventral anterior insula (vAI). In addition, we independently confirmed the enhancement of right VST-vAI association reported as the main activation-based finding in Oberlin et al. (2016). Most notably, proposed statistical approach to dFC analysis accounted for a complex structure of the data and experimental design uncovering numerous associations undetected by the traditional static FC analysis.

In the third part of the dissertation, we proposed to utilize the estimated dFC for the gustatory fMRI data to study the brain's modularity - a measure of mutually exclusive division of brain regions into blocks with intra-connectivity greater than the one obtained by chance. Specifically, we fist estimated dFC by applying methods from Section 3 and then to study the brain's modularity and incorporate the dFC information, we optimized the quality function (see Mucha et al. (2010)) by using the Louvain algorithm. The dynamic modularity was calculated at a network and a region level for the whole group and all subjects individually. We discovered at a network level three predominant communities: 1) visual-subcortical, 2) somatomotor-attentional, and 3) frontoparietal-default mode network regions. To summarize and compare the community assignment results for each flavor, we

proposed to use an entropy - a measure of uncertainty of community assignment. We found that the entropy measure was significantly greater for Gatorade than beer in orbitofrontal, somatomotor, and default mode networks. This finding was reproduced regionally, with reward-related orbitofrontal and ventrostriatal regions also implicated in the alcohol cue response (Oberlin et al. (2016)). In summary, we quantified changes in dynamic functional connectivity during the gustatory task fMRI using the state-of-the-art brain network modularity approach in combination with applications of modern statistical methodology.

The main contribution of this work is in its unique blending of complex methodology from the fields of statistics, machine learning and network theory to provide statistical tools for studying dynamic brain connectivity from a holistic, multi-disciplinary perspective. The proposed approach assesses uncertainty and quantifies changes in dFC. The techniques developed here provide a novel analytical framework for a discovery of previously hidden associations in task and resting state time series data.

Bibliography

Allen, E. A., E. Damaraju, S. M. Plis, E. B. Erhardt, T. Eichele, and V. D. Calhoun (2012). Tracking whole-brain connectivity dynamics in the resting state. *Cerebral cortex*, bhs352.

Amico, E., D. Marinazzo, C. DiPerri, L. Heine, J. Annen, C. Martial, M. Dzemidzic, S. Laureys, and J. Goñi (2016). Mapping the functional connectome traits of levels of consciousness. *arXiv preprint arXiv:1605.03031*.

Arenas, A., A. Diaz-Guilera, and C. J. Pérez-Vicente (2006). Synchronization reveals topological scales in complex networks. *Physical review letters 96*(11), 114102.

Beckmann, C. F., M. DeLuca, J. T. Devlin, and S. M. Smith (2005). Investigations into resting-state connectivity using independent component analysis. *Philosophical Transactions of the Royal Society of London B: Biological Sciences 360*(1457), 1001–1013.

Benjamini, Y. and D. Yekutieli (2001). The control of the false discovery rate in multiple testing under dependency. *Annals of statistics*, 1165–1188.

Blondel, V. D., J.-L. Guillaume, R. Lambiotte, and E. Lefebvre (2008). Fast unfolding of communities in large networks. *Journal of statistical mechanics: theory and experiment 2008*(10), P10008.

Bolt, T., J. S. Nomi, M. Rubinov, and L. Q. Uddin (2017). Correspondence between evoked and intrinsic functional brain network configurations. *Human Brain Mapping*.

Bretz, F., T. Hothorn, P. H. Westfall, et al. (2011). *Multiple comparisons using R*. CRC Press Boca Raton.

Brumback, B. A., D. Ruppert, and M. P. Wand (1999). Comment on "variable selection and function estimation in additive nonparametric regression using a data-based prior". *Journal of the American Statistical Association 94*, 794–797.

Buckner, R. L., J. R. Andrews-Hanna, and D. L. Schacter (2008). The brain's default network. *Annals of the New York Academy of Sciences 1124*(1), 1–38.

Calhoun, V., M. Yaesoubi, B. Rashid, and R. Miller (2013). Characterization of connectivity dynamics in intrinsic brain networks. In *Global Conference on Signal and Information Processing (GlobalSIP), 2013 IEEE*, pp. 831–834. IEEE.

Calhoun, V. D., T. Adali, G. D. Pearlson, and J. Pekar (2001). A method for making group inferences from functional mri data using independent component analysis. *Human brain mapping 14*(3), 140–151.

Chai, X. J., A. N. Castañón, D. Öngür, and S. Whitfield-Gabrieli (2012). Anticorrelations in resting state networks without global signal regression. *Neuroimage 59*(2), 1420–1428.

Chang, C. and G. H. Glover (2010). Time–frequency dynamics of resting-state brain connectivity measured with fmri. *Neuroimage 50*(1), 81–98.

Congdon, E., J. A. Mumford, J. R. Cohen, A. Galvan, A. R. Aron, G. Xue, E. Miller, and R. A. Poldrack (2010). Engagement of large-scale networks is related to individual differences in inhibitory control. *Neuroimage 53*(2), 653–663.

Contreras, J. A., J. Goñi, S. L. Risacher, E. Amico, K. Yoder, M. Dzemidzic, J. D. West, B. C. McDonald, M. R. Farlow, O. Sporns, et al. (2016). Cognitive complaints in older adults at risk for alzheimer's disease are associated with altered resting-state networks. *Alzheimer's & Dementia: Diagnosis, Assessment & Disease Monitoring*.

Coupé, P., J. V. Manjón, E. Gedamu, D. Arnold, M. Robles, and D. L. Collins (2010). Robust rician noise estimation for mr images. *Medical image analysis 14*(4), 483–493.

Coupé, P., P. Yger, S. Prima, P. Hellier, C. Kervrann, and C. Barillot (2008). An optimized blockwise nonlocal means denoising filter for 3-d magnetic resonance images. *IEEE transactions on medical imaging 27*(4), 425–441.

Cribben, I., R. Haraldsdottir, L. Y. Atlas, T. D. Wager, and M. A. Lindquist (2012). Dynamic connectivity regression: determining state-related changes in brain connectivity. *Neuroimage 61*(4), 907–920.

Cribben, I., T. D. Wager, and M. A. Lindquist (2013). Detecting functional connectivity change points for single-subject fmri data. *Frontiers in computational neuroscience 7*.

Cribben, I. and Y. Yu (2016). Estimating whole-brain dynamics by using spectral clustering. *Journal of the Royal Statistical Society: Series C (Applied Statistics)*.

Debener, S., M. Ullsperger, M. Siegel, and A. K. Engel (2006). Single-trial eeg–fmri reveals the dynamics of cognitive function. *Trends in cognitive sciences 10*(12), 558–563.

Doucet, G., M. Naveau, L. Petit, L. Zago, F. Crivello, G. Jobard, N. Delcroix, E. Mellet, N. Tzourio-Mazoyer, B. Mazoyer, et al. (2012). Patterns of hemodynamic low-frequency oscillations in the brain are modulated by the nature of free thought during rest. *Neuroimage 59*(4), 3194–3200.

Durbán, M., J. Harezlak, M. Wand, and R. Carroll (2005). Simple fitting of subject-specific curves for longitudinal data. *Statistics in medicine 24*(8), 1153–1167.

Filippini, N., B. J. MacIntosh, M. G. Hough, G. M. Goodwin, G. B. Frisoni, and S. M. e. a. Smith (2009). Distinct patterns of brain activity in young carriers of the apoe-ε4 allele. *Proceedings of the National Academy of Sciences 106*(17), 7209–7214.

Fornito, A., A. Zalesky, and M. Breakspear (2015). The connectomics of brain disorders. *Nature Reviews Neuroscience 16*(3), 159–172.

Fornito, A., A. Zalesky, and E. Bullmore (2016). *Fundamentals of brain network analysis*. Academic Press.

Fortunato, S. (2010). Community detection in graphs. *Physics reports 486*(3), 75–174.

Fox, M. D., A. Z. Snyder, J. L. Vincent, M. Corbetta, D. C. Van Essen, and M. E. Raichle (2005). The human brain is intrinsically organized into dynamic, anticorrelated functional networks. *Proceedings of the National Academy of Sciences of the United States of America 102*(27), 9673–9678.

Friston, K. J. (1994). Functional and effective connectivity in neuroimaging: a synthesis. *Human brain mapping 2*(1-2), 56–78.

Friston, K. J. (2011). Functional and effective connectivity: a review. *Brain connectivity 1*(1), 13–36.

Girvan, M. and M. E. Newman (2002). Community structure in social and biological networks. *Proceedings of the national academy of sciences 99*(12), 7821–7826.

Green, B. G., P. Dalton, B. Cowart, G. Shaffer, K. Rankin, and J. Higgins (1996). Evaluating the 'labeled magnitude scale'for measuring sensations of taste and smell. *Chemical senses 21*(3), 323–334.

Greicius, M. D., B. Krasnow, A. L. Reiss, and V. Menon (2003). Functional connectivity in the resting brain: a network analysis of the default mode hypothesis. *Proceedings of the National Academy of Sciences 100*(1), 253–258.

Hagmann, P., L. Cammoun, X. Gigandet, R. Meuli, C. J. Honey, V. J. Wedeen, and O. Sporns (2008). Mapping the structural core of human cerebral cortex. *PLoS Biol 6*(7), e159.

Handwerker, D. A., V. Roopchansingh, J. Gonzalez-Castillo, and P. A. Bandettini (2012). Periodic changes in fmri connectivity. *Neuroimage 63*(3), 1712–1719.

Hastie, T., R. Tibshirani, and J. Friedman (2009). *The Elements of Statistical Learning: Data Mining, Inference, and Prediction, Second Edition.* Springer Series in Statistics. Springer New York.

Hindriks, R., M. H. Adhikari, Y. Murayama, M. Ganzetti, D. Mantini, N. K. Logothetis, and G. Deco (2016). Can sliding-window correlations reveal dynamic functional connectivity in resting-state fmri? *NeuroImage 127*, 242 – 256.

Hutchison, R. M., T. Womelsdorf, E. A. Allen, P. A. Bandettini, V. D. Calhoun, and C. et al. (2013). Dynamic functional connectivity: promise, issues, and interpretations. *Neuroimage 80*, 360–378.

Jenkinson, M., C. F. Beckmann, T. E. Behrens, M. W. Woolrich, and S. M. Smith (2012). {FSL}. *NeuroImage 62*(2), 782 – 790. 20 {YEARS} {OF} fMRI20 {YEARS} {OF} fMRI.

Jentsch, C., D. N. Politis, et al. (2015). Covariance matrix estimation and linear process bootstrap for multivariate time series of possibly increasing dimension. *The Annals of Statistics 43*(3), 1117–1140.

Jones, D. T., P. Vemuri, M. C. Murphy, J. L. Gunter, M. L. Senjem, and M. et al. (2012). Non-stationarity in the "resting brain's" modular architecture. *PloS one 7*(6), e39731.

Kareken, D. A., M. Dzemidzic, L. Wetherill, W. Eiler, B. G. Oberlin, J. Harezlak, Y. Wang, and S. J. O'Connor (2013). Family history of alcoholism interacts with alcohol to affect brain regions involved in behavioral inhibition. *Psychopharmacology 228*(2), 335–345.

Kashtan, N. and U. Alon (2005). Spontaneous evolution of modularity and network motifs. *Proceedings of the National Academy of Sciences of the United States of America 102*(39), 13773–13778.

Kiviniemi, V., T. Vire, J. Remes, A. A. Elseoud, T. Starck, O. Tervonen, and J. Nikkinen (2011). A sliding time-window ica reveals spatial variability of the default mode network in time. *Brain connectivity 1*(4), 339–347.

Kreiss, J.-P. and E. Paparoditis (2011). Bootstrap methods for dependent data: A review. *Journal of the Korean Statistical Society 40*(4), 357–378.

Kudela, M., J. Harezlak, and M. A. Lindquist (2017). Assessing uncertainty in dynamic functional connectivity. *NeuroImage*.

Lancichinetti, A. and S. Fortunato (2009). Community detection algorithms: a comparative analysis. *Physical review E 80*(5), 056117.

Lancichinetti, A. and S. Fortunato (2012). Consensus clustering in complex networks. *Scientific reports 2*.

Landman, B. A., A. J. Huang, A. Gifford, D. S. Vikram, I. A. L. Lim, and J. A. F. et al.

Leonardi, N. and D. Van De Ville (2015). On spurious and real fluctuations of dynamic functional connectivity during rest. *Neuroimage 104*, 430–436.

Lindquist, M. A., Y. Xu, M. B. Nebel, and B. S. Caffo (2014). Evaluating dynamic bivariate correlations in resting-state fmri: A comparison study and a new approach. *NeuroImage 101*, 531–546.

McMurry, T. L. and D. N. Politis (2010). Banded and tapered estimates for autocovariance matrices and the linear process bootstrap. *Journal of Time Series Analysis 31*(6), 471–482.

Mucha, P. J., T. Richardson, K. Macon, M. A. Porter, and J.-P. Onnela (2010). Community structure in time-dependent, multiscale, and multiplex networks. *science 328*(5980), 876–878.

Newman, M. E. (2006). Modularity and community structure in networks. *Proceedings of the national academy of sciences 103*(23), 8577–8582.

Oberlin, B. G., M. Dzemidzic, J. Harezlak, M. A. Kudela, S. M. Tran, C. M. Soeurt, K. K. Yoder, and D. A. Kareken (2016). Corticostriatal and dopaminergic response to beer flavor with both fmri and [11c] raclopride positron emission tomography. *Alcoholism: Clinical and Experimental Research 40*(9), 1865–1873.

Oberlin, B. G., M. Dzemidzic, S. M. Tran, C. M. Soeurt, D. S. Albrecht, K. K. Yoder, and D. A. Kareken (2013). Beer flavor provokes striatal dopamine release in male drinkers: mediation by family history of alcoholism. *Neuropsychopharmacology 38*(9), 1617–1624.

Oberlin, B. G., M. Dzemidzic, S. M. Tran, C. M. Soeurt, S. J. O'Connor, K. K. Yoder, and D. A. Kareken (2015). Beer self-administration provokes lateralized nucleus accumbens dopamine release in male heavy drinkers. *Psychopharmacology 232*(5), 861–870.

Patenaude, B., S. M. Smith, D. N. Kennedy, and M. Jenkinson (2011). A bayesian model of shape and appearance for subcortical brain segmentation. *Neuroimage 56*(3), 907–922.

Power, J. D., K. A. Barnes, A. Z. Snyder, B. L. Schlaggar, and S. E. Petersen (2012). Spurious but systematic correlations in functional connectivity mri networks arise from subject motion. *Neuroimage 59*(3), 2142–2154.

Power, J. D., A. Mitra, T. O. Laumann, A. Z. Snyder, B. L. Schlaggar, and S. E. Petersen (2014). Methods to detect, characterize, and remove motion artifact in resting state fmri. *Neuroimage 84*, 320–341.

Power, J. D., B. L. Schlaggar, and S. E. Petersen (2015). Recent progress and outstanding issues in motion correction in resting state fmri. *Neuroimage 105*, 536–551.

Ptak, R. (2012). The frontoparietal attention network of the human brain: action, saliency, and a priority map of the environment. *The Neuroscientist 18*(5), 502–515.

Robinson, P., J. Henderson, E. Matar, P. Riley, and R. Gray (2009). Dynamical reconnection and stability constraints on cortical network architecture. *Physical review letters 103*(10), 108104.

Ruppert, D., M. P. Wand, and R. J. Carroll (2003). *Semiparametric regression*. Number 12. Cambridge university press.

Sadaghiani, S., G. Hesselmann, and A. Kleinschmidt (2009). Distributed and antagonistic contributions of ongoing activity fluctuations to auditory stimulus detection. *Journal of Neuroscience 29*(42), 13410–13417.

Sakoğlu, Ü., G. D. Pearlson, K. A. Kiehl, Y. M. Wang, A. M. Michael, and V. D. Calhoun (2010). A method for evaluating dynamic functional network connectivity and task-modulation: application to schizophrenia. *Magnetic Resonance Materials in Physics, Biology and Medicine 23*(5-6), 351–366.

Shanahan, M. (2010). Metastable chimera states in community-structured oscillator networks. *Chaos: An Interdisciplinary Journal of Nonlinear Science 20*(1), 013108.

Shen, X., F. Tokoglu, X. Papademetris, and R. T. Constable (2013). Groupwise whole-brain parcellation from resting-state fmri data for network node identification. *Neuroimage 82*, 403–415.

Siegel, J. S., J. D. Power, J. W. Dubis, A. C. Vogel, J. A. Church, B. L. Schlaggar, and S. E. Petersen (2014). Statistical improvements in functional magnetic resonance imaging

analyses produced by censoring high-motion data points. *Human brain mapping 35*(5), 1981–1996.

Simon, H. A. (1962). The architecture of complexity. *Proceedings of the American philosophical society 106*(6), 467–482.

Singleton, E. G., S. T. Tiffany, and J. E. Henningfield (2000). Alcohol craving questionnaire (acq-now): Background, scoring, and administration. *Intramural Research Program*.

Smith, S. M., C. F. Beckmann, J. Andersson, E. J. Auerbach, J. Bijsterbosch, G. Douaud, E. Duff, D. A. Feinberg, L. Griffanti, M. P. Harms, et al. (2013). Resting-state fmri in the human connectome project. *Neuroimage 80*, 144–168.

Sporns, O. and R. F. Betzel (2016). Modular brain networks. *Annual review of psychology 67*, 613–640.

Starck, T., J. Nikkinen, J. Rahko, J. Remes, T. Hurtig, and H. e. a. Haapsamo (2013). Resting state fmri reveals a default mode dissociation between retrosplenial and medial prefrontal subnetworks in asd despite motion scrubbing. *Frontiers in human neuroscience 7*.

Thesen, S., O. Heid, E. Mueller, and L. R. Schad (2000). Prospective acquisition correction for head motion with image-based tracking for real-time fmri. *Magnetic Resonance in Medicine 44*(3), 457–465.

Turk-Browne, N. B. (2013). Functional interactions as big data in the human brain. *Science 342*(6158), 580–584.

Uddin, L. Q. (2015). Salience processing and insular cortical function and dysfunction. *Nature Reviews Neuroscience 16*(1), 55–61.

Wakefield, J. (2013). *Bayesian and frequentist regression methods*. Springer Science & Business Media.

Wand, M. and J. Ormerod (2008). On semiparametric regression with o'sullivan penalized splines. *Australian & New Zealand Journal of Statistics 50*(2), 179–198.

Whitfield-Gabrieli, S. and J. M. Ford (2012). Default mode network activity and connectivity in psychopathology. *Annual review of clinical psychology 8*, 49–76.

Xu, Y. and M. A. Lindquist (2015). Dynamic connectivity detection: an algorithm for determining functional connectivity change points in fmri data. *Frontiers in neuroscience 9*.

Yeo, B. T., F. M. Krienen, J. Sepulcre, M. R. Sabuncu, D. Lashkari, M. Hollinshead, J. L. Roffman, J. W. Smoller, L. Zöllei, J. R. Polimeni, et al. (2011). The organization of the human cerebral cortex estimated by intrinsic functional connectivity. *Journal of neurophysiology 106*(3), 1125–1165.

Curriculum vitae

Maria Aleksandra Kudela

EDUCATION

- Ph.D. in Biostatistics, Minor in Epidemiology, Indiana University, Indianapolis, IN, 2017
- B.S./M.S. in Mathematics, Wroclaw University of Technology, Poland, 2009

WORKING EXPERIENCE

- Research Assistant, Department of Biostatistics, Indiana University School of Medicine, Indianapolis, IN, 09/2011 - 01/2017
- Teaching Assistant, Department of Biostatistics, Indiana University Purdue University Indianapolis, Indianapolis, IN, 07/2013 - 06/2014
- Associate Instructor, Department of Biostatistics, Indiana University Purdue University Indianapolis, Indianapolis, IN, 07/2014 - 06/2015

HONORS AND AWARDS

- The 2nd Summer Institute in Statistics for Big Data Scholarship Award, Department of Biostatistics, University of Washington, Seattle, WA 2016
- Outstanding Advanced Graduate Student Award, School of Science IUPUI 2016
- ENAR Distinguished Student Paper Award at the 2016 ENAR Spring Meeting in Austin, TX
- Graduate - Professional Educational Grant, IUPUI, March 2015

SELECTED PUBLICATIONS

- Kudela, M.A., Harezlak J., Lindquist M.A. (2016), Assessing uncertainty in dynamic functional connectivity, Neuroimage, 2017
- Oberlin, B. G., Dzemidzic, M., Harezlak, J., Kudela, M. A., Tran, S. M., Soeurt, C. M., Yoder, K. K. and Kareken, D. A. (2016), Corticostriatal and Dopaminergic Response to Beer Flavor with Both fMRI and [11C]raclopride Positron Emission Tomography. Alcoholism: Clinical and Experimetal Research, Volume 40, Issue 9, 1865–1873
- Tsai W., Chan Y., Hsueh C., Everett IV T., Chang P., Choi E., Lin S., Shen C., Kudela M. A. et.al. (2016), Small conductance calcium-activated potassium current and the mechanism of atrial arrhythmia in mice with dysfunctional melanocyte-like cells. Heart Rhythm , Volume 13 , Issue 7 , 1527 - 1535